九州大学学術情報リポジトリ
Kyushu University Institutional Repository

Point mutations in yeast oligosaccharyltransferase decouple the oligosaccharyl transfer and hydrolysis of lipid-linked oligosaccharide reactions: an improved purification strategy and peptide substrate for the oligosaccharyltransferase researches

山﨑, 貴大

https://hdl.handle.net/2324/4474954

出版情報：Kyushu University, 2020, 博士（システム生命科学）, 課程博士
バージョン：
権利関係：

Point mutations in yeast oligosaccharyltransferase decouple the oligosaccharyl transfer and hydrolysis of lipid-linked oligosaccharide reactions: an improved purification strategy and peptide substrate for the oligosaccharyltransferase researches

by

TAKAHIRO YAMASAKI

A DISSERTATION

Submitted in partial fulfillment of the requirements for the degree

DOCTOR OF PHILOSOPHY (Ph.D.) IN SYSTEM LIFE SCIENCES

Graduate School of Systems Life Sciences

KYUSHU UNIVERSITY
Fukuoka, Japan

February 2021

Supervised by:

Professor Daisuke Kohda

Table of Contents

Acknowledgments

Upon the completion of this thesis, I am grateful to those who have offered me support during my study.

Firstly, I would like to express my sincere gratitude to my supervisor, Prof. Daisuke Kohda, whose suggestions and encouragement are beneficial to me a lot.

I appreciate Dr. Atsushi Shimada and Dr. Kouta Mayanagi giving professional technical supports about respectively X-ray crystal structure analysis and electron microscopy analysis.

I thank Dr. Shunsuke Matsumoto, Dr. Rei Matsuoka, Dr. Daisuke Fujinami, Dr. Yuya Taguchi, and Dr. Hiromi Ogino for technical supports in the experiments. Also, I learned how to think scientifically from many discussions.

Finally, I would like to thank all the people I have met, both directly and indirectly through literature and lectures, for their knowledge and experiments that helped me complete this paper.

Abbreviations used in this thesis:

2-AP, 2-aminopyridine
CBB, Coomassie Brilliant Blue
CPY, carboxypeptidase Y
ER, endoplasmic reticulum
FNG, free N-glycan
5-FOA, 5-fluoroorotic acid
GPD, glyceraldehyde 3-phosphate dehydrogenase
LLO, lipid-linked oligosaccharide
OD, optical density
OST, oligosaccharyltransferase
PA, a high-affinity tag
PNGase, peptide : N-glycanase
TAMRA, 5(6)-carboxytetramethylrhodamine
tam, TAMRA
UPLC, ultra-performance liquid chromatography
WT, wild-type
O-GlcNacylation, O-linked-N-acetylglucosaminylation
GPI, Glycosylphosphatidylinositol
HA, Human influenza hemagglutinin
MALDI-TOF-MS, Matrix-Assisted Laser Desorption/Ionization Time of Flight Mass Spectrometry
DTT, 1,4-dithiothreitol
SDS-PAGE, Sodium dodecyl sulfate Polyacrylamide gel electrophoresis
EDTA, ethylenediaminetetraacetic acid
DMSO, Dimethyl Sulfoxide
Tm, Tunicamycin
H_2O_2, hydrogen peroxide
Cryo-EM, Cryo-electron microscopy
PyMOL, molecular visualization system software

Abstract

Oligosaccharyltransferase (OST) is responsible for the first step in the N-linked glycosylation, transferring an oligosaccharide chain onto asparagine residues to create glycoproteins. In the absence of the acceptor asparagine, OST hydrolyzes the oligosaccharide donor, lipid-linked oligosaccharide (LLO), and releases free N-glycans (FNGs) into the endoplasmic reticulum (ER) lumen constitutively. Here, I established a purification method for mutated OSTs using a high-affinity epitope tag attached to the catalytic subunit Stt3, from yeast cells co-expressing the wild-type OST to support growth. A high-affinity epitope tag attached to the catalytic subunit Stt3 enabled the preparation of functionally impaired OSTs free from the genome-derived native Stt3. The purified OST protein with mutations is useful for wide-ranging biochemical experiments. I assessed the effects of mutations in the Stt3 subunit on the two enzymatic activities in vitro, as well as their effects on the N-glycan attachment and FNG content levels in yeast cells. The correlations with the growth phenotype suggested that FNG in the ER was dispensable for the growth of yeast cells under laboratory conditions. I found that mutations in the first DXD motif increased the FNG generation activity relative to the oligosaccharyl transfer activity, both in vitro and in vivo, while mutations in the DKM motif had the opposite effect. The decoupling of the two activities may facilitate future deconvolutions of the reaction mechanism. The isolation of the mutated OSTs also enabled me to identify different enzymatic properties in OST complexes containing either the Ost3 or Ost6 subunit and to find a 15-residue peptide as a better quality substrate than shorter peptides. This toolbox of mutants, substrates, and methods will be useful for investigations of the molecular basis and physiological roles of the OSTs in yeast and other organisms.

Chapter 1 Introduction

1.1 Post-translational protein modification

Many proteins function with post-translational modifications [1]. More than 200 post-translational modifications have been reported in eukaryotes [2]. Phosphorylation and O-GlcNacylation are representative of reversible modifications, which are modulated by signaling molecules [3,4]. Among glycosylations, there are N-linked, O-linked, GPI anchor type, etc. In glycosylation, the chemical structure of the transferred oligosaccharide chain is processed by other glycosyltransferases and glycosidases in the endoplasmic reticulum (ER) and Golgi apparatus, which results in various glycan structures in response to the environment and stimuli of cell [5].

1.2 N-glycosylation

N-glycosylation refers to the covalent attachment of an oligosaccharide chain on asparagine residues in proteins (Fig. 1) [6–8]. The N-glycosylation consensus, Asn-X-Ser/Thr (X≠Pro), is the sequon, and the N-oligosaccharide chain attached to a protein is the N-glycan. The oligosaccharide donors are lipid-linked oligosaccharides (LLOs) [9]. The oligosaccharide portion of LLO is transferred to the side-chain carboxamide group of asparagine residues in the sequon by the action of oligosaccharyltransferase (OST) at the luminal side of the rough endoplasmic reticulum [10]. In the absence of the acceptor asparagine, OST hydrolyzes LLO and releases free N-glycans (FNGs) into the ER lumen constitutively [11,12]. In higher eukaryotes, including the budding yeast *Saccharomyces cerevisiae* (*S. cerevisiae*), the transfer of the 14-residue oligosaccharide chain, Glc3Man9GlcNAc2. N-linked glycosylation serves as a marker for folding, hydrophilic surface, and signaling molecules, contributing to protein quality control and cell-cell interactions [5]. Statistical studies revealed that two-thirds of the sequons are glycosylated [13]. The proper selections of the sequons to be glycosylated or left unmodified are a prerequisite for the protein quality control in the ER and subsequent degradation in the cytosol [6,7]. Genes involved in N-linked glycosylation include glycan donor synthases, glycosidases, and glycosyltransferases. It has been estimated that human glycome requires more than 700 proteins to generate the glycan structures [14]. Congenital disorder of glycosylation (CDG) disease is a human genetic disease involved in glycosylation [6]. Many reports of CDG diseases are caused by mutations in genes involved in N-linked glycosylation [15].

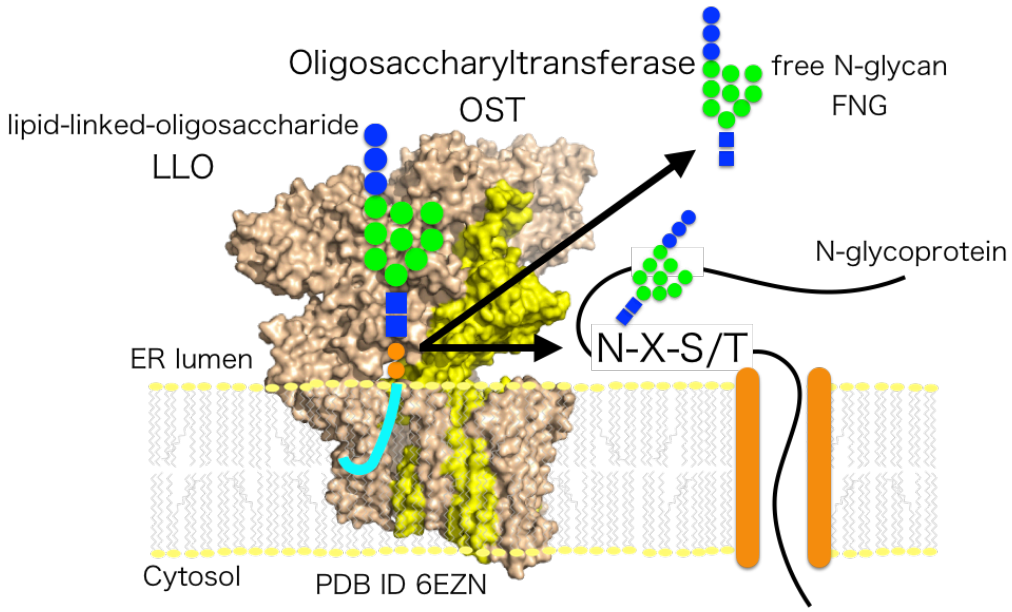

Figure 1. Overview of the oligosaccharyltransferase enzymatic reaction.

The Oligosaccharyltransferase (OST) catalyzes the transfer of a sugar chain to the asparagine residues in the consensus sequence (N-X-S/T, X≠P). The OST also hydrolyzes lipid-linked-oligosaccharide (LLO) to generate free N-glycan (FNG). The yeast OST consists of eight membrane protein subunits, including the catalytic subunit, STT3 (yellow). ER, endoplasmic reticulum.

1.3 Free N-glycan (FNG)

Interestingly, oligosaccharide chains that are not attached to proteins reportedly accumulate inside the ER and the cytosol (Fig. 2) [16]. The peptide:N-glycanase (PNGase), Png1, cleaves the N-glycans from misfolded glycoproteins in the cytosol. The PNGase-derived "free" N-glycans (FNGs) account for 95% of the total FNGs in the yeast cytosol [11]. The yeast OST generates the remaining 5% of FNGs via LLO hydrolysis reaction. No other enzyme had been found that can hydrolyze mature LLO. The OST-derived FNGs are transported from the ER to the cytosol for degradation by a cytosol-vacuolar α-mannosidase, Ams1 [17,18]. The amounts of FNGs generated by OST can be measured using a *png1Δams1Δ* double-knockout strain, by suppressing the generation of the cytosol-originated FNGs [11]. In contrast, most of the FNGs in the ER and the cytosol are attributed to the hydrolytic activity of OST in the ER lumen in mammalian cells [12]. In mammalian cells, Manβ1-4GlcNAc disaccharide is produced by FNGs degradation enzymes and stimulated immune responses [19]. It had also been

suggested that FNG generation activity may differ depending on the subunit composition of the OST complex in mouse embryonic fibroblasts [20]. In plant cells, mass spectrometry analyses had suggested that FNG may be released from the ER to the extracellular space via the Golgi apparatus in the same manner as secretory proteins [21]. In other free oligosaccharide researches, free GPIs, nonprotein-anchor GPI were existed at the plasma membrane in some tissues of mice and modified the same structural remodeling pathway as do protein-linked GPI [22]. It was reported that glucose starvation induced the accumulation of free O-mannosylated glycans in budding yeast [23]. Previously reports showed that N-glycan conjugated asparagines directly promote protein folding [21,24,25]. It should be noted here that the physiological function of the FNG in ER remains largely unexplored.

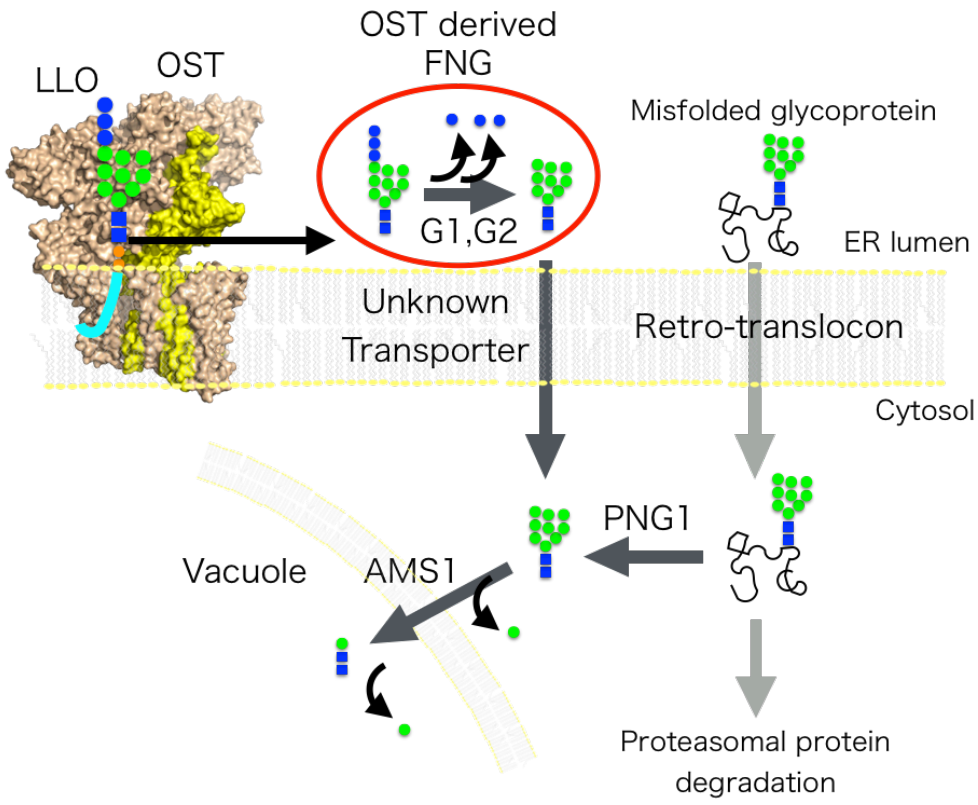

Figure 2. Outline of the FNGs processing pathway in yeast.

OST generates FNG consisting of 14 sugars in the ER lumen by LLO hydrolysis. 14 Sugar FNG is trimmed by the action of ER luminal α-glucosidase I (G1) and α-glucosidase II (G2) as well as sugar chains on glycoproteins. FNGs and misfolded glycoproteins are transported to the cytoplasmic side through their respective

transporters. The sugar chain of the misfolded glycoprotein is cleaved from the protein by the action of cytoplasmic PNGase, and FNGs are produced. Cytosolic FNGs are degraded by the action of Ams1 localized at the vacuole.

1.4 OST complex of Saccharomyces cerevisiae

The budding yeast *Saccharomyces cerevisiae* (*S. cerevisiae*) is a model organism for eukaryotes. The yeast OST complex consists of the same number of subunits as the human OST complex (Table. 1). The yeast OST is a membrane-embedded protein complex consisting of eight membrane-protein subunits in an equimolar ratio. Stt3, Wbp1, Swp1, Ost1, and Ost2 are essential gene products, while Ost3/Ost6, Ost4, and Ost5 are non-essential gene products [10]. The Stt3 subunit has a catalytic site. In general, eukaryotic genomes encode multiple paralogous *stt3* genes [26]. The homologous Stt3 proteins expressed from these paralogous genes generate different OST complexes. Except for *Caenorhabditis* species, the genomes from all sequenced metazoan organisms contain two STT3 genes (STT3A and STT3B). Plant genomes also encode two copies of STT3 genes (STT3A and STT3B) [27]. In the phylum Protista, for example, the *Leishmania major* genome contains four *stt3* genes, *stt3A*, *stt3B*, *stt3C*, and *stt3D* [28]. Despite their similar names, the human and protist genes lack direct orthologous relationships [27,29]. One important exception is fungi, including *S. cerevisiae*, with genomes encoding a single *stt3* gene. The human STT3B protein sequence is more similar to the yeast Stt3 protein sequence, suggesting that the human STT3A is a newcomer in evolution and the human STT3B is orthologous to the yeast Stt3 [29].

	Homo sapiens		*S. cerevisiae*
	STT3A complex	STT3B complex	OST complex
80 kDa	STT3A		
93 kDa		STT3B	Stt3
48 kDa	DDOST/OST48		Wbp1
66 kDa	RPN1/ribophorin I		Ost1
63 kDa	RPN2/ribophorin II		Swp1
13 kDa	DAD1		Ost2
3.6 kDa	OST4		Ost4
40 kDa		TUSC3	Ost3
38 kDa		MAGT1	Ost6
14 kDa	KCP2		
17 kDa	DC2		
9 kDa	TMEM258		Ost5

Table 1. Subunit composition of OST complex in *Homo sapiens* and *S. cerevisiae*

Genes in the same row are a homologous relationship. The left column showed the molecular weight of *Homo sapiens* protein. In *Homo sapiens*, two OST complexes exist, STT3A complex and STT3B complex that contains each STT3A or STT3B as the catalytic subunits. STT3A complex contains either KCP2 or DC2 subunit. STT3B complex contains either TUSC3 or MAGT1 subunit. In *S. cerevisiae*, the OST complex contains either Ost3 or Ost6.

1.5 Interchangeable subunit: OST3 and OST6

In place of the single Stt3, the yeast genome encodes the two paralogous *ost3* and *ost6* genes, which generate two different OST forms containing either Ost3 or Ost6 (Table. 1) [30]. The ratio of the Ost3-containing to Ost6-containing OST complexes is 4:1 [11]. Single deletions of either Ost3 or Ost6 resulted in moderate underglycosylation of proteins, and the Ost3 and Ost6 double knockout led to severe underglycosylation in yeast cells [31].

1.6 Motivation

It is still unclear whether FNGs in the ER have a physiological function or not. Previous studies had suggested that the hydrolysis of LLO may be a side reaction, as the amounts of FNGs were reduced in the cells when impaired OST mutants expressed [11,32]. However, one was in vivo mutant analysis using bacteria cells which OST is not essential for survival [32], another was in vivo mutant analysis over-expressing

Leishmania major OST with lethal phenotypic mutations in yeast [11]. The previous article had suggested that FNG generation activities may differ by the difference of subunit composition of OST complex in mouse embryonic fibroblast [20].

I think it is important to consider FNG generation activity and oligosaccharyl transfer activity separately for exploring the function of FNGs. However, there are few examples of examining it in detail.

In this study, I measured the oligosaccharyl transfer activity and the hydrolytic activity of LLO in vitro, using the OST complexes carrying mutations in the catalytic Stt3 subunit. In parallel, I determined the N-glycosylation status of the glycoproteins and the amounts of FNGs generated by OST in strains harboring the same stt3 mutations. These detailed comparisons of the two activities of a series of mutations provided new insights into the N-glycosylation reactions in vitro and in living cells. Then, I explored under what conditions the amount of intracellular FNG changes and identified the factors that cause changes in OST activity. By studying the relationship between the amount of intracellular FNG and phenotype, I would clarify how the OST-derived FNG in the ER affects the survival of the organism.

Chapter 2 Construction of the experimental system for the study

2.1 The merits of yeast for this study

In this study, I needed to use an experimental organism that would allow us to easily determine the amount of FNG and its phenotype. Therefore, I chose budding yeast, *S. cerevisiae*, which OST is essential for survival. Yeast has only OST and PNG1 enzymes that generate FNG, and few N-glycan trimming enzymes [33]. There is a wealth of information such as OST structural information [34,35], N-glycome analyses [36,37], and glycosidase annotations [11,18,38]. Yeast grows quickly and is a unicellular model genetic organism and used for studies of common cellular processes in higher organisms.

2.2 Gene manipulation

Yeast is easy to allow genetic manipulation and can be selected based on auxotrophy and antibiotic resistance. Sporulation and PCR fragments were used to create a gene knockout strain of yeast. I used a native promoter or constitutive strong expression promoter (glyceraldehyde 3-phosphate dehydrogenase: GPD) for expression from plasmids.

Yeast strains used in this study are listed in Table 2.

Plasmids used in this study are listed in Table 3.

Table 2. Yeast strains used in this study

Strain name	Genotype	Source	Purpose
BY4741	*MAT***a** *his3Δ1 leu2Δ0 met15Δ0 ura3Δ0*	Laboratory strain	Parental strain, Source of LLO
*stt3*Δ-pSTT3	*MAT***a** *stt3*Δ::*KanMX* BY4741-pRS316-STT3	This study	Plasmid shuffling
*stt3*Δ *png1*Δ *ams1*Δ-pSTT3	*MAT***a** *stt3*Δ::*KanMX png1*Δ::*HygMX ams1*Δ::*LEU2* BY4741- pRS316-STT3	This study	Plasmid shuffling
*stt3*Δ *png1*Δ *ams1*Δ-pSTT3/pSTT3(X)	*MAT***a** *stt3*Δ::*KanMX png1*Δ::*HygMX ams1*Δ::*LEU2* BY4741- pRS316-STT3/pRS313-STT3(X)	This study	Plasmid shuffling

*stt3*Δ *png1*Δ *ams1*Δ-pSTT3(X)	*MAT***a** *stt3*Δ::*KanMX png1*Δ::*HygMX ams1*Δ::*LEU2* BY4741- pRS313-STT3(X)	This study	Quantification of the glycosylation status of CPY and Wbp1, and the amounts of FNG, LLO, and mannoprotein N-glycans
*ost6*Δ-pOST3[a]	*MAT***a** *ost6*Δ::*LEU2* BY4741-pOST3	This study	Production of OST[Ost3, PA-Stt3(X)]
*ost6*Δ *ost4*PA-pOST3[a]	*MAT***a** *ost6*Δ::*LEU2 ost4*Δ*::ost4*-PA BY4741- pOST3	This study	Production of OST[Ost3, Ost4-PA]
*ost3*Δ*ost4*PA-pOST6[b]	*MAT***a** *ost3*Δ::*LEU2 ost4*Δ*::ost4*-PA BY4741- pOST6	This study	Production of OST[Ost6, Ost4-PA]
*ost6*Δ-FLAG*stt3*-pOST3[a]	*MAT***a** *ost6*Δ::*LEU2 stt3*Δ::*HygMX*-FLAG-*stt3* BY4741- pOST3	This study	Check contamination of mutated PA-Stt3 by WT FLAG-Stt3
*png1*Δ *ams1*Δ	*MAT***a** *png1*Δ::*HygMX ams1*Δ::*LEU2* BY4741	This study	The amounts of FNG in stress conditions
W303-1A	*MAT***a** {*leu2-3,112 trp1-1 can1-100 ura3-1 ade2-1 his3-11,15*}	Laboratory strain	Determination of the mating type
W303-1B	*MAT* **alpha** {*leu2-3,112 trp1-1 can1-100 ura3-1 ade2-1 his3-11,15*}	Laboratory strain	
*ost6*Δ *ost3*Δ *ost4*PA-pOST3[a]	*MAT***a** *ost6*Δ::*LEU2 ost3*Δ::*HygMX ost4*Δ*::ost4*-PA BY4741- pOST3	This study	Plasmid shuffling

[a]The extra expression of Ost3 from the pOST3 plasmid reduces the deleterious effects by the absence of Ost6.

[b]The extra expression of Ost6 from the pOST6 plasmid reduces the deleterious effects by the absence of Ost3.

Table 3. Plasmids used in this study

Plasmid name	Description	Source	Purpose
pRS316	CEN6/ARS4, URA3	BYP562, National BioResource Project Japan	Parental plasmid
pRS316-STT3	described previously	Reference [39]	Expression of WT Stt3 under the native promoter
pRS313	CEN6/ARS4, HIS3	BYP559, National BioResource Project Japan	Parental plasmid, An empty plasmid in Figs. 5, 17, 18, 35
pRS313-STT3-3HA	described previously	Reference [39]	Expression of WT Stt3 under the native promoter
pRS313-STT3	3×HA tag sequence was removed from pRS313-STT3-3HA	This study	Expression of WT and mutated Stt3 under the native promoter in plasmid shuffling experiments and other *in vivo* experiments
pSTT3(E45A)	pRS313-STT3(E45A)	This study	
pSTT3(E45D)	pRS313-STT3(E45D)	This study	
pSTT3(E45K)	pRS313-STT3(E45K)	This study	
pSTT3(E45Q)	pRS313-STT3(E45Q)	This study	
pSTT3(D47A)	pRS313-STT3(D47A)	This study	
pSTT3(D166A)	pRS313-STT3(D166A)	This study	
pSTT3(E168A)	pRS313-STT3(E168A)	This study	
pSTT3(D583A)	pRS313-STT3(D583A)	This study	
pSTT3(K586A)	pRS313-STT3(K586A)	This study	
pSTT3(K586H)	pRS313-STT3(K586H)	This study	

pSTT3(K586L)	pRS313-STT3(K586L)	This study	
pSTT3(K586R)	pRS313-STT3(K586R)	This study	
pSTT3(K586S)	pRS313-STT3(K586S)	This study	
pSTT3(M590A)	pRS313-STT3(M590A)	This study	
pAG416-GPD-ccdB	CEN6/ARS4, HIS3, GPD, CYC1, ccdB	#14148, Addgene	Parental plasmid
pOST3	pAG416-GPD-OST3	This study	Compensate for the lack of Ost6
pOST6	pAG416-GPD-OST6	This study	Compensate for the lack of Ost3
pPA-STT3	pRS313-GPD-PA-spacer-STT3	This study	Expression of WT and mutated PA-Stt3 under the GPD promoter in the strain, *ost6*Δ-pOST3
pPA-STT3(E45A)	pRS313-GPD-PA-spacer-STT3(E45A)	This study	
pPA-STT3(E45D)	pRS313-GPD-PA-spacer-STT3(E45D)	This study	
pPA-STT3(E45K)	pRS313-GPD-PA-spacer-STT3(E45K)	This study	
pPA-STT3(E45Q)	pRS313-GPD-PA-spacer-STT3(E45Q)	This study	
pPA-STT3(D47A)	pRS313-GPD-PA-spacer-STT3(D47A)	This study	
pPA-STT3(R159A)	pRS313-GPD-PA-spacer-STT3(R159A)	This study	
pPA-STT3(E350A)	pRS313-GPD-PA-spacer-STT3(E350A)	This study	
pPA-STT3(W517A)	pRS313-GPD-PA-spacer-STT3(W517A)	This study	
pPA-STT3(D518A)	pRS313-GPD-PA-spacer-STT3(D518A)	This study	
pPA-STT3(D583A)	pRS313-GPD-PA-spacer-STT3(D583A)	This study	
pPA-STT3(K586A)	pRS313-GPD-PA-spacer-STT3(K586A)	This study	

pPA-STT3(K590A)	pRS313-GPD-PA-spacer-STT3(M590A)	This study	
pGST-C-NVT8	pGEX6p-GST-C-NVT8	This study	Expression of oligosaccharyl transfer substrate peptide
pGST-C-NVT9	pGEX6p-GST-C-NVT9	This study	
pGST-C-NVT18	pGEX6p-GST-C-NVT18	This study	
pGST-C-NVT28	pGEX6p-GST-C-NVT28	This study	
pFA6a-OST4-PA-URA4MX6	pFA6a-OST4-PA-URA4MX6	This study	Preparation of *ost4*PA strain
pFA6a-ura4MX6	pFA6a-ura4MX6	# 49184, Addgene	Parental plasmid
pFA6a-6xGLY-3xFLAG-hphMX4	pFA6a-6xGLY-3xFLAG-hphMX4	# 20755, Addgene	Parental plasmid
pRS313-OST3	pRS313-OST3	This study	Plasmid shuffling
pRS313-OST3 Δ26-175 AA	pRS313-OST3 Δ26-175 AA	This study	
pRS313-OST3 Δ26-205 AA	pRS313-OST3 Δ26-205 AA	This study	
pRS313-OST3 Δ2-175 AA	pRS313-OST3 Δ2-175 AA	This study	
pRS313-OST3 Δ2-205 AA	pRS313-OST3 Δ2-205 AA	This study	
pRS313-OST6	pRS313-OST6	This study	
pRS313-OST6 Δ28-178 AA	pRS313-OST6 Δ28-178 AA	This study	
pRS313-OST6 Δ28-205 AA	pRS313-OST6 Δ28-205 AA	This study	
pRS313-OST6 Δ2-178 AA	pRS313-OST6 Δ2-178 AA	This study	
pRS313-OST6 Δ2-205 AA	pRS313-OST6 Δ28-205 AA	This study	

2.3 Yeast genetic experiments

2.3.1 Common motifs of STT3 protein

Comparison studies revealed that several common motifs in STT3 catalytic subunit conserved in the three domains of life, 1st DXD (Glu^{45}-Asp^{47}), 2nd DXD (Asp^{166}-Glu^{168}), SVSE (Ser^{347}-Glu^{350}), WWDYG (Trp^{516} -Trp^{517}-Asp^{518}-Tyr^{519}-Gly^{520}), and DKM (Asp^{583}-Lys^{586}-Met^{590}) (Fig. 3) [35,39].

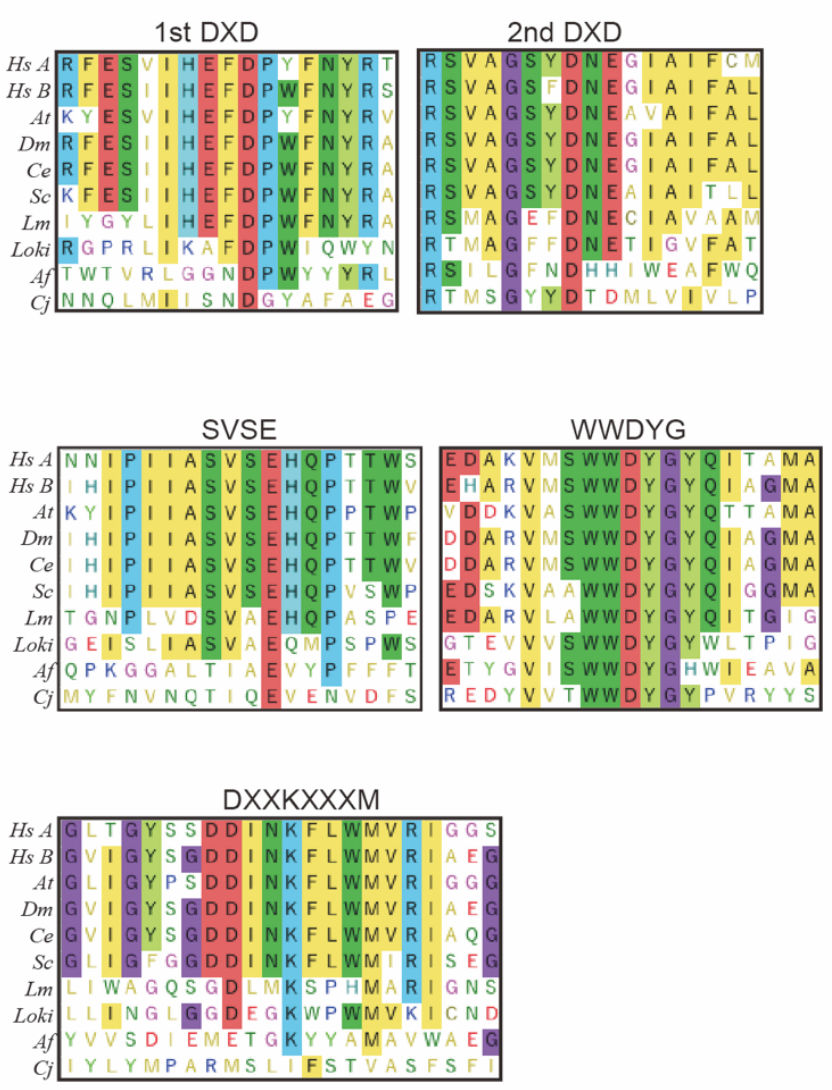

Figure 3. Multiple sequence alignments of amino acid sequences of conserved motifs of STT3 proteins.

STT3 protein sequences contain five evolutionally conserved structural motifs among three domains of life. The species from the top to the 7th line are Eukaryota.

Lokiarchaeum sp. GC14_75 and *Archaeoglobus fulgidus* are Archaea species. *Campylobacter jejuni* is Eubacteria.

Symbols: Hs A, *Homo sapiens* STT3A; Hs B, *Homo sapiens* STT3B; At, *Arabidopsis thaliana* STT3A; Dm, *Drosophila melanogaster* STT3B; Ce, *Caenorhabditis elegans* STT3; Sc, *Saccharomyces cerevisiae* STT3; Lm, *Leishmania major* STT3D; Loki, *Lokiarchaeum* sp. GC14_75 AglB; Af, *Archaeoglobus fulgidus* AglB; Cj, *Campylobacter jejuni* PglB.

2.3.2 Preparation of stt3 knockout strain

For in vivo mutagenesis studies, I prepared an *stt3* knockout strain. Because *stt3* is an essential gene for yeast survival, the *stt3* knockout strain was sustained the *stt3* expression plasmid (pRS316-STT3). Thus, I used the sporulation method for creating an *stt3* knockout strain.

creating a haploid strain stt3Δ-pSTT3

The Yeast Hetero-Diploid Knock Out Strain YGL022W (YSC1021-6716911, *Mat**a**/**alpha** his3/his3 leu2/leu2 lys2/LYS2 MET15/met15 ura3/ura3* Δ*stt3::kanMX4/STT3,* dharmacon) was purchased and transformed with pRS316-STT3 [39]. The STT3 regions of pRS316-STT3 and pRS313-STT3 are 2,680-bp fragment containing the entire *stt3* gene (2,157 bp) plus 299 bp (native promoter) and 224 bp (native terminator) at the 5' and 3' ends, respectively. pRS313-STT3 was generated by the deletion of the 3×HA tag sequence (30 amino acid residues) from the pRS313-STT3-3HA plasmid constructed previously [39]. After sporulated, the haploid strain *stt3*Δ-pSTT3 (*MAT**a** his3 leu2 lys2 ura3* Δ*stt3::kanMX4* [pRS316-STT3]) was selected on a -Met-Ura+G418+alpha-aminoadipate plate (G418 and alpha-aminoadipate, Sigma) (Fig. 4A). The mating type was determined using Yeast Reference strains, W303-1A *MAT**a*** *and* W303-1B *MAT* **alpha**.

2.3.3 Plasmid shuffling

In vivo mutagenesis studies of the individual subunits of the yeast OST have been performed using the spotting plate assay. Switching from the wild-type OST to the mutated OST in cells is accomplished by the plasmid shuffling method [39,40] or the GAL1 promoter switching method [41]. Plasmid shuffling is used to analyze essential

genes in yeast (Fig. 4B) [42]. Plasmid shuffling shows the importance of motifs introduced with mutations by yeast cell growth.

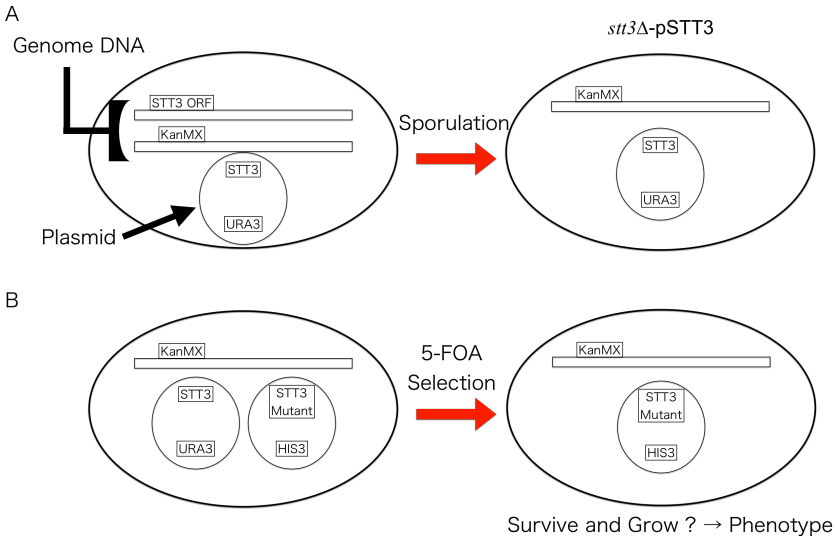

Figure 4. Acquisition of STT3 knockout strain and plasmid shuffling procedure.
pRS316-STT3 was transformed into Yeast Hetero-Diploid Knock Out Strain YGL022W. *STT3*/*stt3*Δ heterozygotes were sporulated to obtain the *stt3* knockout haploid. pSTT3 (X) was transformed into *stt3*Δ-pSTT3 strain, followed by 5-FOA selection was performed to drop pRS316-STT3. Yeast can grow if the STT3 mutant can complement the function of STT3. If not complementary, yeast cannot grow.

plasmid* shuffling *and spotting plate assay

*stt3*Δ cells bearing pRS316-STT3 encoding the wild-type *stt3* were transformed with p(RS313-)STT3(X), encoding the *stt3* gene containing a single-point mutation X. The transformants were grown in SD medium lacking L-histidine until the OD_{600} reached 1. Collected cells were diluted in a 5-fold series. Aliquots (3 µL) of each dilution were spotted onto SD plates lacking L-histidine and those lacking L-histidine supplemented with 5-FOA, at a final concentration of 1 mg mL^{-1}. After incubations at 25, 30, and 37°C for 2 days, cell growth was assessed.

I defined the growth phenotypes as follows, lethal means no growth in any temperatures, normal means the same growth as wild-type STT3, and the others

classified the temperature-sensitive (Fig. 5). 1st DXD motif E45A mutation is temperature-sensitive, D47A mutation is lethal (Fig. 5A). 2nd DXD motif D166A mutation is lethal, E168A mutation is temperature-sensitive. The D583A mutation of DXXKXXXM motif was lethal, the K586A mutation was temperature-sensitive, and the M590A mutation was normal (Fig. 5B). Because the K586A mutation was previously reported as lethal [39,41], I changed to another amino acid and re-experimented to Lys[586] residue. K586A, L, R, S mutations were temperature-sensitive, K586H mutation was normal (Fig. 5C). In previous reports, the K586A and K586R mutations were lethal, both were temperature-sensitive in this experiment. In a previous study, a 3×HA tag was added to the C-terminus of STT3, and I suspect that it affected growth. Chromosomal mutations in the STT3 locus (K586A) experiment resulted in a temperature-sensitive phenotype [35].

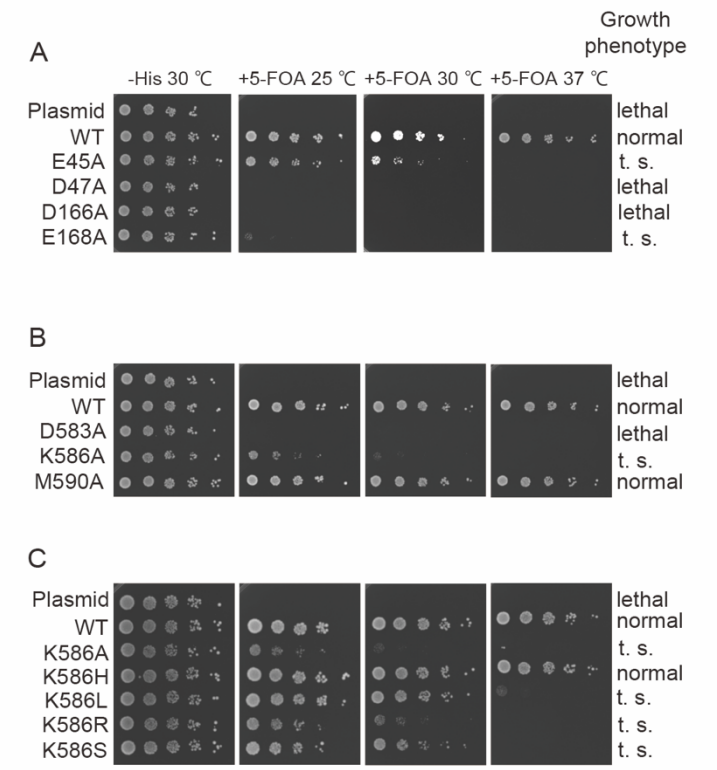

Figure 5. Spotting plate assay of yeast strains expressing mutated Stt3 subunits.
The yeast strains, *stt3*Δ-pRS316-STT3(WT)+p(RS313-)STT3(X), where X denotes a mutation, were spotted on -His + 5-FOA plates. The growth of the colonies at three different temperatures was compared after 2 days 30,37˚C and 3 days 25˚C. 't.s.' stands

for temperature-sensitive. The OST complex expressed in the cells was the mixed type of Ost3 and Ost6.

2.4 Purification of OST complex for studies

The spotting plate assay is quite easy to execute, but its outcome is rather limited: a mutation is just classified into lethal, temperature-sensitive, or normal (i.e., non-conditional) growth phenotypes. Moreover, the different properties of the two OST complexes containing Ost3 or Ost6 in vivo could complicate the interpretation of the results obtained by the spotting plate assays.

In some situations, enzymological studies using purified proteins with a defined subunit composition are preferred. However, the reconstitution of the OST complex in vitro using recombinant proteins has not been successful. Fortunately, the genetic manipulation of the yeast genome is straightforward. Previously, the 3×HA (hemagglutinin) epitope tag encoding sequence was inserted at the 3′-ends of the *stt3* and *ost3* genes in the yeast genome, for immunopurification of the OST complexes and immunodetection of other subunits [40,43]. The tandem IgG-binding domain encoding sequence of Protein A was added to the 3′-end of the *stt3* gene in the yeast genome for the same purpose [44]. Subsequently, other types of epitope tag sequences (FLAG, 3×FLAG, and 1D4) were incorporated into the 3′-end of the *ost4* gene in the yeast genome, and the tagged OST complexes were affinity purified to homogeneity for enzymatic investigation [11] and cryo-EM single-particle analyses [34,35,45].

In the case of conditional mutations, the isolation of OST complexes containing such mutant proteins is possible, provided that the yeast strain can grow under permissive conditions. Yeast strains carrying the *stt3-4* and *stt3-6* (G520D), *stt3-5* (G520S), and *stt3-7* (S552P) alleles have temperature-sensitive phenotypes [44]. These strains were grown at the permissive temperature of 23°C, and the membrane fractions were prepared. In the membrane fractions, the OST complexes with these mutants showed very low oligosaccharyl transfer activities [44]. In contrast, the introduction of lethal or very severe temperature-sensitive mutations into the Stt3 subunit is rather difficult, as the co-expression of the wild-type Stt3 subunit is necessary for cell culture.

In this study, I fused a new epitope tag (PA tag) to the 3'-end of the *ost4* genes in the genome DNA or 5′-end of the *stt3* genes in expression plasmids.

2.4.1 Effect of PA tag to STT3 protein on yeast growth

First of all, I confirmed that the addition of the PA tag to the STT3 subunit protein did not affect the growth of yeast by plasmid shuffling. I selected four mutants from previously reported growth phenotypes, R159A as temperature-sensitive, E350A, W517A, and D518A as lethal [35,40,46].

plasmid construction

The pPA-STT3 plasmid was constructed with a Gibson Assembly kit (NEB). The open reading frame of the *stt3* gene was amplified using genomic DNA from the yeast strain BY4741 as the PCR template. For the construction of pPA-STT3, the GPD promoter, the yeast Stt3 sequence, and the CYC1 terminator were assembled into pRS313. The GPD promoter and the CYC1 terminator were derived from pAG416-GPD-ccdB as the PCR template. pAG416GPD-ccdB was a gift from Susan Lindquist (Addgene plasmid # 14148; http://n2t.net/addgene:14148; RRID:Addgene_14148). Then, the DNA sequences corresponding to the PA tag, GVAMPGAEDDVV, and the spacer sequence, $(GGGGS)_2$, were inserted between the GPD promoter and the Stt3 sequence (Fig. 6A). An inverse PCR-based site-directed mutagenesis kit (SMK-101, TOYOBO) was used to generate single-point mutations to generate pPA-STT3(X).

plasmid* shuffling *and spotting plate assay

*Stt3*Δ cells bearing pRS316-STT3 encoding the wild-type *stt3* were transformed with pPA-STT3(X), encoding the *stt3* gene containing a single-point mutation X. The transformants were grown in SD medium lacking L-histidine until the OD_{600} reached 1. Collected cells were diluted in a 5-fold series. Aliquots (3 µL) of each dilution were spotted onto SD plates lacking L-histidine and those lacking L-histidine supplemented with 5-FOA, at a final concentration of 1 mg mL^{-1}. After incubations at 25, 30, and 37°C, cell growth was assessed.

The WT phenotype did not change with the addition of the PA tag to the STT3 protein (Fig. 6B). As reported for mutants, R159A was temperature-sensitive and E350A, W517A, D518A were lethal [35,40,46]. I decided that STT3 expressed with the addition of the PA tag did not significantly change the properties of OST function, and proceeded to the next experiments.

2.4.2 Purification of OST complex including Stt3 subunit protein expressed by plasmid

In vitro analysis required the mutated OST protein in addition to WT OST protein. Next, I tried to purify the OST complex from the yeast transformed a plasmid to verify if it was possible to purify WT, temperature-sensitive, and lethal mutants of STT3 proteins.

yeast strain

PCR-based methods were used to disrupt of yeast *ost6* gene, replacing *ost6* to *LEU2*. Correct gene knockout was confirmed by PCR and DNA sequencing. The pOST3 plasmids were constructed with a Gibson Assembly kit (NEB). The open reading frames of the *ost3*, the gene was amplified using genomic DNA from the yeast strain BY4741 as the PCR template. For the construction of pOST3, the DNA sequence encoding Ost3 was inserted into the multiple cloning site of pAG416-GPD-ccdB.

affinity purification of the yeast OST complex bearing the PA tag

The OST complex was purified from yeast strains as previously described, with modifications [34]. Yeast cells transformed with pPA-STT3(X) were grown in SD media lacking appropriate nutrients (-Ura and -His). Recovered yeast cells were lysed with glass beads, and microsome fractions were collected by ultracentrifugation at 100,000 × g. The membrane pellets were resuspended and dissolved in 20 mM Tris-HCl buffer, pH 7.5, 1.5% digitonin, 0.5 M NaCl, 1 mM $MgCl_2$, 1 mM $MnCl_2$, 1 mM EDTA, 1 mM phenylmethylsulfonyl fluoride, protease inhibitor cocktail (Roche), and 10% (v/v) glycerol. After 1 h incubation, the mixture was ultracentrifuged for 30 min at 100,000 × g, and the clarified supernatant was mixed with pre-washed anti-PA tag antibody beads (Fujifilm Wako Pure Chemicals) at 4°C overnight with gentle shaking. The affinity beads were collected by centrifugation and washed five times with 20 mM Tris-HCl buffer, pH 7.5, 0.1% digitonin, 150 mM NaCl, 1 mM $MgCl_2$, and 1 mM $MnCl_2$. Finally, the OST complex was eluted with the same buffer containing 0.1 mg mL^{-1} PA-tag peptide (Fujifilm Wako Pure Chemicals).

Affinity purification of the OST complexes containing mutations in the Stt3 subunit. The PA epitope tag sequence was inserted into the region encoding the N-terminus of

the Stt3 subunit via a 10-residue spacer sequence. The tagged Stt3 protein was expressed under the control of the constitutive GPD (glyceraldehyde 3-phosphate dehydrogenase) promoter from the expression plasmid, pPA-STT3. An Ost6-knockout strain (*ost6*Δ) was used as the host to prepare the Ost3-containing OST complex (referred to as OST[Ost3]). Deleterious effects caused by the absence of Ost6 were compensated by the extra expression of Ost3 from the pOST3 plasmid [35,47]. The purified samples contained bands corresponding to the subunits of STT3, OST1, WBP1, OST3, SWP1, and OST2, respectively (Fig. 6C). I confirmed that the OST complex can be purified by this method in temperature-sensitive and lethal mutants as well as in WT STT3.

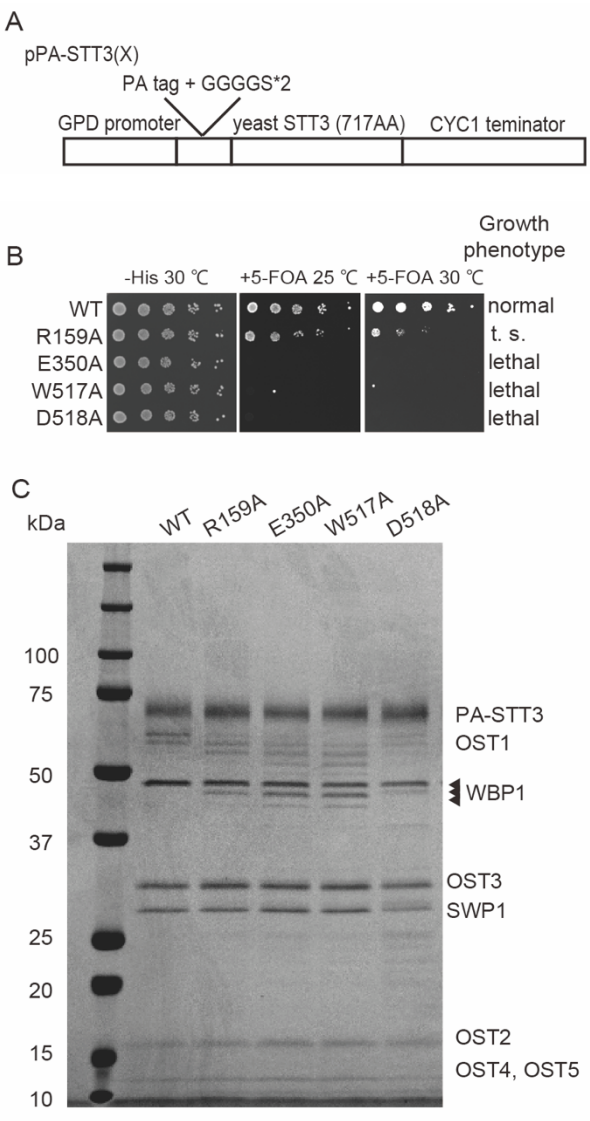

Figure 6. Effect on the cell growth and protein purification by point mutations of Stt3 subunit protein expressed by the plasmid.

A. Schematic representation of the gene construction for expression of the PA tag-fused Stt3 protein. The PA tag sequence, GVAMPGAEDDVV, is inserted at the N-terminus of the Stt3 protein *via* a 10-residue spacer sequence, $(GGGGS)_2$. Transcription is controlled by the GPD promoter and the CYC1 terminator. *B*. The yeast strains, *stt3*Δ-pRS316-STT3(WT)+pPA-STT3(X), where X denotes a mutation, were spotted on -His + 5-FOA plates. The growth of the colonies at three different temperatures was compared after 2 days 30 and 3 days 25˚C. 't.s.' stands for temperature-sensitive. The OST complex expressed in the cells was the mixed type of Ost3 and Ost6. *C*. CBB-stained gel image of the purified OST proteins. The triangles indicate the three bands corresponding to the non-, mono-, and diglycosylated forms of the Wbp1 subunit.

2.5 Check contamination of the yeast OST preparation

The epitope tag has a high affinity to a specific antibody and enables the preparation of the OST complex containing STT3 expressed by plasmid free from the native OST complex. I must confirm that the OST preparation with the mutated Stt3 subunit is not contaminated with the native OST complex containing the wild-type Stt3 subunit.

Preparation of FLAGstt3 yeast strain

The PCR-based method was used to create fusion to epitope tags (FLAG*stt3*). PCR fragments that contain the DNA sequences corresponding to the FLAG tag and the spacer sequence, $(GGGGS)_2$, were inserted before the Stt3 sequence, and a selectable marker *HygMX* was integrated into the yeast genome DNA by homologous recombination and selected strain based on antibiotic resistance. *HygMX* sequence was derived from pFA6a-6xGLY-3xFLAG-hphMX4 as the PCR template. pFA6a-6xGLY-3xFLAG-hphMX4 was a gift from Mark Hochstrasser (Addgene plasmid # 20755 ; http://n2t.net/addgene:20755 ; RRID:Addgene_20755) [48]. Correct insertion was confirmed by PCR and DNA sequencing. The N-terminal amino acid sequence fused to Stt3 is DYKDDDDK-$(GGGGS)_2$ (the FLAG epitope tag sequence followed by spacer sequence).

affinity purification of the yeast OST complex

Yeast cells (*ost6*Δ-FLAG*stt3*-pOST3) transformed with pPA-STT3(WT) were grown in SD media lacking appropriate nutrients (-Ura and -His). The materials containing FLAG-Stt3(WT) were immunoprecipitated from yeast cells expressing the chromosomal *stt3* gene using anti-FLAG affinity gel (A2220 Millipore). The materials absorbed were eluted with the SDS sample buffer. Separately, the OST complex containing PA-Stt3(WT) expressed from the plasmid was immunopurified from the same yeast cells as described above (chapter 2.4.1). The collected materials were separated on SDS-PAGE using gradient gels (10–20%). The proteins in the gels were transferred to Immobilon-P PVDF membranes (Millipore), probed with the indicated antibodies, and visualized by chemiluminescence with the SuperSignal West Femto Maximum Sensitivity Substrate (ThermoFisher). The anti-FLAG antibody(PM020 MBL) and anti-STT3 antiserum [39] were used at dilutions of 1:5000 and 1:1000, respectively. The peroxidase-conjugated anti-rabbit IgG antibody (NA934VS Amersham ECL) was used at a dilution of 1:12500. The chemiluminescent images were recorded with an LAS-3000 multicolor image analyzer (Fuji Photo Film).

I checked the incorporation of the wild-type Stt3 protein expressed from the chromosome into the OST sample preparations, considering the oligomeric interactions between the OST molecules [45]. I created a strain carrying an *stt3* gene in the chromosome with a FLAG epitope tag encoding sequence. The immunoprecipitated materials with the anti-FLAG antibody (FLAG-IP) and those with the anti-PA antibody (PA-IP) were analyzed by western blotting (Fig. 7). As a positive control experiment, the FLAG-IP sample was analyzed with the anti-FLAG antibody, indicating the presence of a single band (Fig. 7, lane 1). In contrast, the PA-IP sample contained no detectable bands with the anti-FLAG antibody (lane 2), even though much larger amounts of the OST complex protein were loaded to the lanes of PA-IP (lanes 2 and 4) than those of FLAG-IP (lanes 1 and 3). I concluded that the genome-derived Stt3 was virtually absent in the OST preparations purified with the PA-epitope tag.

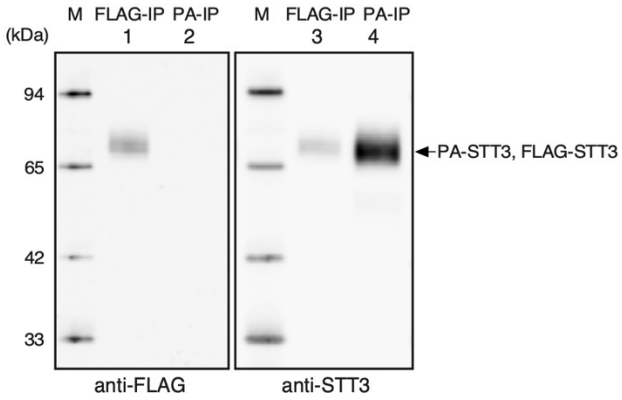

Figure 7. Check wild-type Stt3 incorporation into the OST preparation.

Immunoprecipitated samples with the anti-FLAG tag antibody (FLAG-IP) and the anti-PA tag antibody (PA-IP) were analyzed by western blotting. The wild-type Stt3 expressed from the chromosome was detected with the anti-FLAG antibody (left). The amounts of the Stt3 protein in the same sample volumes were measured with an anti-STT3 antibody (right).

2.6 In vitro assay

An in vitro experimental system was established to study the oligosaccharyl transfer and the FNG generation activity in purified OST (Fig. 8). Time course was measured using NVT9-tam as substrate peptide used previously in oligosaccharyl transfer activity experiments [49]. FNG generation activity was quantified by reacting with LLO in the absence of substrate peptide and then labeling the generated FNGs with 2-AP.

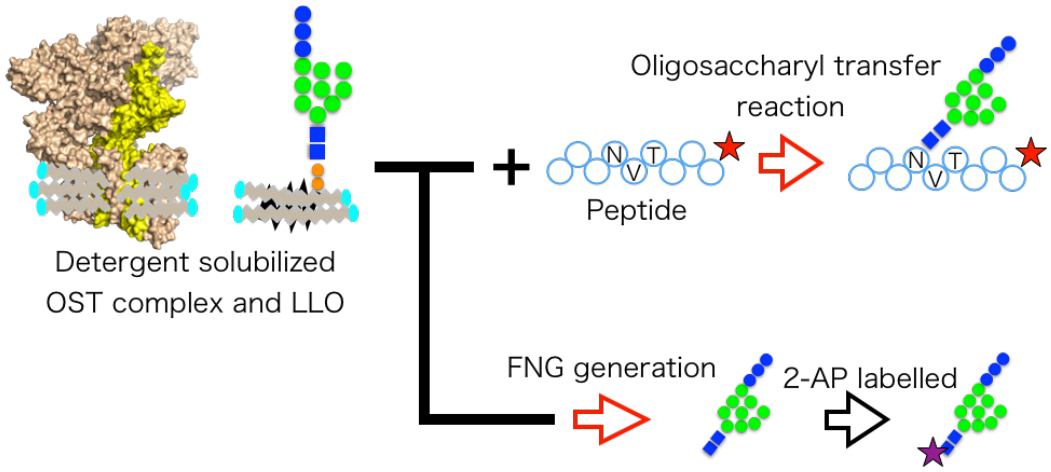

Figure 8. Scheme of in vitro assays.

Fluorescently labeled peptides were mixed with detergent-solubilized OST complex and LLOs for oligosaccharyl transfer reaction. After the reaction, N-glycosylated peptides were detected and quantified by UPLC equipment. Detergent-solubilized OST complex and LLOs were incubated without peptide for FNG generation. After the reaction, FNGs were labeled by 2-AP. 2-AP labeled oligosaccharides were detected and quantified by UPLC equipment.

extraction of LLO for in vitro assays

The yeast cells, strain BY4741, were grown in a 3-L flask containing 1-L synthetic complete medium at 30°C until the OD_{600} reached 10. Cells were collected and used for the extraction of LLO, as described previously [50]. To determine the amount of LLO, I used the endpoint assay and acid-hydrolysis methods. The endpoint assay measures the maximum amount of the N-glycosylated peptide produced by OST in the presence of an excess of the peptide substrate. The acid hydrolysis method measures the oligosaccharide released from LLO by acid hydrolysis. The LLO was hydrolyzed using 20 mM hydrochloride in a 2-propanol-water mixture (1:1, v/v) at 100°C for 30 min. After evaporation to dryness, the pellet was labeled with 2-AP (see below). The pyridylaminated oligosaccharides were separated by Infinity 1290 UPLC (Agilent) with an AdvanceBio Glycan Mapping column (Agilent) and quantified by an in-line fluorescence detector. Solvent A was 100 mM ammonium acetate buffer, pH 4.5, and solvent B was 100% acetonitrile. The column was equilibrated with 20% solvent A at a flow rate of 0.5 ml min^{-1}. A linear gradient of solvent A was applied from 20 to 40% over 8.5 min. Typically, 10-20 nmol of LLO was obtained from 10 grams of wet yeast cells from a 1-L culture.

pyridylamination of FNG

The reducing end of the oligosaccharides was derivatized with 2-aminopyridine (AP) as described previously, with some modifications [18]. The dried oligosaccharides were incubated with 20 µL of 2-AP in acetic acid at 80°C for 1 h. After the reaction, the mixture was incubated with 20 µL of dimethylamine borane reagent in acetic acid at 80°C for 30 min. The excess 2-AP was removed using a MonoFas silica gel spin column (GL Sciences). The spin column was washed with water and then preequilibrated twice with 800 µL of 100% acetonitrile before use. The sample solution was mixed with 460 µL of 100% acetonitrile and loaded onto the spin column. The column was washed twice with 800 µL of 95% (v/v) acetonitrile. Water was added to the column to elute the fluorescently labeled oligosaccharides.

2.6.1 Oligosaccharyl transfer assay

The oligosaccharyl transfer assay was performed using the fluorescent peptide substrate method [51,52]. The reaction mixture (total 10 µL) contained 1 µM yeast LLO, 1 µM substrate peptide, and 1 – 5 nM purified OST protein, in 20 mM Tris-HCl buffer, pH 7.5, 5 mM $MnCl_2$, 5 mM $MgCl_2$, and 0.1% (v/v) Triton X-100. The substrate peptides were labeled with a fluorescent dye, 5(6)-carboxytetramethylrhodamine (TAMRA) for detection (Table 4). The reaction mixture was incubated for the indicated time at 30°C. The reaction was stopped by the addition of 2 µL of 60 mM EDTA-NaOH, pH 8.0. The reaction products were separated by Infinity 1290 UPLC (Agilent) with an AdvanceBio Glycan Mapping column and quantified by an in-line fluorescence detector. Solvent A was 100 mM ammonium acetate buffer, pH 4.5, and solvent B was 100% acetonitrile. The column was equilibrated with 20% solvent A at a flow rate of 0.5 ml min^{-1}. A linear gradient of solvent A was applied from 20 to 41.5% over 16 min.

Table 4. Information of substrate peptide used in this section

Peptide name	Amino acid sequence[a]	Preparative method
NVT9-tam	Ac-AAYNVTKRK(TAMRA) -COOH	Chemical synthesis[b]

[a]The N-glycosylation sequon is underlined. TAMRA and tam denote the fluorescent dye, 5(6)-carboxytetramethylrhodamine. The peptide concentrations were determined by the absorbance at 555 nm, with an extinction coefficient of 90,000 M^{-1} cm^{-1}. The N-

terminal α-amino group is modified with an acetyl group (Ac-). The C-terminal α-carboxyl group is unmodified (-COOH).
[b]TAMRA is attached to the side-chain ε-amino group of the C-terminal lysine residue.

Oligosaccharyl transfer activity was measured in vitro using purified OST (Fig. 9). The peak was recovered and measured by MALDI-TOF-MS, and the observed MS was consistent with a 14-residue oligosaccharide chain-added peptide. The amounts of N-glycosylated peptide increased over time and reacted linearly up to 60 minutes.

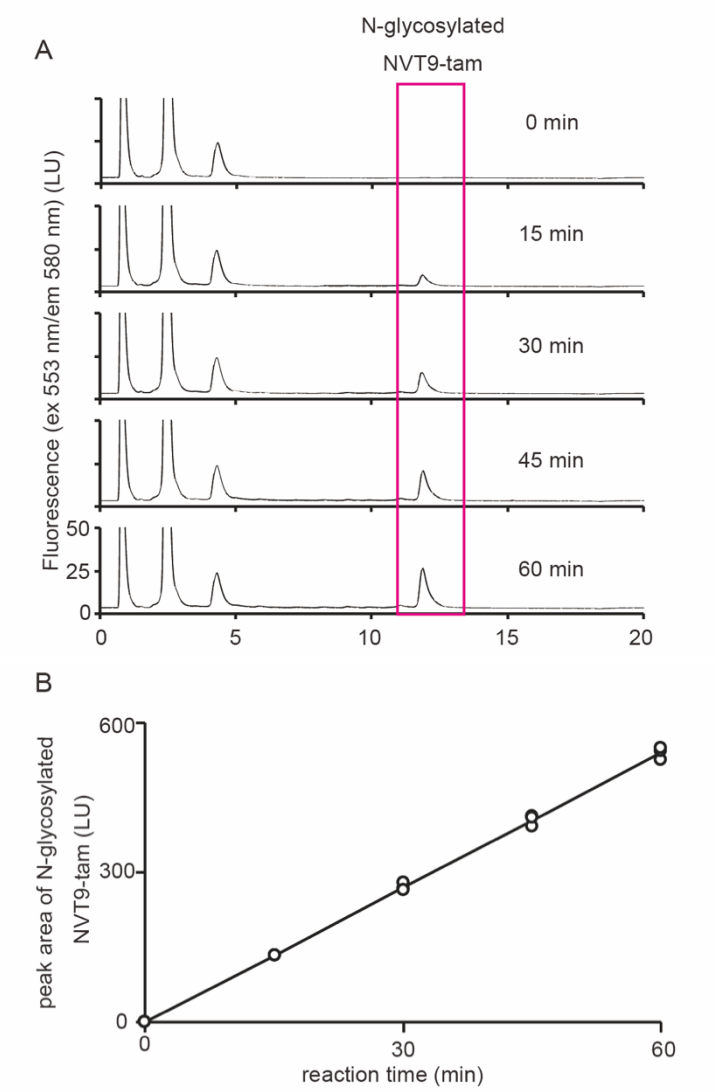

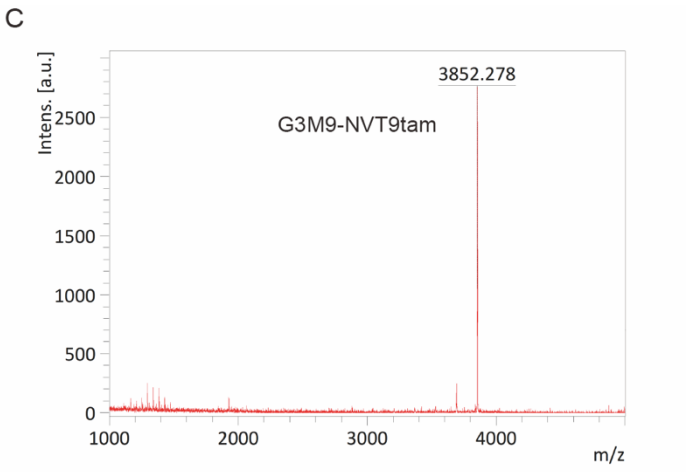

Figure 9. UPLC chromatograms for the oligosaccharyl transfer assay of the purified OST complexes and mass spectrum (MALDI-TOF) of N-glycosylated NVT9-tam peptides.

A. The original chromatogram data. *B*. The amounts of N-glycosylated NVT9-tam peptides generated by the OST protein were plotted versus reaction time each 0, 15, 30, 45, and 60 minutes. Triplicate measurements were performed for each time point. The straight line showed the approximate straight line generated from the plots. *C*. Observed molecular mass (m/z) was shown on the peak. The observed molecular mass was in good agreement with the calculated theoretical molecular mass of Glc3Man9GlcNAc2 - NVT9tam = 3854.54.

2.6.2 FNG generation assay

The purified OST complex was incubated with 1 μM LLO for indicated time at 30°C in a 100 μL reaction solution, containing 20 mM Tris-HCl, pH 7.5, 5 mM $MnCl_2$, 5 mM $MgCl_2$, and 0.1% (v/v) Triton X-100. The incubation time was longer (24 h) than that for the oligosaccharyl transfer assay (1 h) to compensate for the low hydrolytic activity. The reaction was terminated by the addition of 1 μL of 0.5 M EDTA-NaOH, pH 8.0. A 300 μL aliquot of ethanol was added, and the reaction solution was incubated for 15 min at 4°C. After centrifugation at 15,000 × g for 15 min, the supernatant was evaporated to dryness. The resultant pellet was labeled with 2-AP. The pyridylaminated oligosaccharides were separated by Infinity 1290 UPLC with an AdvanceBio Glycan Mapping column and quantified by an in-line fluorescence detector. Solvent A was 100 mM ammonium acetate buffer, pH 4.5, and solvent B was 100% acetonitrile. The

column was equilibrated with 20% solvent A at a flow rate of 0.5 ml min^{-1}. A linear gradient of solvent A was applied from 20 to 40% over 14 min.

The FNG-generating activity was measured in vitro using purified OST (Fig. 10). The peak was recovered and measured by MALDI-TOF-MS, and the observed MS was consistent with the addition of 2-AP to the 14 sugar. FNG increases in the test tube over time and reacted linearly up to 28 hours, indicated that the OST complex had not denatured or inactivated during 28 hours.

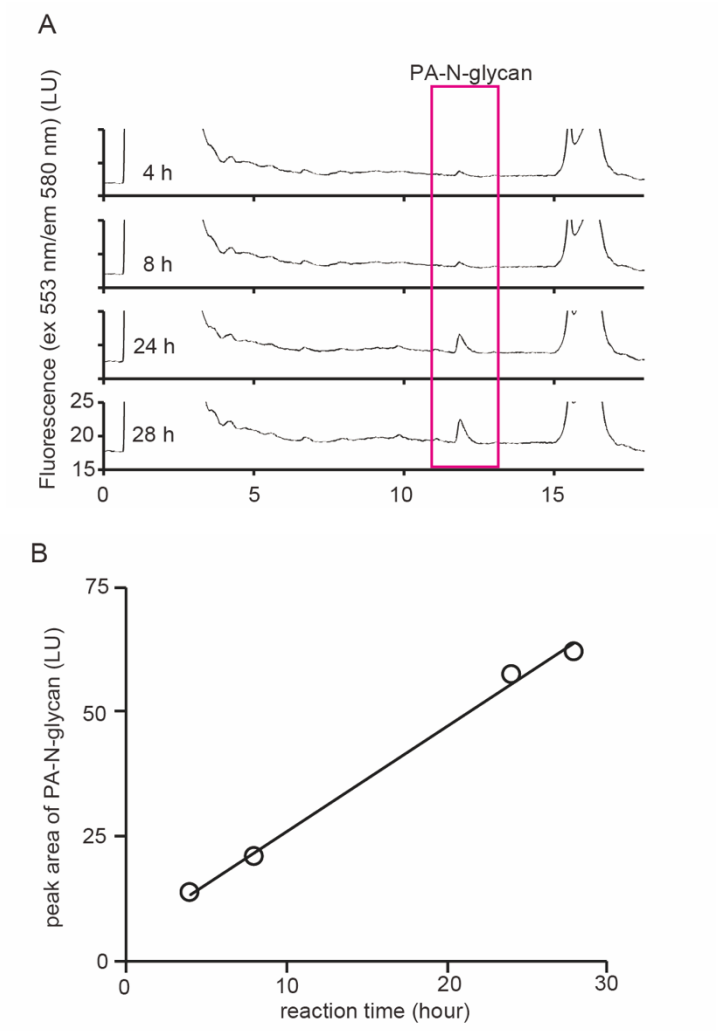

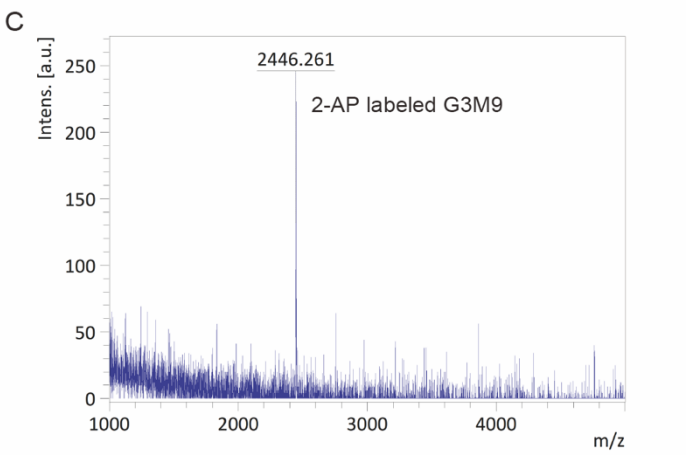

Figure 10. UPLC chromatograms for the FNG generation assay of the purified OST complexes and mass spectrum (MALDI-TOF) of 2-AP labeled G3M9GlcNac2 oligosaccharide.

A. The original chromatogram data. *B*. the amount of FNGs generated by the OST protein were plotted versus reaction time each 4, 8, 24, and 28 hours. The straight line showed the approximate straight line generated from the plots. Mass spectrum (MALDI-TOF) of 2-AP labeled oligosaccharide. *C*. Observed molecular mass (m/z) was shown on the peak. The observed molecular mass was in good agreement with the calculated theoretical molecular mass of 2-AP labeled Glc3Man9GlcNAc2 oligosaccharide = 2447.87.

2.7 Preparation of peptide substrate

Previous studies have used peptides with less than 10 residues due to their simplicity of synthesis and detection [11,35]. However, it is not known how OST interacts with the substrate peptide to place the sequon at the active center. Therefore, a developed assay is required using a peptide having a sufficient length, which is closer to the reaction in vivo. In this section, peptides were prepared by expressing substrate peptides as a glutathione S-transferase (GST)-fusion protein and after cleavage with proteases. Peptides were labeled with thiol-reactive TAMRA-maleimide fluorophore.

expression and purification

OST substrate peptides were expressed as a GST-fusion protein using the pGEX-6P-1 vector (GE Healthcare) as a template, pGEX6p-GST-C-NVT(X). X indicates the total number of amino acids in the peptide to be prepared. The transformed *Escherichia coli*

strain BL21(DE3) cells were grown using the ZYM-5052 medium at 30°C for 24 hours [53]. The cells were harvested by centrifugation at 5,000 × g at 4°C for 10 min and resuspended in 20 mM Tris-HCl, pH 8.0, containing 300 mM NaCl, 5 mM 1,4-dithiothreitol (DTT), and 10% (v/v) glycerol (buffer A). After disruption by sonication and centrifugation at 7,500 × g at 4°C for 10 min, the supernatant was centrifuged 50,000 × g at 4°C for 30 min. The supernatant loaded onto a Glutathione Sepharose 4B (GE Healthcare) column equilibrated with buffer A. The column was then washed with buffer A. After cleavage with 3C protease on the column overnight, the protein was eluted with buffer A.

The eluted materials were loaded on a COSMOSIL 5C18-AR-II reverse phase column (Nacalai Tesque, Kyoto, Japan) in trifluoroacetic acid (TFA) and acetonitrile. Solvent A was 0.1% (v:v) TFA, and Solvent B was 80% (v:v) acetonitrile, 0.1% (v:v) TFA. A linear gradient of solvent B was applied from 20% B to 60% B. The peaks were collected and dried in a SpeedVac concentrator (Thermo Savant).

Dry up samples were dissolved in water. The alpha-cyano-4-hydroxycinnamic acid was used as the matrix and dissolved at 10 mg/ml in 80% (v:v) acetonitrile, 0.1% (v:v) TFA. Equal volumes (0.5 µl each) of the sample and the matrix solution were mixed on a target plate and dried. MS spectra were acquired in the positive ion reflection mode, using a MALDI-TOF-mass spectrometer Autoflex (Bruker) for C-NVT-8 and C-NVT-18, and C-NVT28.

A fluorophore, carboxytetramethylrhodamine (TAMRA), was attached to the thiol group of the cysteine residue. Each peptide was dissolved in 100 mM HEPES buffer, pH 7.5. 10 mM 5,6-TAMRA-maleimide solution in dimethyl sulfoxide was added, and the solution was incubated overnight at room temperature. Modified peptides were purified by a COSMOSIL 5C18-AR-II reversed-phase column. The peak was collected, dried, and re-dissolved in water (Table 5). The concentration of the peptides was determined by the absorbance at 555 nm, with an extinction coefficient of 90,000 M^{-1} cm^{-1}.

Table 5. Information of substrate peptides used in this section

Peptide name	Amino acid sequence[a]	Preparative method
C(tam)-NVT8	NH_2-GPC(TAMRA)-YNVTK-COOH	Protein expression and chemical modification[b]
C(tam)-NVT9	NH_2-GPC(TAMRA)-SYNVTK-COOH	Protein expression and chemical modification[b]
C(tam)-NVT18	NH_2GPC(TAMRA) GAGGSYNVTKGAGGS-COOH	Protein expression and chemical modification[b]
C(tam)-NVT28	NH_2-GPC(TAMRA)-GAGGSGAGGSYNVTKGAGGSGAGGS-COOH	Protein expression and chemical modification[b]

[a]The N-glycosylation sequon is underlined. TAMRA and tam denote the fluorescent dye, 5(6)-carboxytetramethylrhodamine. The peptide concentrations were determined by the absorbance at 555 nm, with an extinction coefficient of 90,000 M^{-1} cm^{-1}. The N-terminal α-amino group is unmodified (NH_2-). The C-terminal α-carboxyl group is unmodified (-COOH).

[b]TAMRA is attached to the side-chain sulfhydryl group of the cysteine residue *via* the thiol-maleimide reaction.

oligosaccharyl transfer assay

The oligosaccharyl transfer assay was performed the same as described above (chapter 2.6.1).

The peptide expressed as a GST-fusion protein was further purified on a reverse-phase column. The fraction was measured the mass spectrum by MALDI-TOF-MS, which was almost the same as the theoretical molecular weight. The peptide was labeled with TAMRA-maleimide and used as a substrate peptide for oligosaccharide transfer activity. Oligosaccharyl transfer reaction was confirmed with all the prepared peptides (Fig. 11).

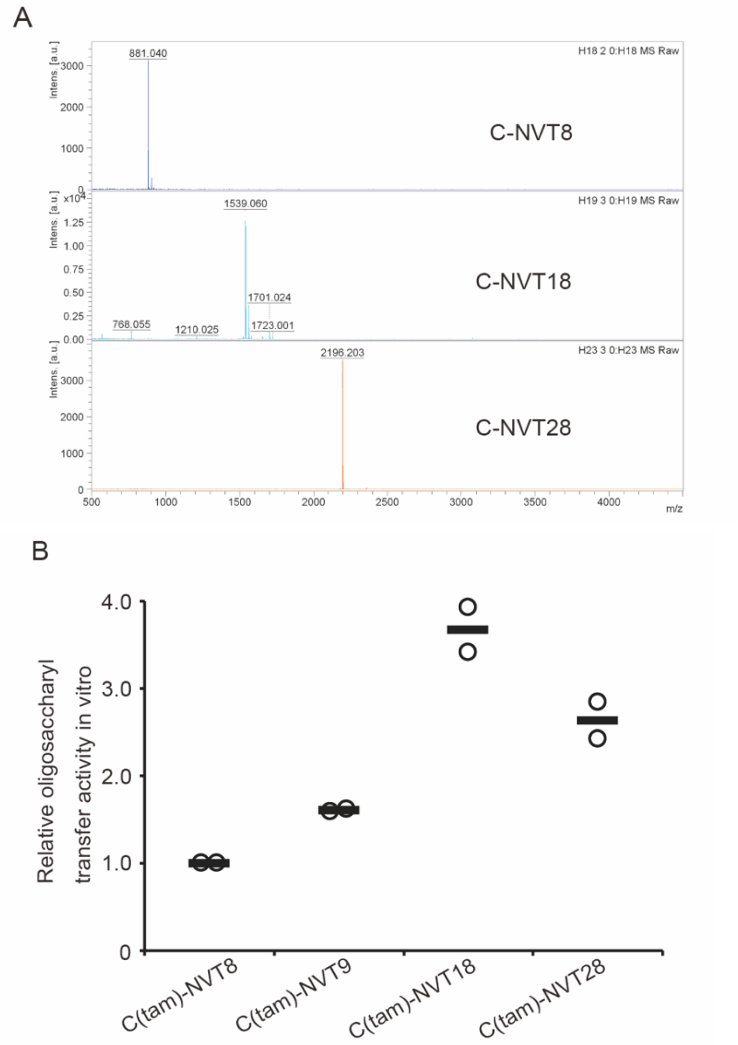

Figure 11. Mass spectra (MALDI-TOF) of HPLC purified peptides and the effects of the acceptor peptide on the enzymatic activities.

A. Observed molecular mass (m/z) was shown on the peak. The observed molecular mass was in good agreement with the theoretical molecular mass of each peptide C-NVT8 = 881.01, C-NVT18 = 1539.64, and C-NVT28 = 2198.20. *B*. In vitro oligosaccharyl transfer activities of the OST complexes using each peptide as acceptor. The activities of OST[Ost3, Ost4-PA] using C(tam)-NVT8 were set to 1. Open circles indicated the measurement of each trial. The bar heights indicate the mean values of duplicate measurements.

2.8 Effect of tag position

I need to make sure that the position of the tag does not change the substrate specificity for the peptide. Markerless strain *ost4*PA was prepared by a two-step method, plasmid integration followed by counter selection using 5-fluoroorotic acid [54]. The C-terminal amino acid sequence fused to Ost4 is $(GGGGS)_3$-GVAMPGAEDDVV (spacer sequence followed by the PA epitope) (Fig. 12).

creating ost4PA strain

The OST4 regions of pFA6a-OST4-PA-URA4MX6 are containing the entire *ost4* gene followed by GGGGS×3 linker and PA tag encoding sequence plus 250 bp (native promoter) and 250 bp (native terminator) at the 5' and 3' ends, respectively. URA4MX6 sequence was derived from pFA6a-ura4MX6 as the PCR template. pFA6a-ura4MX6 was a gift from Eishi Noguchi (Addgene plasmid # 49184 ; http://n2t.net/addgene:49184 ; RRID:Addgene_49184) [55]. pFA6a-OST4-PA-URA4MX6 was digested with the Xho1 restriction enzyme and the purified fragments were integrated into the yeast genome. Correct integration was confirmed by PCR and DNA sequencing. For the selection of yeast strain *ost4*PA, a fresh colony of pFA6a-OST4-PA-URA4MX6 integrated yeast strain was inoculated on a synthetic complete medium containing 5-FOA. Correct PA tag integration was confirmed by PCR and DNA sequencing.

The pOST6 plasmid was constructed with a Gibson Assembly kit (NEB). The open reading frame of the *ost6* gene was amplified using genomic DNA from the yeast strain BY4741 as the PCR template. For the construction of pOST6, the DNA sequence encoding Ost6 was inserted into the multiple cloning site of pAG416-GPD-ccdB.

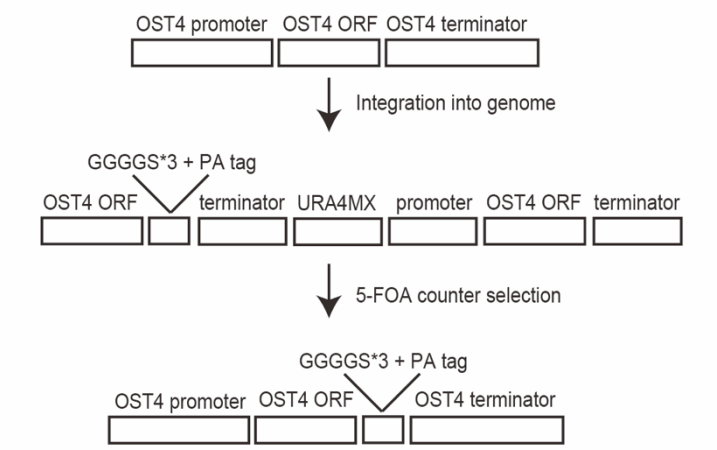

Figure 12. Integration of the PA tag encoding sequence into the yeast genome at OST4 gene locus.

The genomic *ost4* gene was C-terminally tagged with the PA epitope by two-step markerless gene replacement. pFA6a-OST4-PA-URA4MX6 plasmid integrated into the yeast genome. Target strain was selected by counter selection using 5-FOA, induced homologous recombination.

In addition to the OST complexes with the PA tag added to the Stt3 subunit, I prepared the OST complexes with the PA tag in the Ost4 subunit (Fig. 13). The tag was inserted at the region encoding the C-terminus of the *ost4* gene in the genome via a 15-residue spacer, (GGGGS)3. To prepare the yeast OST complexes containing the Ost3 subunit alone, the *ost6*Δ knockout strain was used. The resulting strain and OST complex are referred to as *ost6*Δ-*ost4*PA-pOST3 and OST[Ost3, Ost4-PA], respectively. The extra expression of Ost3 from the pOST3 plasmid reduces the deleterious effects caused by the absence of Ost6. In the same manner, I constructed the strain *ost3*Δ-*ost4*PA-pOST6 and purified the OST[Ost6, Ost4-PA] complex. As for the Ost3-containing OST complex, two constructs bearing the PA tag in different subunits are available. I assessed the influence of the tag position.

quantification of OST protein amounts

OST[Ost3, PA-STT3], [Ost3, Ost4-PA], and [Ost6, Ost4-PA] proteins were purified the same as described above (chapter 2.4.1). The eluted fractions were separated by SDS-PAGE using gradient gels (10–20%). Fluorescence measurement after western blotting (Fig. 13) was used for protein quantification. In the western blotting, proteins in

gels were transferred to Immobilon-FL PVDF membranes (Millipore). Anti-Wbp1 antiserum [39] was used as the primary antibody at a dilution of 1:5,000, and IRDye-labeled goat anti-rabbit IgG (LI-COR) was used as the secondary antibody at a dilution of 1:25,000. The fluorescence of the IRDye was measured by an Odyssey (LI-COR) imaging system.

oligosaccharyl transfer assay

The oligosaccharyl transfer assay was performed the same as described above with slight modification. The reaction mixture (total 10 μL) contained 1 μM yeast LLO, 5 μM substrate peptide, and 1 – 5 nM purified OST protein, in 20 mM Tris-HCl buffer, pH 7.5, 5 mM $MnCl_2$, 5 mM $MgCl_2$, and 0.1% (v/v) Triton X-100. The reaction mixture was incubated for 1 h at 30°C. A linear gradient of solvent A was applied from 25 to 57% over 8.5 min.

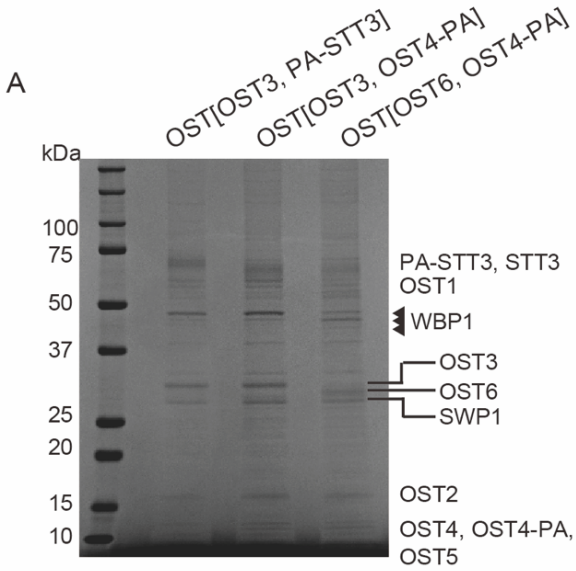

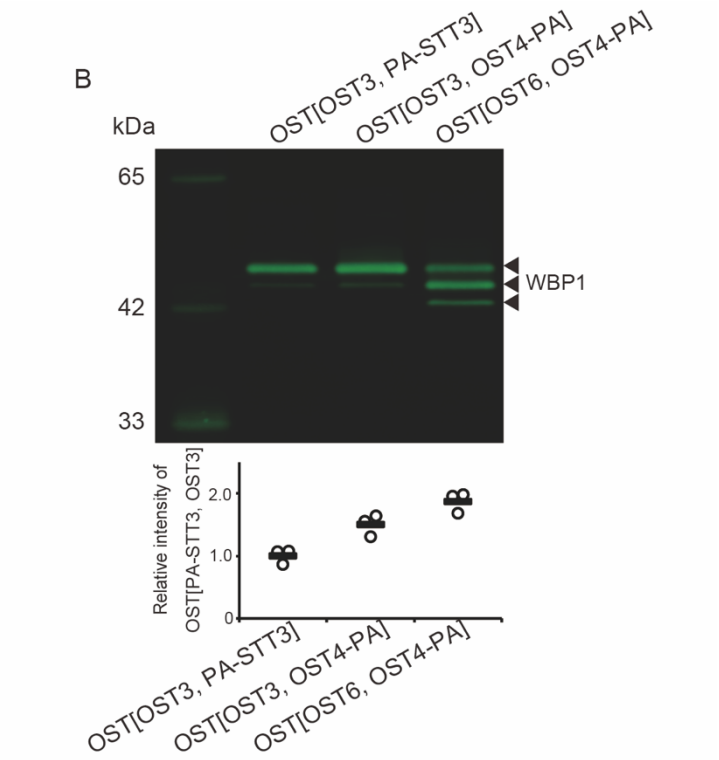

Figure 13. CBB-stained gel image of the purified OST proteins and the result of quantitative Western blotting.

A. The triangles indicate the three bands corresponding to the non-, mono-, and diglycosylated forms of the Wbp1 subunit. *B*. The relative amounts of the OST complexes were estimated by fluorescent Western blotting of the Wbp1 subunit and used to normalize the activities. The yield of the OST complex containing the WT Stt3 subunit with the PA tag is set to 1. Open circles indicated the measurement of each trial. The bars indicate the mean values of triplicate measurements.

Comparison of peptide substrates in the in vitro oligosaccharyl transfer assay. The OST[Ost3, PA-Stt3] and OST[Ost3, Ost4-PA] complexes had the same specific activities for the oligosaccharyl transfer activity with the four different peptides substrates, indicating the negligible effects of the insertion and position of the PA tag (Fig. 14). Additionally, the growth rates of the cells expressing the PA-tagged Ost4 and the PA-tagged Stt3 were the same as that of the wild-type cells. These results indicate that the added PA tag has no detectable harmful effects, and the PA-tagged Ost4 and Stt3 proteins are fully functional in vitro and in vivo.

Table 6. Information of substrate peptides used in this section

Peptide name	Amino acid sequence[a]	Preparative method
NVT9-tam	Ac-AAYNVTKRK(TAMRA) -COOH	Chemical synthesis[b]
tam-NVT9	(TAMRA)-GAYNVTAKR-COOH	Chemical synthesis
tam-NVT15	(TAMRA)-GAGGSYNVTKGAGGS-$CONH_2$	Chemical synthesis Reference [51]
C(tam)-NVT28	NH_2-GPC(TAMRA)-GAGGSGAGGSYNVTKGAGGSGAGGS-COOH	Protein expression and chemical modification[c]

[a]The N-glycosylation sequon is underlined. TAMRA and tam denote the fluorescent dye, 5(6)-carboxytetramethylrhodamine. The peptide concentrations were determined by the absorbance at 555 nm, with an extinction coefficient of 90,000 M^{-1} cm^{-1}. The N-terminal α-amino group is either unmodified (NH_2-), modified with an acetyl group (Ac-), or modified with the TAMRA group (TAMRA-). The C-terminal α-carboxyl group is either unmodified (-COOH) or modified with an amide group (-$CONH_2$).
[b]TAMRA is attached to the side-chain ε-amino group of the C-terminal lysine residue.
[c]TAMRA is attached to the side-chain sulfhydryl group of the cysteine residue *via* the thiol-maleimide reaction.

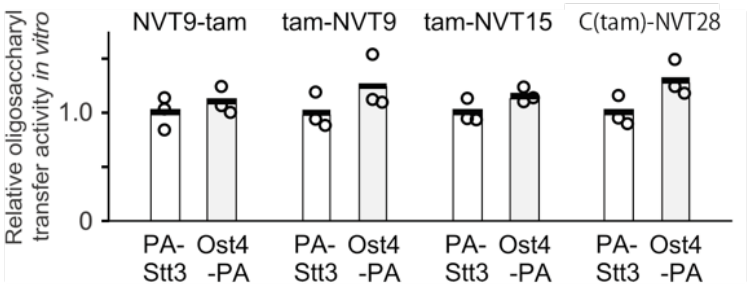

Figure 14. Effects of the epitope tag position on the oligosaccharyl transfer activity.
The PA tag was attached to either the N-terminus of the Stt3 subunit (PA-STT3) or the C-terminus of the Ost4 subunit (Ost4-PA). The two OST complexes contain the Ost3 subunit alone. The four peptides in Table 6 were used as acceptor peptide substrates. The relative amounts of the PA-tagged OST complexes were estimated by fluorescent western blotting of the Wbp1 subunit (Fig. 13) and used to normalize the activities. The activities of the OST with the tag in Stt3 were set to 1. Open circles indicated the measurement of each trial. The bar heights indicate the mean values of triplicate

measurements. For statistical analysis, Welch's t-test was applied for each peptide, but no significant differences were detected (p=0.44, 0.14, 0.26, and 0.073).

2.9 Kinetic parameters for peptide substrates

Enzymatic parameters were determined for the peptides used above section (Table 6). The oligosaccharyl transfer activities of the purified OST complexes were measured with LLO prepared from yeast cells as the oligosaccharide donor, and various peptides containing the sequon Asn-Val-Thr as the oligosaccharide acceptor. The glycopeptide products were separated by normal-phase UPLC and quantified with in-line fluorescence detection of the TAMRA dye attached to the peptide substrates. I designed four peptide substrates for the selection of a peptide substrate suitable for the oligosaccharyl transfer assay (Table 6). Kinetic parameters were determined using the OST[Ost3, PA-Stt3(WT)] complex. There were few differences in the maximal velocity Vm, whereas considerable variations in the Michaelis-Menten constant Km were observed (Fig. 15, Table 7). The 15-residue peptide substrate, tam-NVT15, had the smallest Km value, indicating the highest affinity for the OST[Ost3].

oligosaccharyl transfer assay

The oligosaccharyl transfer assay was performed the same as described above with slight modification. The reaction mixture (total 10 µL) contained 2 µM yeast LLO, 0.4 to 40 µM substrate peptide, and purified wild-type OST protein, in 20 mM Tris-HCl buffer, pH 7.5, 5 mM $MnCl_2$, 5 mM $MgCl_2$, and 0.1% (v/v) Triton X-100. The reaction mixture was incubated for 1 h at 30°C. A linear gradient of solvent A was applied from 25 to 57% over 8.5 min. Kinetic parameters for peptide substrates were determined by nonlinear least-squares fitting of the initial rates in the presence of 2 µM LLO to the Michaelis-Menten equation, using the program Kaleidagraph version 4.5.1 (Synergy Software).

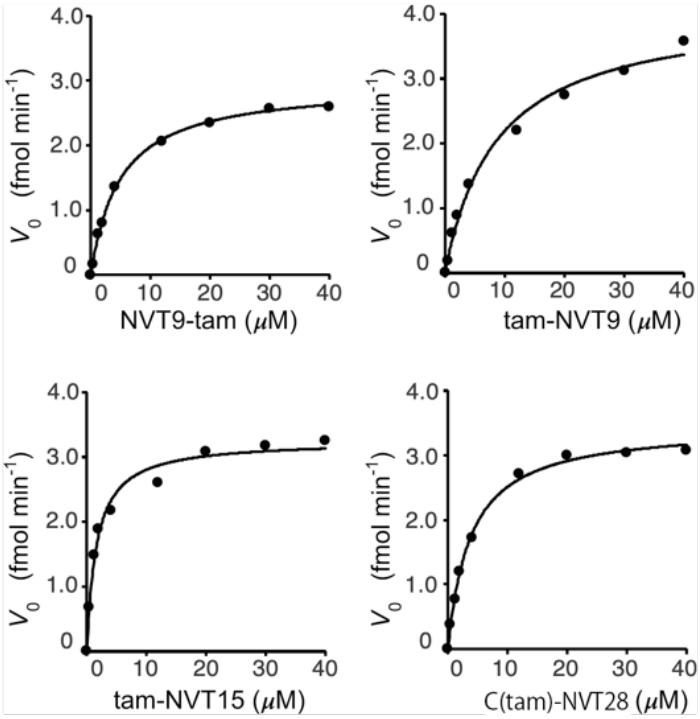

Figure 15. Kinetic parameter determinations with four different peptide substrates.

The peptide sequences are listed in Table 6. The initial rate of the oligosaccharyl transfer reaction (V_0) was plotted as a function of the peptide concentration. The maximum velocities (V_m) and substrate affinities (K_m) were derived by nonlinear regression to the Michaelis-Menten model (continuous lines). The kinetic constants are presented as best-fitted values with the standard errors in Table 7.

Table 7. Enzyme kinetic parameters of the oligosaccharyl transfer reaction[a] of the yeast OST complex[b] for various peptide substrates

peptide	K_m (μM)	V_m (fmol min^{-1})
NVT9-tam	4.9 ± 0.3	2.9 ± 0.04
tam-NVT9	8.8 ± 1.3	4.1 ± 0.19
tam-NVT15	1.6 ± 0.2	3.3 ± 0.09
C(tam)-NVT28	3.8 ± 0.3	3.5 ± 0.06

[a]In the presence of 2 μM LLO.

[b]OST[Ost3, PA-Stt3(WT)].

2.10 Discussion

In this chapter, I inserted the recently developed PA affinity tag into the region encoding the N-terminus in the mutated stt3 gene, under the control of the strong GPD promoter on the expression plasmid (Fig. 6). The co-expression of the wild-type *stt3* gene from the yeast genome maintains the growth of yeast cells, even if the mutation is lethal. The phenotype did not change with the addition of the PA tag to the STT3 protein.

In previous studies, affinity tags were introduced to the C-terminus of the Stt3 subunit [39,40,43,44]. Considering the membrane topology of the OST complex, the attachment to the N-terminus would be better, because the N-terminus is located on the opposite side of the ER membrane and is distant from the large luminal soluble domain, to avoid the risk of affecting the enzymatic activity. The 12-residue PA tag has a high affinity for the specific monoclonal antibody, NZ-1 [56], and the binding of the PA tag (Kd = 0.49 nM) is 10- to 100-fold stronger than those of other frequently used tags, including the FLAG tag (Kd = 100 nM) [57] and the 1D4 tag (Kd = 20 nM) [58]. The ultrahigh affinity withstands vigorous washing and hence ensures the minimal co-purification of the tag-less OST complex containing the wild-type Stt3 subunit (Fig. 7). It is important to check the impacts of the tag attachment on the enzymatic activities. Good linearities were obtained in two enzymatic reactions oligosaccharyl transfer and FNG generation using purified OST protein (Figs 9, 10). I compared the oligosaccharyl transfer activities between the two OST complexes containing the PA tag on the N-terminus of the Stt3 subunit and that on the C-terminus of the Ost4 subunit (Fig. 14). The results confirmed that the tag had no adverse effects on the enzymatic activity.

Experiments were performed using purified OSTs to determine how oligosaccharide transfer activity changes for peptides of different lengths (Fig. 11). I then determined the enzymatic parameters for the WT OST complex by changing the length of the peptide and the position of the fluorescent label (Fig. 15). I found that tam-NVT15 was a better acceptor substrate for the glycosylation of yeast OST than the shorter peptides used in previous reports (Table 7).

Chapter 3 Mutation study of yeast STT3 subunit

3.1 Determination of mutation sites

I decided to perform the mutation analysis of the OST to clarify if the FNG generation activity was just a side reaction of the oligosaccharyl transfer activity, and how the amount of intracellular FNG affects the growth of yeast. As mutational sites, I selected the two conserved short amino acid motifs, the first DXD motif from the two DXD motifs, and the DKM motif in the Stt3 subunit (Fig. 3) [39,59].

model building of the yeast OST-peptide complex

The three-dimensional structure model of the yeast OST-peptide complex was constructed, based on the cryo-EM structures of the yeast OST protein (PDB entry 6EZN) by reference to the *Archaeoglobus fulgidus* AglB-peptide complex (5GMY)(Fig. 16). AglB is a single-subunit OST in the archaeal domain. The figures were generated with the PyMOL program, version 2.3.2 (Schrödinger).

The DXD and the DKM motifs are located close to the bound peptide substrate in the three-dimensional structure and are involved in the recognition of the amino acid residues in or close to the sequon (Fig. 16). Glu^{45} is the first acidic residue of the DXD motif and is positioned to interact with the residue at position -1 of the sequon [35,59], whereas Asp^{47} is the second acidic residue in the same motif and coordinates to the divalent metal ion in the catalytic center. Asp^{583}, Lys^{586}, and Met^{590} are the three signature amino acid residues that constitute the DKM motif [39]. Asp^{583} and Lys^{586} are directly and Met^{590} is indirectly involved in the formation of the Ser/Thr-binding pocket, which recognizes the hydroxy amino acid residue at position +2 in the sequon [60].

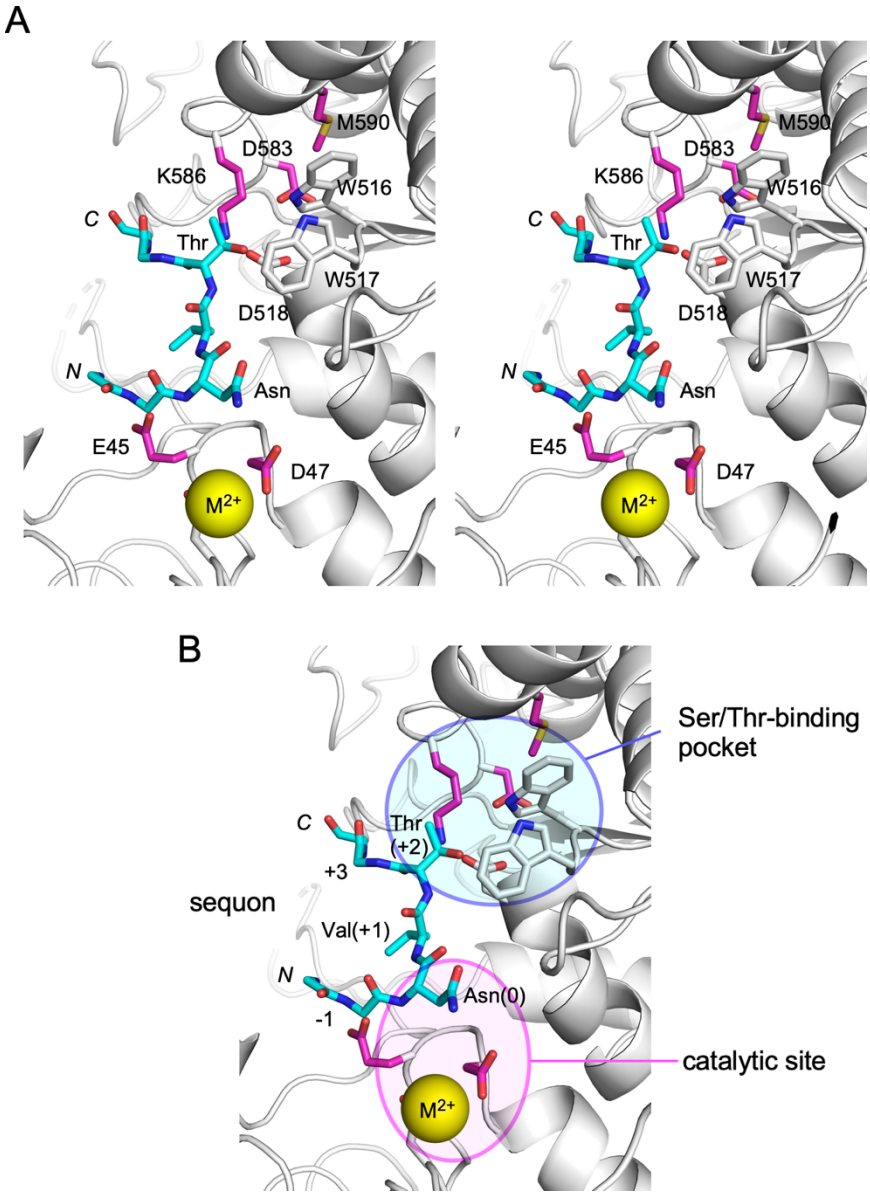

Figure 16. Point mutation sites in the three-dimensional structure of yeast OST.

A. Stereoview of the sequon binding site of the yeast Stt3 subunit (PDB entry 6EZN). The 7-residue peptide containing a sequon, Asn-Val-Thr, was adopted from the archaeal AglB-peptide complex (5GMY) after the superimposition of the AglB structure on the Stt3 structure and is shown in cyan. The side-chains of the residues mutated in this study are highlighted in magenta. *B*. Catalytic site around the bound divalent metal cation for the activation of the side-chain carboxamide group of the Asn residue at position 0 in the sequon. The Ser/Thr-binding pocket is formed by the residues in the WWDYG motif (Trp^{516}-Trp^{517}-Asp^{518}) and the DKM motif (Asp^{583}-Lys^{586}-Met^{590}) for the recognition of the side-chain hydroxyl group of the Ser/Thr residue at position +2 in the sequon.

3.2 Plasmid shuffling

The conserved amino acid in the motif was changed to alanine and plasmid shuffling was performed again. Because little attention has been paid to Glu^{45} in previous researches so far, I changed it to an amino acid other than alanine and proceed with the experiments.

strains and culture conditions

*Stt3*Δ cells bearing pRS316-STT3 encoding the wild-type *stt3* were transformed with p(RS313-)STT3(X), encoding the *stt3* gene containing a single-point mutation X. The transformants were grown in SD medium lacking L-histidine until the OD_{600} reached 1. Collected cells were diluted in a 5-fold series. Aliquots (3 μL) of each dilution were spotted onto SD plates lacking L-histidine and those lacking L-histidine supplemented with 5-FOA, at a final concentration of 1 mg mL^{-1}. After incubations at 25, 30, and 37°C for 3 days, cell growth was assessed.

The phenotypes of alanine mutation were different in each position even in the same conserved motif (Fig. 17). Alanine mutation result was the same as Fig. 5. In Glu^{45} mutation, aspartic acid with the same negative charge was normal, lysine with the positive charge was lethal, and uncharged glutamine was temperature-sensitive.

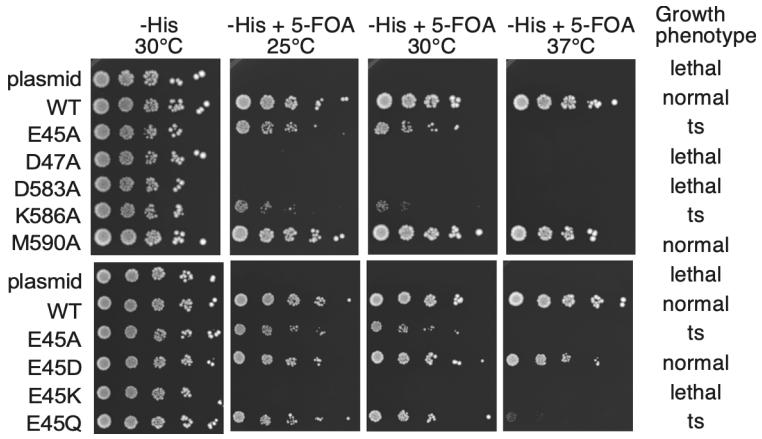

Figure 17. Spotting plate assay of yeast strains expressing mutated Stt3 subunits.

The yeast strains, *stt3*Δ-pRS316-STT3(WT)+p(RS313-)STT3(X), where X denotes a mutation, were spotted on -His + 5-FOA plates. The growth of the colonies at three

different temperatures was compared after 3 days. 'ts' stands for temperature-sensitive. The OST complex expressed in the cells was the mixed type of Ost3 and Ost6.

3.3 Protein purification

OST[Ost3, PA-STT3(X)] proteins were purified from the *ost6*Δ-pOST3+pPA-STT3(X) yeast strain. Yeast cells transformed with pPA-STT3(X) were grown in SD media lacking appropriate nutrients (-Ura and -His). Recovered yeast cells were lysed with glass beads, and microsome fractions were collected by ultracentrifugation at 100,000 × g. The membrane pellets were resuspended and dissolved in 20 mM Tris-HCl buffer, pH 7.5, 1.5% digitonin, 0.5 M NaCl, 1 mM $MgCl_2$, 1 mM $MnCl_2$, 1 mM EDTA, 1 mM phenylmethylsulfonyl fluoride, protease inhibitor cocktail, and 10% (v/v) glycerol. After 1 h incubation, the mixture was ultracentrifuged for 30 min at 100,000 × g, and the clarified supernatant was mixed with pre-washed anti-PA tag antibody beads at 4°C overnight with gentle shaking. The affinity beads were collected by centrifugation and washed five times with 20 mM Tris-HCl buffer, pH 7.5, 0.1% digitonin, 150 mM NaCl, 1 mM $MgCl_2$, and 1 mM $MnCl_2$. Finally, the OST complex was eluted with the same buffer containing 0.1 mg mL^{-1} PA-tag peptide.

The eluted fractions were separated by SDS-PAGE using gradient gels (10–20%). Staining with Coomassie Brilliant Blue (CBB) was used for protein quantification (Fig. 18). Even if a lethal mutation was introduced in the catalytic Stt3 subunit, the growth of the yeast host cells is supported by the native *stt3* gene in the genome. The E45K, D47A, and D583A mutations were lethal in the spotting plate assay (Fig. 17). The OST complexes containing Ost3 and the PA-tagged Stt3 subunit with a mutation (OST[Ost3, PA-Stt3(X)], where X denotes a mutation) were affinity-purified from digitonin-solubilized microsomal fractions and subjected to SDS-PAGE and CBB staining (Fig. 18). No bands were present in the sample from the yeast cells transformed with the empty plasmid, indicating the absence of the native OST complex without the PA tag in the purified samples. The Wbp1 subunit contains two potential N-glycosylation sites. The total amount of Wbp1 was used to estimate the relative amounts of the mutation-bearing OST complexes to the wild-type OST complex with the PA tag (Fig. 18B). The quantification of the other subunits is less useful, due to diffused, adjacent, or high-mobility bands. The protein yields were variable, but not lower than 30% of the wild-type OST with the PA tag.

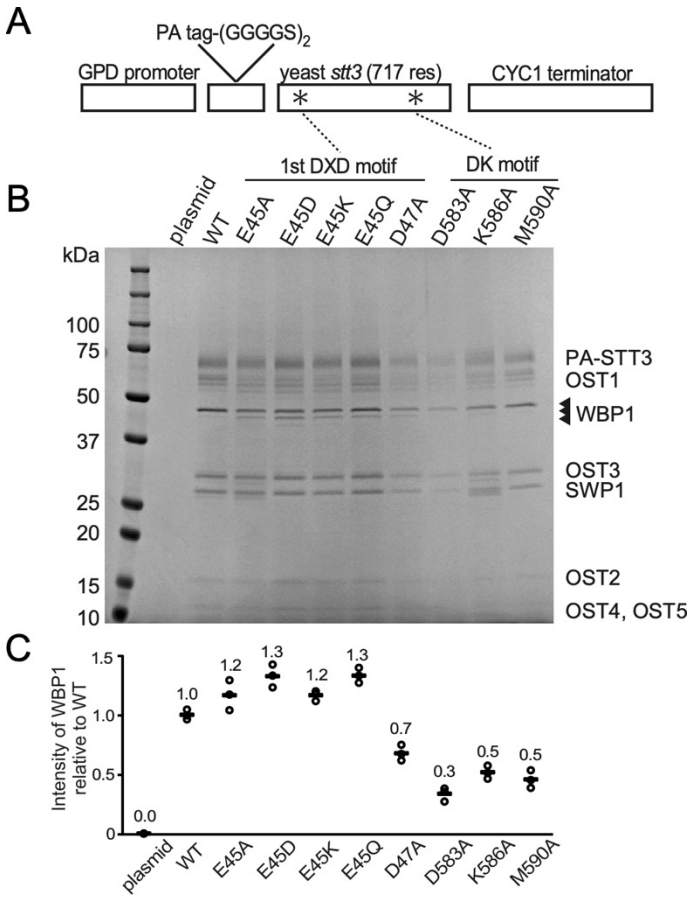

Figure 18. Purification of yeast OST complexes containing a point mutation in the Stt3 subunit.

A. Schematic representation of the gene construction for expression of the PA tag-fused Stt3 protein. The asterisks indicate the positions of the mutations. *B*. CBB-stained gel image of the purified OST proteins, OST[Ost3, PA-Stt3(X)], where X denotes a point mutation. The *ost6*Δ-pOST3 yeast strain was used as the host to prepare the OST complex containing the Ost3 subunit alone. The triangles indicate the three bands corresponding to the non-, mono-, and di-glycosylated forms of the Wbp1 subunit. *C*. Protein yields based on the Wbp1 band intensities. The yield of the OST complex containing the wild-type Stt3 subunit with the PA tag is set to 1. Open circles indicated the measurement of each trial. The bar heights indicate the mean values of triplicate measurements.

3.4 In vitro assay

Next, I assessed separately oligosaccharyl transfer activity and FNG generation activity using purified OST protein for the effects of single-point mutations in the Stt3 subunit on the enzymatic activities in vitro (Figs. 19, 20).

3.4.1 Oligosaccharyl transfer assay

I measured the oligosaccharyl transfer activity of the OST complexes bearing mutations in the Stt3 subunit, OST[Ost3, PA-Stt3(X)], using the tam-NVT15 peptide as the oligosaccharide acceptor. The raw chromatographic data are presented (Fig. 19).

oligosaccharyl transfer assay

The oligosaccharyl transfer assay was performed the same as described above. The reaction mixture (total 10 µL) contained 1 µM yeast LLO, 5 µM substrate peptide, and 1 – 5 nM purified OST protein, in 20 mM Tris-HCl buffer, pH 7.5, 5 mM $MnCl_2$, 5 mM $MgCl_2$, and 0.1% (v/v) Triton X-100. The reaction mixture was incubated for 1 h at 30°C. The reaction was stopped by the addition of 2 µL of 60 mM EDTA-NaOH, pH 8.0. The reaction products were separated by Infinity 1290 UPLC (Agilent) with an AdvanceBio Glycan Mapping column and quantified by an in-line fluorescence detector. Solvent A was 100 mM ammonium acetate buffer, pH 4.5, and solvent B was 100% acetonitrile. The column was equilibrated with 20% solvent A at a flow rate of 0.5 ml min^{-1}. A linear gradient of solvent A was applied from 25 to 57% over 8.5 min.

Table 8. Information of substrate peptide used in this section

Peptide name	Amino acid sequence[a]	Preparative method
tam-NVT15	(TAMRA)-GAGGSYNVTKGAGGS-$CONH_2$	Chemical synthesis Reference [51]

[a]The N-glycosylation sequon is underlined. TAMRA and tam denote the fluorescent dye, 5(6)-carboxytetramethylrhodamine. The peptide concentrations were determined by the absorbance at 555 nm, with an extinction coefficient of 90,000 M^{-1} cm^{-1}. The N-terminal α-amino group is modified with the TAMRA group (TAMRA-). The C-terminal α-carboxyl group is modified with an amide group (-$CONH_2$).

The peak of N-glycosylated tam-NVT15 peptide was not detected using empty plasmid fraction in oligosaccharyl transfer reaction (Fig. 19). Furthermore, the OST complex containing the lethal Stt3(D47A) subunit had no detectable oligosaccharyl transfer activity, confirming the negligible wild-type OST complex contamination in the final preparations. The oligosaccharyl transfer activity was calculated from the peak area.

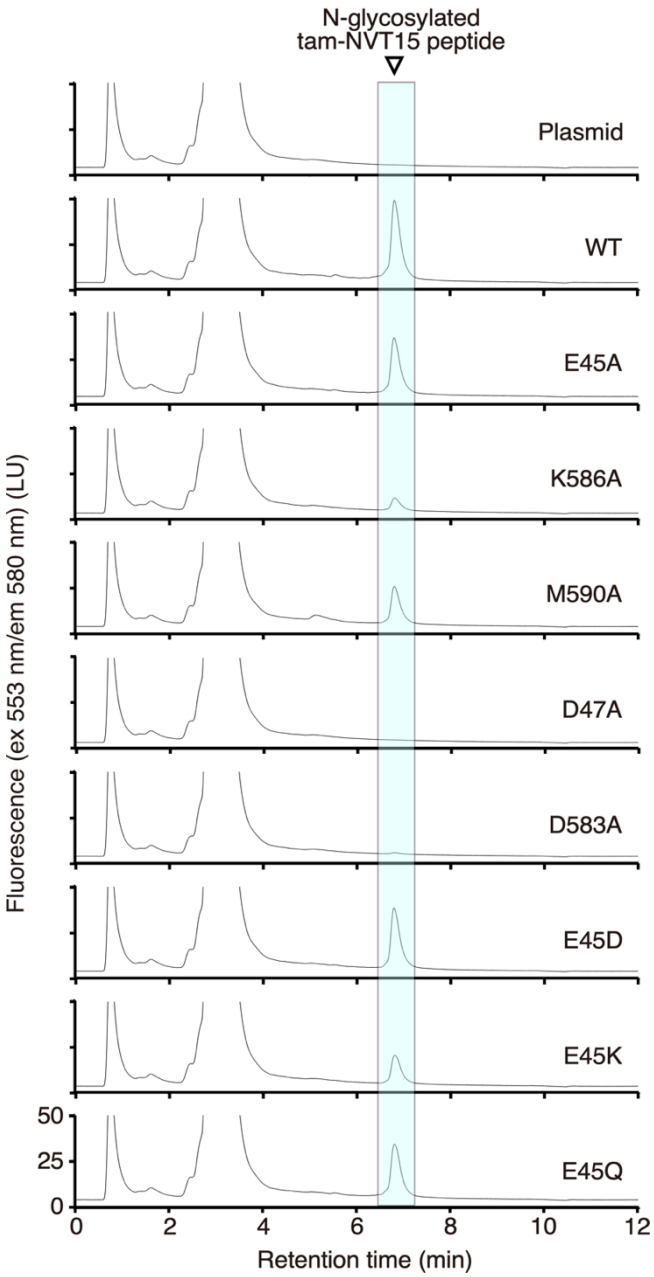

Figure 19. UPLC chromatograms for the oligosaccharyl transfer assay of the purified OST complexes containing a mutated Stt3 subunit.

The original chromatogram data. The fluorescence of the TAMRA label attached to the peptide was detected. The unreacted peptide was contained in the peak at 3 minutes. The N-glycosylated tam-NVT15 peptide was eluted for about 7 minutes. The cyan color peak area was calculated as the oligosaccharide transfer activity.

3.4.2 FNG generation assay

In parallel, I measured the FNG generation activity (i.e., the hydrolytic activity of LLO). The mutated OST complexes were incubated with LLO in the absence of the peptide substrate. The released N-oligosaccharide chain was recovered by ethanol precipitation and fluorescently labeled by pyridylamination. Normal-phase UPLC was used to separate and quantify the 2-AP-labeled N-oligosaccharides. Note that the incubation time was longer (24 h) than that for the oligosaccharyl transfer assay (1 h), to compensate for the low hydrolytic activity.

FNG generation assay

The purified OST complex was incubated with 1 μM LLO for 24 h at 30°C in a 100 μL reaction solution, containing 20 mM Tris-HCl, pH 7.5, 5 mM $MnCl_2$, 5 mM $MgCl_2$, and 0.1% (v/v) Triton X-100. The reaction was terminated by the addition of 1 μL of 0.5 M EDTA-NaOH, pH 8.0. A 300 μL aliquot of ethanol was added, and the reaction solution was incubated for 15 min at 4°C. After centrifugation at 15,000 × g for 15 min, the supernatant was evaporated to dryness. The dried oligosaccharides were incubated with 20 μL of 2-AP in acetic acid at 80°C for 1 h. After the reaction, the mixture was incubated with 20 μL of dimethylamine borane reagent in acetic acid at 80°C for 30 min. The excess 2-AP was removed using a MonoFas silica gel spin column. The spin column was washed with water and then preequilibrated twice with 800 μL of 100% acetonitrile before use. The sample solution was mixed with 460 μL of 100% acetonitrile and loaded onto the spin column. The column was washed twice with 800 μL of 95% (v/v) acetonitrile. Water was added to the column to elute the fluorescently labeled oligosaccharides. The pyridylaminated oligosaccharides were separated by Infinity 1290 UPLC with an AdvanceBio Glycan Mapping column and quantified by an in-line fluorescence detector. Solvent A was 100 mM ammonium acetate buffer, pH 4.5, and solvent B was 100% acetonitrile. The column was equilibrated with 20% solvent A

at a flow rate of 0.5 ml min^{-1}. A linear gradient of solvent A was applied from 20 to 40% over 14 min.

The peak of 2-Aminopyridine derivatives of oligosaccharides was not detected using empty plasmid, K586A, D47A, D583A fraction in the FNG generation reaction (Fig. 20). The FNG generation activity was calculated from the peak area.

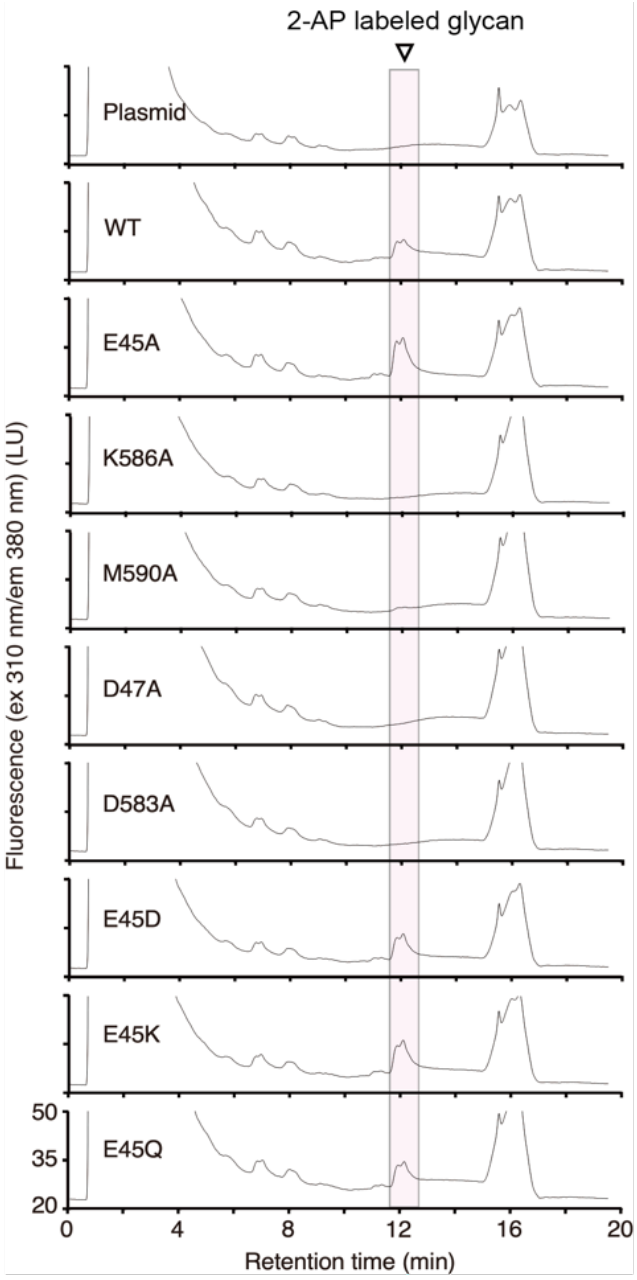

Figure 20. UPLC chromatograms for the FNG generation assay of the purified OST complexes containing a mutated Stt3 subunit.

The original chromatogram data. The fluorescence of the 2-AP label attached to the oligosaccharide was detected. The 2-AP labeled FNG was eluted for about 12 minutes. The pink color peak area was calculated as the FNG generation activity.

3.5 Comparison of mutated OST complex

A good correlation exists between the phenotypic level and the oligosaccharyl transfer activity (inset of Fig. 21A). There is no obvious correlation between the phenotypic level and the FNG generation activity (inset of Fig. 21B). I then analyzed the correlation between the two in vitro activities (Fig. 21C). If the hydrolysis of LLO were a simple side reaction, then the two activities would show a linear relationship (the dashed line in Fig. 21C). However, the amino acid replacements of Glu^{45} increased, and the amino acid replacements of Lys^{586} and Met^{590} decreased the FNG generation activity relative to the oligosaccharyl transfer activity. These results collectively indicate that the two activities can be uncoupled by single-point mutations in the catalytic Stt3 subunit.

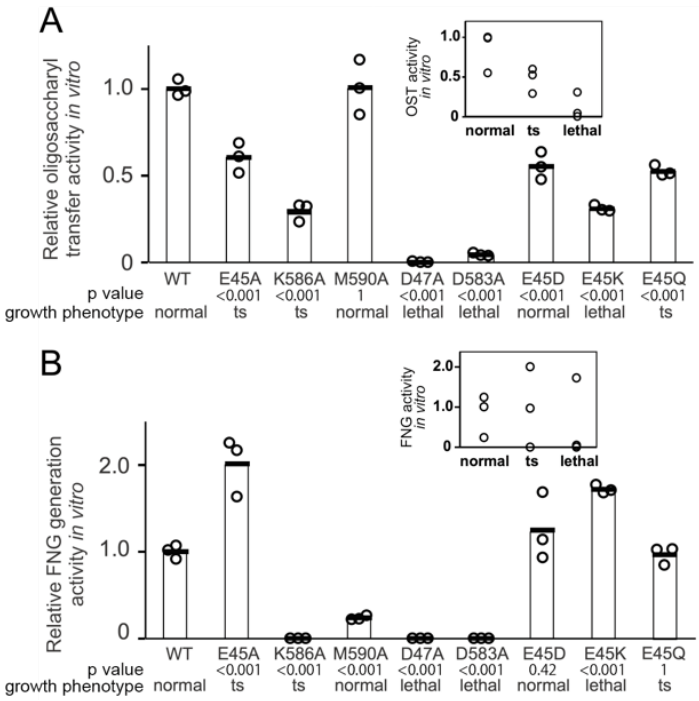

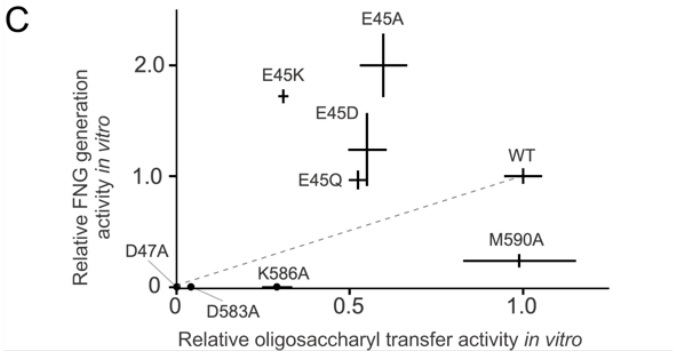

Figure 21. Oligosaccharyl transfer and FNG generation activities of the purified OST complexes containing a mutated Stt3 subunit.

A. Oligosaccharyl transfer activities of the purified OST[Ost3, PA-Stt3(X)] complexes, where X denotes a mutation. The peptide substrate was tam-NVT15. *B*. Free N-glycan generation activities of the purified OST[Ost3, PA-Stt3(X)] complexes. In *A* and *B*, the relative amounts of the OST complexes bearing mutations were determined by CBB staining, as shown in Fig. 18*B*, and used to normalize the two activities. Open circles indicated the measurement of each trial. The bar heights indicate the mean values of triplicate measurements, and the horizontal axes in the *insets* represent the growth phenotypic level scored with a 3-point ordinal scale. Statistical analyses were by one-way ANOVA followed by Dunnett post-hoc test between the wild type and mutants. *C*. Correlation plot between the oligosaccharyl transfer and FNG generation activities. The error bars represented the standard deviations. Data from *A* and *B*.

3.6 In vivo assay

Next, I assessed the effects of single-point mutations in the Stt3 subunit on the N-glycosylation and FNGs levels in yeast cells. In this section, I used a triple knockout strain (*stt3*Δ*png1*Δ*ams1*Δ) that expresses STT3 only from the pSTT3(X) plasmid using a native promoter. The D47A, D583A, and E45K mutants, within the mutants whose activity was examined in vitro, were excluded from the in vivo analysis because their phenotype was lethal.

yeast strains

PCR-based methods were used to disruption of yeast genes (*ams1*, *png1*), replacing *ams1* to *LEU2* and *png1* to *HygMX*. Correct gene knockout was confirmed by PCR and DNA sequencing.

For the selection of yeast strains containing pRS313-STT3(X) alone, a fresh colony of yeast strains, *stt3*Δ *png1*Δ *ams1*Δ containing pRS316-pSTT3 and pRS313-pSTT3(X) together, were inoculated on synthetic dropout medium (SD) containing 5-FOA and lacking L-histidine. Plates were incubated in an inverted position at 30°C. The series of operations was repeated three times.

3.6.1 N-glycosylation status

The N-glycosylation statuses of the carboxypeptidase Y (CPY) protein and the Wbp1 subunit were measured to assess the N-glycosylation level in vivo. The CPY protein contains four potential N-glycosylation sites and the Wbp1 subunit contains two potential sites. Since the N-glycans of the two glycoproteins are dispensable for the growth of yeast cells, they are useful markers for monitoring the N-glycosylation level in yeast cells.

determination of the N-glycosylation status of glycoproteins

The *stt3*Δ *png1*Δ *ams1*Δ-pSTT3(X) strains were cultured in YPD medium at the permissive temperature (30°C) until the OD_{600} reached 10. Ten OD_{600} units of cells were harvested and washed twice with 1 mL of water. The whole-cell lysate was prepared as described previously [61]. After centrifugation at 15,000 × g for 2 min, 6 μl aliquots of the supernatants were subjected to SDS-PAGE using gradient gels (10–20%). SDS sample buffer (50 mM Tris-HCl, pH 6.8, 1% (w/v) SDS, 10% (w/v) glycerol, 0.025% (w/v) bromophenol blue, and 100 mM DTT) was used for protein denaturation. The proteins in the gels were transferred to Immobilon-P PVDF membranes (Millipore), probed with the indicated antibodies, and visualized by chemiluminescence with the SuperSignal West Femto Maximum Sensitivity Substrate (ThermoFisher). The anti-carboxypeptidase Y (CPY) antibody (10A5B5 Abcam) and anti-Wbp1 antisera were used at dilutions of 1:10,000 and 1:5,000, respectively. The peroxidase-conjugated anti-mouse and anti-rabbit IgG antibodies were used at a dilution of 1:12,500. The chemiluminescent images were recorded with an LAS-3000 multicolor image analyzer (Fuji Photo Film). The average numbers of N-glycans attached to the CPY and the Wbp1 glycoproteins were calculated.

The CPY protein contains four potential N-glycosylation sites and the Wbp1 subunit contains two potential sites, as mentioned above, resulting in five and three bands on the SDS-PAGE gels, respectively (Fig. 22A and B). Note that all of the in vivo experiments were conducted using yeast strains expressing both the Ost3 and Ost6 subunits from the genome (*stt3*Δ *png1*Δ *ams1*Δ-pSTT3(X)), and the OST complexes (OST[Ost3+Ost6, Stt3(X)]) did not contain any tags. The sequons in the two proteins were almost fully modified in yeast cells expressing OSTs containing the wild-type Stt3 or the Stt3(M590A) with normal growth phenotypes, but only partially modified in yeast cells expressing OSTs containing temperature-sensitive mutations, Stt3(E45A) and Stt3(K586A). A good correlation exists between the oligosaccharyl transfer activities in vitro and the N-glycosylation statuses of CPY (Fig. 22A) and Wbp1 (Fig. 22B).

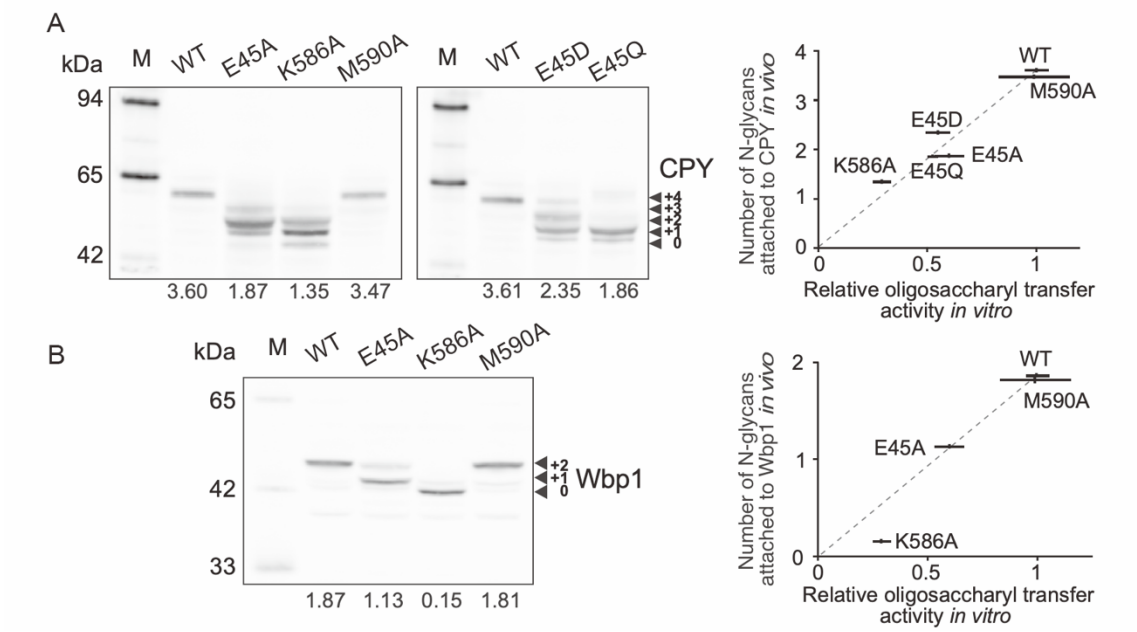

Figure 22. N-glycosylation levels in mutated Stt3-expressing cells.

A. N-glycosylation status of the CPY protein, determined by immunoblotting with the anti-CPY antibody. The figures below the gel images are the average numbers of N-glycans attached to the CPY protein. The whole-cell lysates were obtained from the *stt3*Δ *png1*Δ *ams1*Δ-pSTT3(X) yeast strains, where X denotes a mutation. The right panel shows the correlation plot between the N-glycosylation levels (the number of N-glycans) of CPY in cells and the oligosaccharyl transfer activities of the purified OST[Ost3, PA-Stt3(X)], adopted from Fig. 21*A*. *B*. N-glycosylation status of the Wbp1 subunit of the OST complex, determined by immunoblotting with the anti-Wbp1

antibody. The figures below the gel image are the average numbers of N-glycans attached to the Wbp1 protein. The whole-cell lysates were the same as those used in the CPY analyses. The right panel shows the correlation plot between the N-glycosylation levels (the number of N-glycans) of Wbp1 in cells and the oligosaccharyl transfer activities of the purified OST[Ost3, PA-Stt3(X)], adopted from Fig. 21*A*. In the correlation plots in *A* and *B*, the horizontal and vertical error bars represent the standard deviations from three independent experiments, except for six independent experiments for WT in *A*.

3.6.2 *Quantification of FNG in cells*

I then measured the amounts of FNGs generated by OST in cells. Since FNGs derived from OST are considered to be accumulated in the ER and cytoplasm, the whole cells were disrupted by ethanol precipitation and extracted FNG.

extraction and quantification of FNG

FNGs were extracted from yeast cells as previously described, with modifications [11]. Yeast strains, *stt3*Δ *png1*Δ *ams1*Δ-pSTT3(X), were cultured in YPD medium until the OD_{600} reached 10. One hundred OD_{600} units of cells were harvested and washed with phosphate-buffered saline (PBS). The washed cells were resuspended in 1 mL of lysis buffer (20 mM Tri-HCl, pH 7.5, 10 mM EDTA), and then 3 mL of ice-cold ethanol was added. The solution was vortexed for 10 sec and cooled on ice for 5 min, and this procedure was repeated 3 times. The homogenate was centrifuged at 7,500 × g for 15 min, and the supernatant was recovered and evaporated to dryness. The dried soluble oligosaccharide fraction was desalted on a column packed with AG 501-X8 ion exchange resin (Bio-Rad), and then on an InertSep GC column (GL Sciences). After elution, the dried pellets were labeled with 2-AP. The pyridylaminated FNGs were separated by Infinity 1290 UPLC with an AdvanceBio Glycan Mapping column and quantified by an in-line fluorescence detector. Solvent A was 100 mM ammonium acetate buffer, pH 4.5, and solvent B was 100% acetonitrile. The column was equilibrated with 20% solvent A at a flow rate of 0.5 ml min^{-1}. A linear gradient of solvent A was applied from 20 to 40% over 25 min.

As expected, a good correlation exists between the FNG generation activity of the purified mutated OSTs in vitro and the amounts of FNGs in the *stt3*Δ *png1*Δ *ams1*Δ-pSTT3(X) strains (Fig. 23). In particular, yeast cells expressing Stt3(E45A) accumulated much more OST-derived FNGs than yeast cells expressing Stt3(WT).

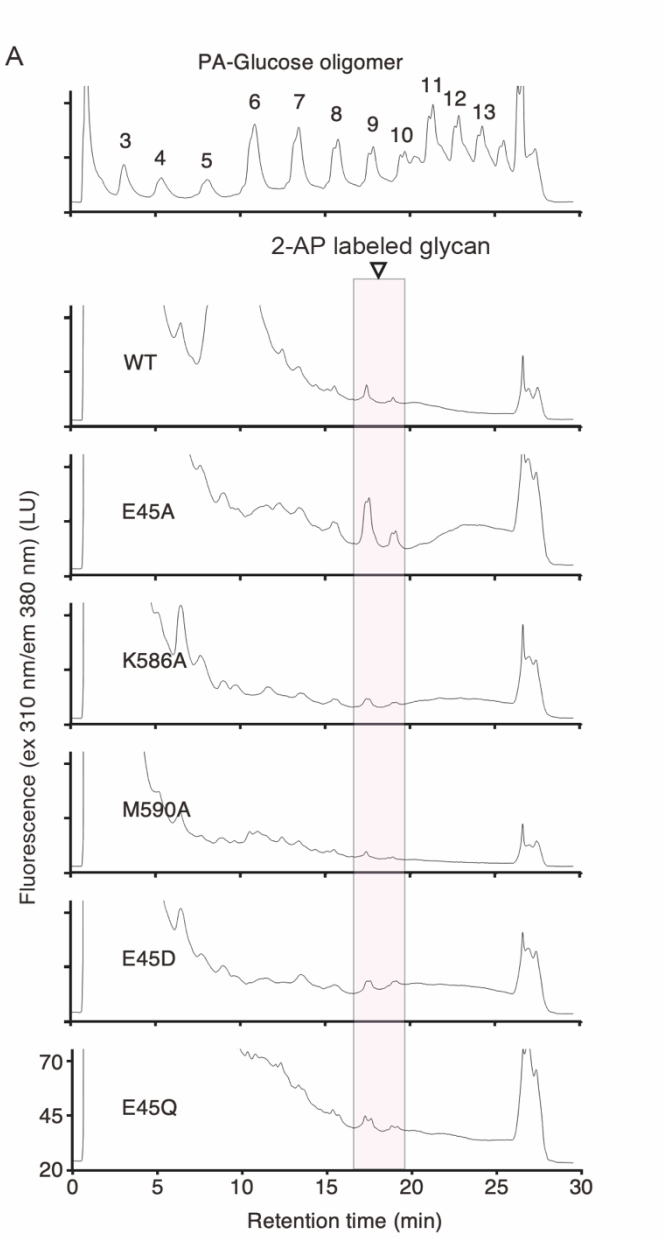

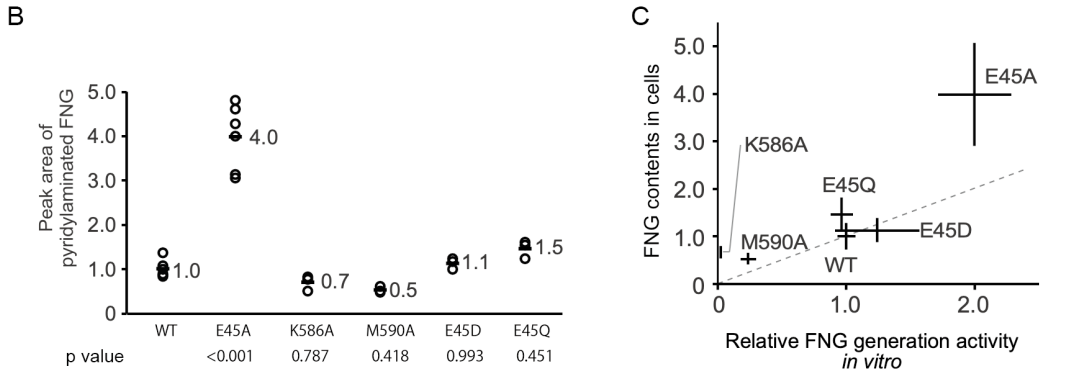

Figure 23. N-glycosylation and FNG levels in mutated Stt3-expressing cells. UPLC chromatograms for the quantitative estimation of FNG contents in yeast cells.

A. Original chromatogram data showed. *B*. Contents of FNG in yeast strains, *stt3*Δ *png1*Δ *ams1*Δ-pSTT3(X), relative to that in the yeast strain harboring pSTT3(WT). Open circles indicated the measurement of each trial. The bar heights indicate the mean values of triplicate measurements, except for six independent experiments for WT and E45A. Statistical analysis was by one-way ANOVA followed by Dunnett post-hoc test between the wild type and mutants. *C*. The panel shows the correlation plot between the FNGs contents in cells and the FNG generation activities of the purified OST[Ost3, PA-Stt3(X)], adopted from Fig. 21*B*. In the correlation plots in *C*, the horizontal and vertical error bars represent the standard deviations from three independent experiments, except for six independent experiments for WT and E45A.

3.6.3 Quantification of LLO in cells

The increase of FNG amount in Stt3(E45A) cells could be caused by the increased supply of LLO. Thus, I measured the LLO contents in whole cells. LLO was extracted from yeast cells and hydrolyzed to measure the amounts of released oligosaccharides.

extraction and quantification of LLO

The yeast strains, *stt3*Δ *png1*Δ *ams1*Δ-pSTT3(X), were grown in YPD medium at 30°C until the OD_{600} reached 10. One hundred OD_{600} units were harvested and washed twice with 4 mL of water. The extraction and acid hydrolysis of LLOs were performed as described above (chapter 2.6). After evaporation to dryness, the pellet was labeled with 2-AP. The pyridylaminated oligosaccharides were separated by Infinity 1290 UPLC with an AdvanceBio Glycan Mapping column and quantified by an in-line fluorescence detector. Solvent A was 100 mM ammonium acetate buffer, pH 4.5, and

solvent B was 100% acetonitrile. The column was equilibrated with 20% solvent A at a flow rate of 0.5 ml min^{-1}. A linear gradient of solvent A was applied from 20 to 40% over 8.5 min.

The amount of LLO was significantly accumulated in Stt3(K586A) cells (Fig. 24). The Stt3(E45A) cells had a similar amount of LLO relative to the wild-type, indicating that the excessive supply of LLO is not the reason for the elevated FNGs level in the Stt3(E45A)-expressing cells.

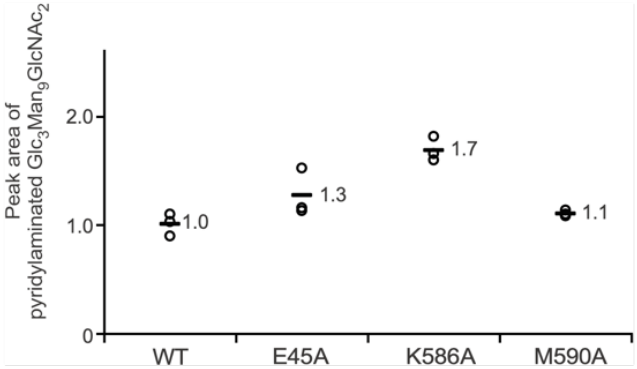

Figure 24. Amounts of LLO in yeast cells expressing mutated Stt3 subunits.
The yeast strains were *stt3*Δ *png1*Δ *ams1*Δ-pSTT3(X), where X denotes a mutation. The main component of the oligosaccharide moiety of LLO was the canonical 14-residue $Glc_3Man_9GlcNAc_2$ chain. Only small amounts of other LLO species with shorter oligosaccharide chains were detected. Open circles indicated the measurement of each trial. The bar heights indicate the mean values of triplicate measurements. Statistical analysis was by one-way ANOVA followed by Dunnett post-hoc test between the wild type and mutants. (adjusted p=0.101, <0.001, and 0.705)

3.6.4 Quantification of the total N-glycans from mannoproteins

I also measured the quantity of the total N-glycans attached to highly glycosylated mannoproteins expressed on the cell wall of yeast cells. The mannoproteins were recovered from the soluble fractions of cells after autoclave treatment, and the N-glycans were released from the mannoproteins by PNGase F digestion.

extraction and quantification of mannoproteins

The total N-glycans from mannoproteins were extracted from yeast strains as previously described, with modifications [11]. The yeast strains, *stt3*Δ *png1*Δ a*ms1*Δ-pSTT3(X), were grown in YPD medium (1% yeast extract, 2% peptone, and 2% glucose) at 30°C until the OD_{600} reached 10. Ten OD_{600} units of cells were harvested and washed twice with 4 mL of water. The washed cell pellets were resuspended in 1 mL of 10 mM sodium citrate buffer, pH 6.0, and autoclaved for 2 hours at 121°C. After centrifugation at 15,000 × g for 5 min, the supernatant was incubated with 3 mL of ethanol on ice for 15 min. The solution was centrifuged at 7,500 × g for 15 min, and the pellet was dried and dissolved in 200 µL of 0.1 M ammonium bicarbonate containing 50 units of PNGase F (New England Biolabs). The solution was incubated for 16 h at 37°C. After inactivation by heating for 5 min at 95°C, ethanol was added to the reaction mixture at a final volume percentage of 75%. After centrifugation at 15,000 × g for 15 min, the supernatant was dried and labeled with 2-AP. The pyridylaminated N-glycans were separated by Infinity 1290 UPLC with an AdvanceBio Glycan Mapping column and quantified by an in-line fluorescence detector. Solvent A was 100 mM ammonium acetate buffer, pH 4.5, and solvent B was 100% acetonitrile. The column was equilibrated with 28% solvent A, at a flow rate of 0.5 ml min^{-1}. A linear gradient of solvent A was applied from 28 to 40.8% over 19 min.

In contrast to the N-glycans on CPY and Wbp1, the total N-glycan amounts remained the same in yeast cells expressing the mutated Stt3 subunit (Fig. 25). This result indicates that the cell-wall integrity was maintained in yeast cells expressing these Stt3 mutants.

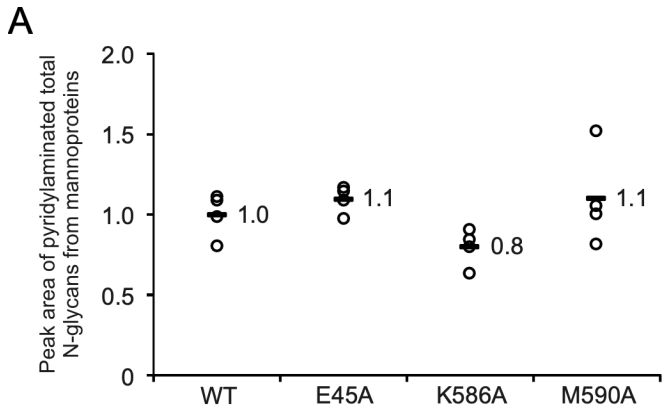

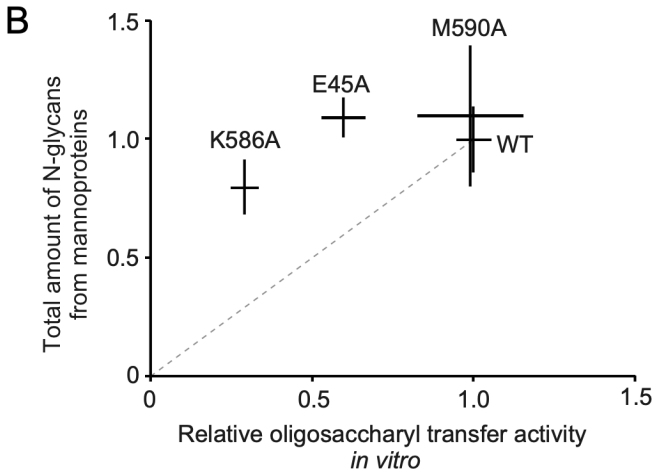

Figure 25. Amounts of total N-glycans attached to mannoproteins on a yeast cell wall.

A. Amounts of fluorescently labeled N-glycans recovered from cell wall fractions after PNGase F digestion. The yeast strains were *stt3*Δ *png1*Δ *ams1*Δ-pSTT3(X), where X denotes a mutation. Open circles indicated the measurement of each trial. The bar heights indicate the mean values of quadruplicate measurements. Statistical analysis was by one-way ANOVA followed by Dunnett post-hoc test between the wild type and mutants, but no significant differences were detected between WT and each of the mutants (p=0.799, 0.309, and 0.773). *B*. Correlation between the oligosaccharyl transfer activities of the purified OST[Ost3, PA-Stt3(X)] *in vitro,* and the amounts of total N-glycans on a yeast cell wall. The error bars represented the standard deviations. The dashed lines simply connect the origin and the point corresponding to WT, as a visual guide.

3.7 Peptide optimization for studies

For the OST of WT, enzymatic parameters showed that tam-NVT-15 is a good acceptor substrate (Table 7). However, it was not defined whether the oligosaccharyl transfer activity of in vivo was properly reflected only by the WT experiment. Therefore, I measured the activity of each peptide with STT3 mutants to see if they reflected their glycosylation activity in vivo.

oligosaccharyl transfer assay

The oligosaccharyl transfer assay was performed the same as described above (chapter 3.4.1).

The changes in the oligosaccharyl transfer activity in vitro by mutations are well correlated with the changes in the N-glycosylation level in cells (i.e., the number of N-glycans attached to CPY) induced by mutation (Fig. 26). However, the K586A mutant showed different oligosaccharyl transfer activities not only the length of the peptide but also the position of the TAMRA label.

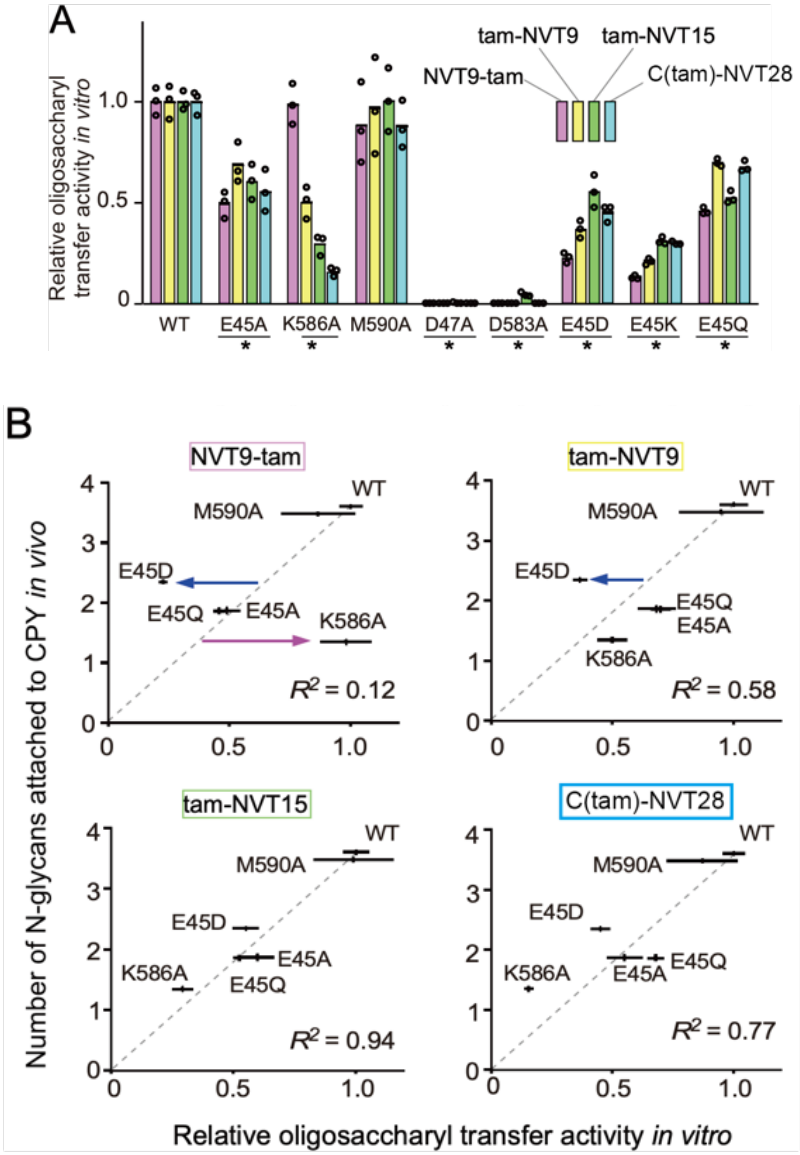

Figure 26. Correlation plots for the quality evaluation of peptide substrates.

A. Oligosaccharyl transfer activities of the OST[Ost3, PA-Stt3(X)] complexes, where X denotes a mutation, relative to those of the OST[Ost3, PA-Stt3(WT)] complex. The four peptides listed in Table 6 were used as acceptor substrates. Open circles indicated

the measurement of each trial. The bar heights indicate the mean values of triplicate measurements. Statistical analyses were by one-way ANOVA followed by Dunnett post-hoc test between the wild type and mutants. *adjusted $p < 0.05$. *B*. Correlation plots. The horizontal axis represents the oligosaccharyl transfer activity *in vitro* taken from *A*, and the vertical axis represents the N-glycosylation status of CPY taken from Fig. 22. The D47A, D583A, and E45K mutants were excluded because their phenotype was lethal and did not quantify the CPY glycosylation level. Note that the plot with tam-NVT15 is identical to the correlation plot in the *inset* of Fig. 22. The square of the correlation coefficient, R^2, is shown for each plot. The dashed lines simply connect the origin and the point corresponding to WT as a visual guide and are not the regression lines. The magenta and blue horizontal arrows indicate the outlier data points (see text).

3.8 Conclusion of mutation study

The data in Figs. 21, 22, and 23 are replotted from the standpoint of the individual mutants (Fig. 27).

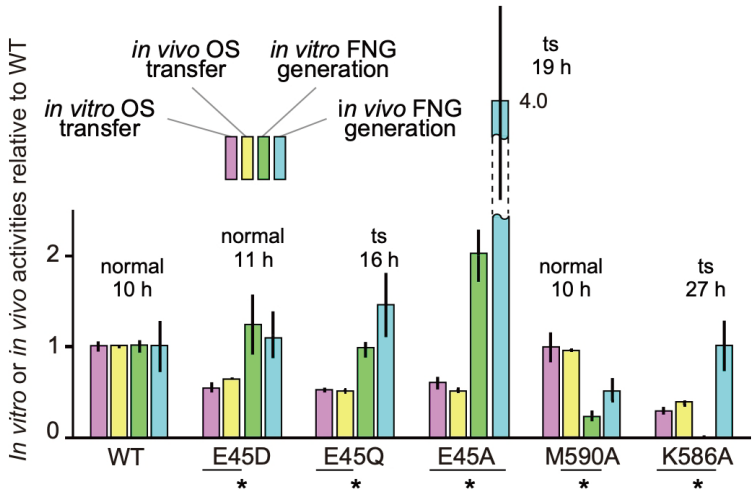

Figure 27. Comparison of the two *in vitro* and two *in vivo* activities for each of the OST complexes containing a mutated Stt3 subunit.

The *in vitro* data were obtained with the purified OST[Ost3, PA-Stt3(X)] proteins, whereas the *in vivo* data were obtained with the yeast strains *stt3*Δ *png1*Δ *ams1*Δ-pSTT3(X), where X denotes a mutation. These data are redisplayed from Figs. 21, 22, and 23 for a detailed comparison. Statistical analyses were by one-way ANOVA followed by Dunnett post-hoc test between the wild type and mutants. *adjusted p <

0.05. The growth phenotype and the time required to reach OD_{600} 10 from 0.2 in the YPD medium at 30°C are shown.

3.9 Discussion

Cell growth spotting assays have been used for mutational analyses of the yeast OST, based on the fact that N-glycosylation is essential for the survival and growth of yeast cells. The problem with these assays is that the dysfunction of the OST results in a simple growth phenotype, either lethal or temperature-sensitive. Moreover, the OST catalyzes the hydrolysis of the oligosaccharide donor, LLO, to release free N-glycans (FNGs) into the ER lumen. Although the physiological significance of the FNGs generated in the ER remains elusive, the functional modulation of the two activities in yeast cells could have diverse influences, eventually leading to an unpredictable growth phenotype. Thus, independent assessments of the two activities are desirable, using purified enzyme samples in vitro.

I selected amino acid residues in the first DXD motif (Glu^{45}-Asp^{47}) and the DKM motif (Asp^{583}-Lys^{586}-Met^{590}) in the Stt3 sequence as mutational sites (Fig. 16) [39]. These residues are positioned close to the peptide substrates in the bound state [34,35]. I purified the OST complexes containing the PA-tagged wild-type and mutated Stt3 subunits, OST[Ost3, PA-Stt3(WT or X)], and measured their oligosaccharyl transfer and FNG generation activities in the presence and absence of the peptide substrates (Fig. 21). I also determined the growth phenotypes of the mutated yeast strains (*stt3*Δ-pSTT3(X)) (Fig. 17). Among them, I selected the Stt3 mutants with temperature-sensitive and normal growth phenotypes for further in vivo studies. The *stt3*Δ *png1*Δ *ams1*Δ-pSTT3(X) strains were cultured to stationary phase in YPD medium at a permissive temperature (30°C) until the OD600 reached 10. I measured the N-glycosylation statuses of the CPY and Wbp1 glycoproteins in vivo (Fig. 22). CPY (carboxypeptidase Y) is a hydrolytic enzyme that catalyzes the release of amino acid residues from the C-terminus of peptides in the vacuole. CPY is a soluble glycoprotein containing four N-glycosylation sites. Wbp1 is one of the eight subunits of the OST, with a single-spanning transmembrane helix and a large N-terminal soluble domain on the luminal side. The soluble domain contains two N-glycosylation sites. I also measured the FNGs (Fig. 23), LLO (Fig. 24) contents in cells, and the total amounts of N-glycans attached to the cell-wall mannoproteins (Fig. 25).

Considering these results, I gained new insights as follows.

Firstly, the two activities of the OST can be uncoupled by single-point mutations in the Stt3 subunit. The replacements of Glu^{45} by Ala, Asp, Gln, and Lys enhanced the FNG generation activity relative to the oligosaccharyl transfer activity, and conversely, the replacements of Lys^{586} and Met^{590} by Ala suppressed the FNG generation activity (Fig. 21). Lys^{586} and Met^{590} are distant from the catalytic center formed around the divalent metal ion (Fig. 16). Interestingly, the LLO hydrolytic activity can be manipulated by modulating the peptide binding mode remotely.

Secondly, under physiological conditions, the sequons are embedded in long, unfolded polypeptide chains in the co-translational mode or conformationally restricted, yet flexible segments of folded polypeptides in the post-translational mode of the oligosaccharyl transfer reaction. In the oligosaccharyl transfer assays in vitro, short peptides up to 10 residues have conventionally been used. Thus, the use of peptides longer than 10 residues might be better in in-vitro assays, to obtain a more realistic assessment of the OST activity inside the cells. I used the correlative relationship between the oligosaccharyl transfer activity in vitro and the N-glycosylation level of glycoproteins in vivo as an evaluating criterion. Figure 26 shows the correlation plots for each of the four peptide substrates. Each point in the plots represents the data from a different mutation in the Stt3 subunit (Fig. 26A). With all data points considered, the 15-residue tam-NVT15 peptide shows the best correlation between the in vitro and in vivo activities (Fig. 26B). Therefore, I used this peptide in the subsequent oligosaccharyl transfer assays. A closer look at the data revealed some exceptions (the magenta and blue horizontal arrows in Fig. 26B). These exceptional preferences may be attributable to unwanted interactions of the positively charged, hydrophobic TAMRA dye with the mutation sites in the OST complex. This unexpected finding advises us to pay careful attention to the peptide substrate design.

Finally, the data in Figs. 21, 22, and 23 are replotted from the standpoint of the individual mutants, for a more detailed discussion (Fig. 27). The five Stt3 mutants in Fig. 27 have a normal or temperature-sensitive phenotype. Even if the N-glycosylation level of CPY is retained to an extent of at least 30% of that in the wild-type cells, yeast cells can survive and grow at the permissive temperature, 30°C. In the Stt3(E45Q) and Stt3(E45A) cells, the contents of FNGs generated by OST increased 1.5-fold and 4-fold, respectively, suggesting that the high FNG levels formed in the ER lumen have no

adverse effects on yeast cell growth. In Stt3(M590A) cells, the content of FNGs generated by OST decreased by 50%. The fact that the Stt3(M590A) strain has a normal growth phenotype indicates that a decrease in the FNG level in cells down to 50% is tolerable for yeast cell growth. These results are consistent with the previous report [11]. The FNG levels as low as 10% of the wild-type cells in the *png1*Δ *ams1*Δ *ost3*Δ *ost6*Δ and the *png1*Δ *ams1*Δ *alg6*Δ strains sustained yeast cell growth.

Together, I did not find any vital functions of the FNGs formed in the ER. However, it is tempting to speculate that the hydrolytic activity of LLO could be a second enzymatic activity preserved throughout eukaryotic evolution, during which the number of glycoproteins and the total number of modified sequons have expanded 10–20-fold [62]. The FNGs generated in the ER might be necessary for yeast in special environments and other eukaryotic organisms even in normal growth environments and may serve as an organic osmolyte. In the case of the Gram-negative bacterium Campylobacter, the FNG generated by the bacterial OST in the periplasmic space is considered to play a role in balancing the osmotic pressure between the cytosol and extracellular environment [32,63].

In conclusion, detailed comparisons of the two activities of a series of mutations in the Stt3 subunit in vitro and in vivo have provided new knowledge about the yeast OST. Specifically, (1) the single-point mutations that change the relative activity of the LLO hydrolytic reaction to the oligosaccharyl transfer reaction, (2) the better design of peptide substrates, and (3) the dispensable function of FNGs generated by OST under standard laboratory conditions. From a future perspective, the uncoupling of the two activities by single-point mutations can offer useful insights into the generation mechanism and the physiological roles of the FNGs generated in the ER. Previous in vivo knockout analyses of HEK293 and liver cells suggested that the human STT3B-containing OST complex generated FNGs in cells, but the STT3A-containing OST complex did not [20]. The mutations in the DXD motif and DKM motif in the human STT3A/STT3B subunits will be helpful to confirm and investigate the functional differences between the two catalytic STT3 subunits in the human OSTs.

Chapter 4 The response to environmental stress conditions

4.1 Growth plate assay with chemical compounds

Because the physiological function of FNGs could not be found under normal culture conditions, the growth of mutants in a stressful environment was investigated. In this section, The E45A, K586A, M590A mutants were used for the assay. The E45A mutant showed a temperature-sensitive growth phenotype and increase the amount of FNG in the cells. The K586A mutant showed a temperature-sensitive growth phenotype same as the E45A mutant and low FNG generation activity in vitro. The M590A mutant showed a normal growth phenotype and low FNG generation activity in vitro. By using these mutants, I hoped to be able to show the function of FNGs more clearly for environmental stress conditions.

4.1.1 Effect of mutation

I performed a growth spotting assay on agar plates containing stress inducers. DTT and tunicamycin are chemical compounds that cause ER stress through different mechanisms [64]. Tunicamycin is an inhibitor of the biosynthesis of LLO. DMSO was used as a negative control of tunicamycin. Sorbitol and hydrogen peroxide (H_2O_2) are inducers of hyperosmotic stress and oxidative stress, respectively [65].

strains and culture condition

To test the growth under stress, *stt3*Δ *ams1*Δ *png1*Δ +p(RS313-)STT3(X) cells were spotted on YPD agar plates containing 24 mM DTT, 5 mM H_2O_2, 0.1% DMSO, or 1 μg mL^{-1} tunicamycin, and after incubation at 30˚C, cell growth was assessed. For each strain, 3 μL of the culture to 1.0 OD600nm units and five subsequent dilutions (5-1dilution factor) were spotted on plates. Tunicamycin was dissolved in 100% DMSO. The changes by the addition of tunicamycin were examined with the addition of DMSO as a control.

Mutant growth was not significantly different for DTT, sorbitol, and DMSO than when cultured in YPD (Fig. 28). I found that the Stt3(E45A) mutant was extra-sensitive to Tunicamycin at the concentration of 1 μg mL^{-1}, and the Stt3(M590A) was tolerant to

H_2O_2 at the concentration of 5 mM. K586A grew at a slower rate than WT in the YPD, yet there was little difference between K586A and WT in the tunicamycin condition.

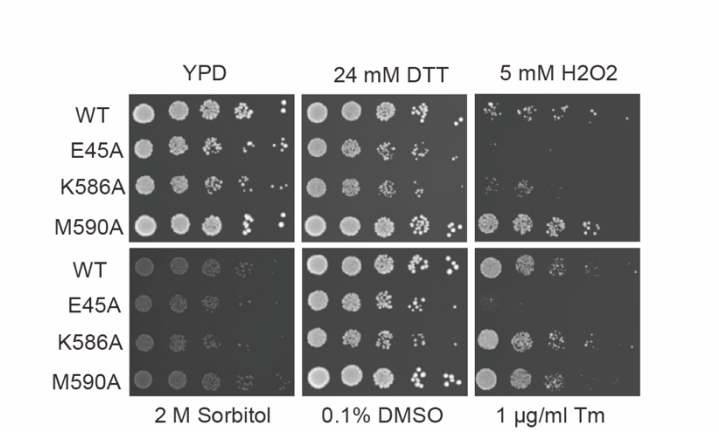

Figure 28. Spotting plate assay of yeast strains expressing mutated Stt3 subunits.
The yeast strains, *stt3*Δ *ams1*Δ *png1*Δ +p(RS313-)STT3(X), where X denotes a mutation, were spotted on YPD containing no chemicals as a control, 24 mM DTT, 5 mM H_2O_2, 2 M sorbitol, 0.1% DMSO, 1 µg/ml tunicamycin. For each strain, 3 µL of the culture to 1.0 OD600nm units and five subsequent dilutions (5-1dilution factor) were spotted on plates. Growth was monitored after 2 days. The OST complex expressed in the cells was the mixed type of Ost3 and Ost6.

4.1.2 Effect of gene knockout

E45A and K586A mutant showed different sensitivity for tunicamycin. In *png1* and *ams1* double-knockout strain, the amounts of cytosolic FNGs were dramatically decreased in yeast. Thus, *stt3* single knockout strains were used for spotting plate assay if the knockout of *png1* and *ams1* affected the phenotype or not.

culture conditions

To test the growth under stress, *stt3*Δ *ams1*Δ *png1*Δ +p(RS313-)STT3(X) and *stt3*Δ +p(RS313-)STT3(X) cells were spotted on YPD agar plates containing 0.1% DMSO, or 1 µg mL^{-1} tunicamycin, and after incubation at 30˚C, cell growth was assessed.

The growth phenotypes were the same as Fig. 28 in 1 μg mL^{-1} tunicamycin condition. The Stt3(E45A) mutant was sensitive to tunicamycin independent of knockout of the genes, *png1*, and *ams1* (Fig. 29). These results indicated that the high FNG generation activity linked to the sensitivity of tunicamycin in the Stt3(E45A) mutant.

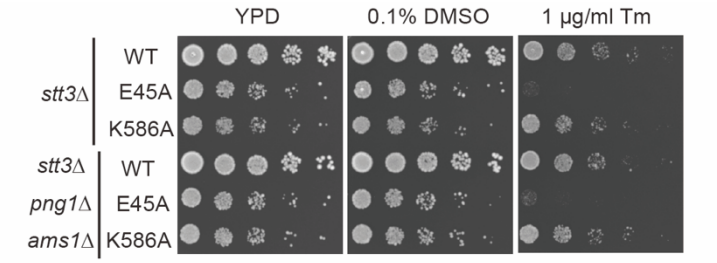

Figure 29. Spotting plate assay of yeast strains expressing mutated Stt3 subunits.
The yeast strains, *stt3*Δ+p(RS313-)STT3(X) or *stt3*Δ *ams1*Δ *png1*Δ +p(RS313-)STT3(X), where X denotes a mutation, were spotted on YPD containing no chemicals as a control, 0.1% DMSO, 1 μg/ml tunicamycin. For each strain, 3 μL of the culture to 1.0 OD600nm units and five subsequent dilutions (5-1dilution factor) were spotted on plates. Growth was monitored after 2 days. The OST complex expressed in the cells was the mixed type of Ost3 and Ost6.

4.1.3 Tolerance of tunicamycin

Tunicamycin induces the ER stress responses by inhibiting the enzymatic reaction of ALG7 protein, which acts as the first step of LLO biosynthesis. The growth of yeast impaired by tunicamycin inducing ER stress even if Stt3(WT) expressed. However, the change of growth rate was limited against the tunicamycin in the Stt3(K586A) mutant. Focusing on the growth rate of K586A in the presence of tunicamycin, the concentration of tunicamycin was increased in the experiment.

culture conditions

To test the growth under stress, *stt3*Δ *ams1*Δ *png1*Δ +p(RS313-)STT3(X) cells were spotted on YPD agar plates containing 1 μg mL^{-1} Tunicamycin or 3 μg mL^{-1} Tunicamycin, and after incubation at 30˚C, cell growth was assessed. Growth was monitored after 5 days, was longer than the above experiments

Although the presence of high concentrations of tunicamycin strongly suppressed the growth of WT, the K586A mutant had a low inhibitory effect (Fig. 30). It has been shown that the Stt3(K586A) mutant has acquired resistance to the high concentration of tunicamycin for some reason. It has been reported previously that deletion of genes enhanced tunicamycin tolerance [66,67].

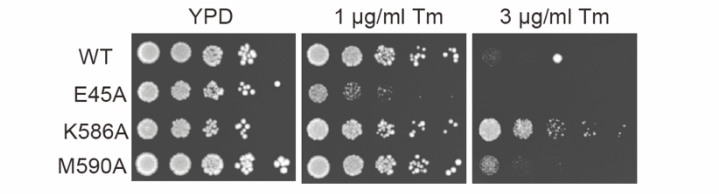

Figure 30. Spotting plate assay of yeast strains expressing mutated Stt3 subunits.
The yeast strains, *stt3*Δ *ams*1Δ *png1*Δ +p(RS313-)STT3(X), where X denotes a mutation, were spotted on YPD containing no chemicals as a control, 1 μg/ml tunicamycin, 3 μg/ml tunicamycin. For each strain, 3 μL of the culture to 1.0 OD600nm units and five subsequent dilutions (5-1dilution factor) were spotted on plates. Growth was monitored after 5 days. The OST complex expressed in the cells was the mixed type of Ost3 and Ost6.

4.2 Growth liquid culture assay with chemical compounds

A plate assay was used to check the long-term effects of stress. However, liquid media are more suitable for assessing the effects of unstable compounds such as DTT. Then, experiments of addition to the liquid medium were performed to explore the changes in cells under environmental stresses.

4.2.1 Growth rate

Because I would assess the effect of the stress, the compounds were added to the yeast medium in the exponential growth phase (OD600=0.9). The wild-type STT3 strain (*png1*Δ*ams1*Δ) was used instead of the mutant to avoid altering the response to stress by the STT3 mutation.

culture conditions

Cultures of the *ams1*Δ *png1*Δ were grown at 30 ˚C in YPD medium to an OD600 of 0.9. Then the compounds, H_2O, DTT, H_2O_2, DMSO, and tunicamycin, were added to yeast cultures at final concentration 0.1%, 5 mM, 0.3 mM, 0.1%, and 2 μM respectively and incubated with absorbance at 600 nm measurements taken every 30 min. After 2 hours, the cells were harvested and quantified the FNG.

In this study, compounds were added at the late exponential growth phase of yeast. The cell concentrations in the media after 2 hours with DTT and H_2O_2 were lower than that of H_2O (Fig. 31). The changes by the addition of tunicamycin were examined with the addition of DMSO as a control. The cell concentration in the media after 2 hours with tunicamycin was lower than that of DMSO.

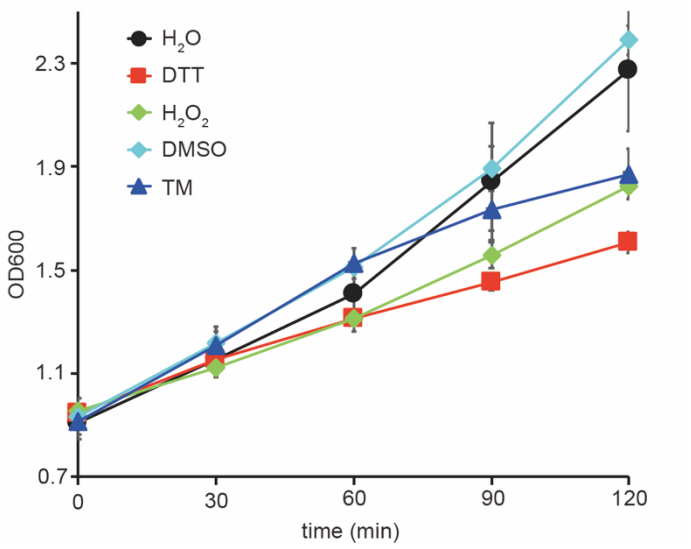

Figure 31. Growth assay of strain *ams1*Δ *png1*Δ in media supplemented with various chemicals.

OD600 of cells were monitored with 30 minutes intervals in media after the addition of compounds H_2O, DTT, H_2O_2, DMSO, or tunicamycin. Triplicate measurements were performed for each condition. Data points represented average optical density readings ± standard deviation of replicate cultures (n = 3). Statistical analysis was by one-way ANOVA followed by Dunnett post-hoc test between the H_2O and DTT, H_2O_2 of data point at 120 min. (adjusted p=<0.001, 0.003) Welch's t-test was applied for between the DMSO and Tunicamycin of data point at 120 min. (p=0.003)

4.2.2 Amount of FNG in the cell

I investigated whether there is a relationship between yeast growth under stress and the amount of intracellular FNG. Two hours after stress was applied, the culture was stopped, cells were collected.

culture conditions and quantification of FNG

Cultures of the *ams1*Δ *png1*Δ were grown at 30 ˚C in YPD medium to an OD600 of 0.9. Then the compounds, H_2O, DTT, H_2O_2, DMSO, and tunicamycin, were added to yeast cultures at final concentration 0.1%, 5 mM, 0.3 mM, 0.1%, and 2 μM respectively. Tunicamycin was dissolved in 100% DMSO. One hundred OD_{600} units of cells were harvested and washed with phosphate-buffered saline (PBS). The washed cells were resuspended in 1 mL of lysis buffer (20 mM Tri-HCl, pH 7.5, 10 mM EDTA), and then 3 mL of ice-cold ethanol was added. The solution was vortexed for 10 sec and cooled on ice for 5 min, and this procedure was repeated 3 times. The homogenate was centrifuged at 7,500 × g for 15 min, and the supernatant was recovered and evaporated to dryness. The dried soluble oligosaccharide fraction was desalted on a column packed with AG 501-X8 ion exchange resin (Bio-Rad), and then on an InertSep GC column (GL Sciences). After elution, the dried pellets were labeled with 2-AP. The dried oligosaccharides were incubated with 20 μL of 2-AP in acetic acid at 80°C for 1 h. After the reaction, the mixture was incubated with 20 μL of dimethylamine borane reagent in acetic acid at 80°C for 30 min. The excess 2-AP was removed using a MonoFas silica gel spin column. The spin column was washed with water and then preequilibrated twice with 800 μL of 100% acetonitrile before use. The sample solution was mixed with 460 μL of 100% acetonitrile and loaded onto the spin column. The column was washed twice with 800 μL of 95% (v/v) acetonitrile. Water was added to the column to elute the fluorescently labeled oligosaccharides. The pyridylaminated FNGs were separated by Infinity 1290 UPLC with an AdvanceBio Glycan Mapping column and quantified by an in-line fluorescence detector. Solvent A was 100 mM ammonium acetate buffer, pH 4.5, and solvent B was 100% acetonitrile. The column was equilibrated with 20% solvent A at a flow rate of 0.5 ml min^{-1}. A linear gradient of solvent A was applied from 20 to 40% over 25 min.

The amount of intracellular FNG was significantly increased in cells when DTT was added. There was no significant difference in the amount of intracellular FNG in H_2O_2

with suppressed growth (Fig. 32). The changes in the amounts of FNG by the addition of tunicamycin were examined with the addition of DMSO as a control. The addition of tunicamycin reduced the amount of intracellular FNG than the addition of DMSO.

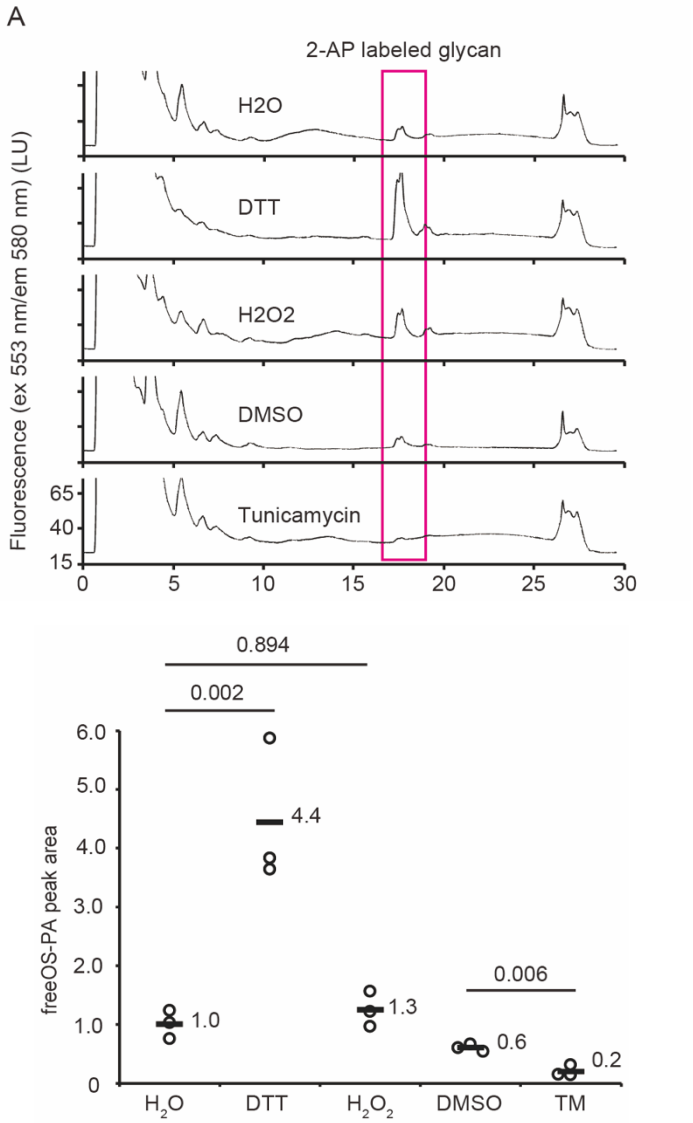

Figure 32 UPLC chromatograms and the plots for the quantification of FNG contents in yeast cells.

A. Contents of FNGs in yeast strains, *png1*Δ *ams1*Δ relative to that in the no chemicals. The primary UPLC chromatograms were shown. *B*. The content of the FNGs in yeast using media containing no additional chemical was set to 1. Triplicate measurements were performed for each condition. Open circles indicated the measurement of each trial. The bars and numbers indicate the mean values of triplicate

measurements. Statistical analysis was by one-way ANOVA followed by Dunnett post-hoc test between the H_2O and DTT, H_2O_2. Welch's t-test was applied for between the DMSO and Tunicamycin.

4.3 Sensitivity of OST to DTT

It was not known if DTT had a direct impact on OST FNG generation activity. The Ost3 and Ost6 proteins have a thioredoxin fold in the N-terminal soluble domain, and the oxidoreductase activity was considered to suppress disulfide bond formation during the oligosaccharyl transfer reaction [36,68]. However, the N-glycosylation status was only affected to a limited extent by the disruption of the CXXC motifs in the Ost3 and Ost6 subunits, suggesting the importance of noncovalent interactions [68]. The actual functions of the Ost3 and Ost6 subunits remain elusive. Different modes of action of the Ost3-containing and the Ost6-containing OST complexes in the in vitro assays. The OST protein samples were used same as Fig. 13. I assessed the effects of the exchange of the homologous Ost3 and Ost6 subunits.

oligosaccharyl transfer assay

The reaction mixture (total 10 µL) contained 1 µM yeast LLO, 5 µM tam-NVT15 peptide, and 1 – 5 nM purified OST protein, in 20 mM Tris-HCl buffer, pH 7.5, 5 mM $MnCl_2$, 5 mM $MgCl_2$, 0.1% (v/v) Triton X-100, and 5 mM DTT or H_2O as negative control. The reaction mixture was incubated for 60 min at 30°C. The reaction was stopped by the addition of 2 µL of 60 mM EDTA-NaOH, pH 8.0. The reaction products were separated by Infinity 1290 UPLC (Agilent) with an AdvanceBio Glycan Mapping column and quantified by an in-line fluorescence detector. Solvent A was 100 mM ammonium acetate buffer, pH 4.5, and solvent B was 100% acetonitrile. The column was equilibrated with 20% solvent A at a flow rate of 0.5 ml min^{-1}. A linear gradient of solvent A was applied from 25 to 57% over 8.5 min.

Table 9. Information of substrate peptide used in this section

Peptide name	Amino acid sequence[a]	Preparative method
tam-NVT15	(TAMRA)-GAGGSYNVTKGAGGS-$CONH_2$	Chemical synthesis Reference [51]

[a]The N-glycosylation sequon is underlined. TAMRA and tam denote the fluorescent dye, 5(6)-carboxytetramethylrhodamine. The peptide concentrations were determined by the absorbance at 555 nm, with an extinction coefficient of 90,000 M^{-1} cm^{-1}. The N-terminal α-amino group is modified with the TAMRA group (TAMRA-). The C-terminal α-carboxyl group is modified with an amide group (-$CONH_2$).

FNG generation assay

The purified OST complex was incubated with 1 μM LLO for 24 hours at 30°C in a 100 μL reaction solution, containing 20 mM Tris-HCl, pH 7.5, 5 mM $MnCl_2$, 5 mM $MgCl_2$, 0.1% (v/v) Triton X-100, and 5 mM DTT or H_2O as negative control. The reaction was terminated by the addition of 1 μL of 0.5 M EDTA-NaOH, pH 8.0. A 300 μL aliquot of ethanol was added, and the reaction solution was incubated for 15 min at 4°C. After centrifugation at 15,000 × g for 15 min, the supernatant was evaporated to dryness. The pyridylaminated oligosaccharides were separated by Infinity 1290 UPLC with an AdvanceBio Glycan Mapping column and quantified by an in-line fluorescence detector. Solvent A was 100 mM ammonium acetate buffer, pH 4.5, and solvent B was 100% acetonitrile. The column was equilibrated with 20% solvent A at a flow rate of 0.5 ml min^{-1}. A linear gradient of solvent A was applied from 20 to 40% over 14 min.

The Ost3-containing OST complex, OST[Ost3, Ost4-PA], had higher oligosaccharyl transfer activity than the Ost6-containing OST complex, OST[Ost6, Ost4-PA], whereas the two OST complexes had similar FNG generation activities (Fig. 33). I then tested the effects of the addition of the reducing agent DTT on the two activities, since Ost3 and Ost6 are redox-related subunits. DTT had no effects on the oligosaccharyl transfer activity of the Ost3-containing OST complex, OST[Ost3, Ost4-PA], but enhanced the FNG generation activity more than two-fold. In contrast, DTT had no effects on the two activities of the Ost6-containing OST complex, OST[Ost6, Ost4-PA]. These results suggest the unique roles of the Ost3 and Ost6 subunits in the recognition of a sequon-containing polypeptide chain and the generation of FNGs in cells.

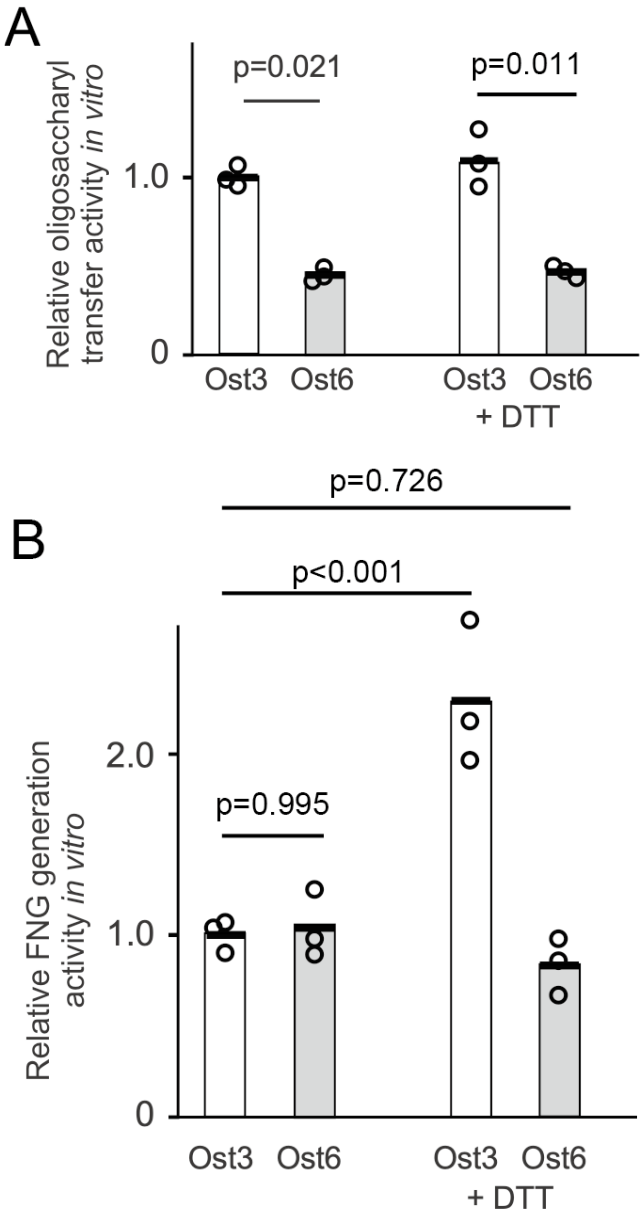

Figure 33. Effects of exchanging the Ost3 and Ost6 subunits on the enzymatic activities.

A. *In vitro* oligosaccharyl transfer activities of the OST complexes containing either Ost3 or Ost6, in the absence and the presence of 5 mM DTT. The tam-NVT15 peptide was used in the oligosaccharyl transfer assay. Welch's *t*-test was applied for statistical analyses between OST[Ost3, Ost4-PA] and OST[Ost6, Ost4-PA] *B*. Same as *A*, but for FNG generation activities. Statistical analysis was by one-way ANOVA followed by Dunnett post-hoc test between the OST[Ost3, Ost4-PA] in the absence of DTT and others. The numbers indicate the adjusted p values. In *A* and *B*, the PA tag was inserted at the C-terminus of the Ost4 subunit. The relative amounts of the OST complexes

containing either Ost3 or Ost6 were estimated by fluorescent western blotting of the Wbp1 subunit and used to normalize the two activities. The activities of OST[Ost3, Ost4-PA] in the absence of DTT were set to 1. Open circles indicated the measurement of each trial. The bar heights indicate the mean values of triplicate measurements.

4.4 Discussion

So far, the function of OST-derived FNGs is not known in the cells. In the case of bacteria, it has been reported that the amount of FNG is regulated by changes in the external salt concentration [32]. In yeast, the addition of tunicamycin and DTT induced the accumulation of unfolded proteins in the ER, followed by, activation of the UPR pathway [69]. Previous reports had suggested that N-glycan conjugated asparagines contribute to protein refolding [24,25]. Experiments with the addition of the compound to plate media showed that the E45A mutant was more sensitive to tunicamycin and the K586A mutant was more resistant than the WT. Due to the elevated FNG generation activity relative to the oligosaccharyl transfer activity, the growth of the E45A mutant requires overload with LLO synthesis. If the LLO synthesis is inhibited by tunicamycin, the growth may be very poor. On the other hand, K586A has a slow growth rate and low FNG-generating activity in vitro, which results in a low load on LLO synthesis. These led that K586A has acquired resistance to tunicamycin. Tunicamycin inhibited LLO synthesis reaction and induce activation of the UPR pathway. UPR activation resulted in decreasing translation activities in cell [69]. There were reported that mutant strains acquired resistance of tunicamycin in low transcription and translation activity [66,67].

In the liquid medium experiments, the growth rates of the yeast were reduced by stress compounds. The amount of FNG in the cells was reduced by Tunicamycin, again indicating that amount of LLOs was related to the amount of FNG [11]. On the other hand, the addition of DTT increased the amount of FNG in the cells. No proteins that generate the FNG had been found other than OST and PNG1 in yeast [11,38]. Therefore, I hypothesized that the activity of OST might be altered by DTT and tried in vitro experiments.

I discuss the different roles of the interchangeable Ost3 and Ost6 subunits. The previous in vivo studies demonstrated that the Ost3-containing and Ost6-containing OST complexes modified distinct repertoires of N-glycosylated proteins [36,68]. Here, I determined the different properties of the two isoforms of the OST complexes, at the

molecular level. The sequence identity (20%) and similarity (46%) are modest between Ost3 and Ost6 [31]. The Ost3-containing OST complex had higher oligosaccharyl transfer activity than the Ost6-containing OST complex (Fig. 33A). The reducing agent DTT enhanced the FNG generation activity of the Ost3-containing OST complex more than two-fold but had no effects on that of the Ost6-containing OST complex (Fig. 33B). DTT increases the FNG level in the ER through the modulation of the OST activity. Thus, the Ost3 and Ost6 subunits can affect the catalytic activity of Stt3 in unique and different manners, through a direct or indirect mechanism. Contrary to previous conceptions, a recent cell biological study has suggested that the oligosaccharyl transfer catalyzed by the yeast OST may not be a co-translational process coupled with the passage across the translocon channel [70], although the Ost3 and Ost6 subunits have been considered to interact with the translocon [34,35]. I expect that the different enzymatic properties of the Ost3-containing and Ost6-containing OST complexes in vitro will serve as a good starting point for future studies on the different roles of the Ost3/Ost6 subunits in yeast cells.

Chapter 5. Electron microscopy analysis of yeast OST complex

5.1 Introduction

Cryo-EM structure of the yeast OST complex had already been reported. However, the reported structures are missing structural information for one transmembrane and soluble domain of OST3 and OST6 [34,35]. In other words, the soluble domain of OST3 and OST6 move flexibly in the absence of the substrate. The difference in substrate specificity between OST3 and OST6 suggests that the soluble domain of OST3 and OST6 may be located close to the active center at some moments. The above-mentioned experiments have shown that differences in OST3/6 affect FNG-generating activity, indicated that the soluble domain may move near the active center. However, how OST3/6 are involved in substrate recognition and FNG generation cannot be explained by structural information so far. Therefore, I used cryo-electron microscopy to test how OST3 in the OST complexes purified in this study was observed.

5.2 Importance of structural domain in OST3 and OST6 for yeast

The structure of the DC2 protein structure of the human STT3A complex is similar to the C-terminal 3TM of OST3 [35,59]. I checked the importance of each structural domain of OST3 and OST6 for yeast growth by plasmid shuffling. OST3 and OST6 proteins were constructed signal sequence, the soluble region containing thioredoxin domain, and four transmembranes. Four deletion constructs were prepared each for OST3 and OST6. The property of constructs showed (Fig. 34).

strains and constructs

The PCR-based method was used to disruption of *ost3* gene in the *ost6*Δ *ost4*PA-pOST3 yeast strain, replacing *ost3* to *HygMX*. Correct gene knockout was confirmed by PCR and DNA sequencing. The OST3 regions of pRS313-OST3 is containing the entire *ost3* ORF region plus 300 bp (native promoter) and 300 bp (native terminator) at the 5' and 3' ends, respectively. The OST6 regions of pRS313-OST6 is containing the entire *ost6* ORF region plus 300 bp (native promoter) and 279 bp (native terminator) at the 5' and 3' ends, respectively. Deletion mutants were obtained by the inverse PCR method.

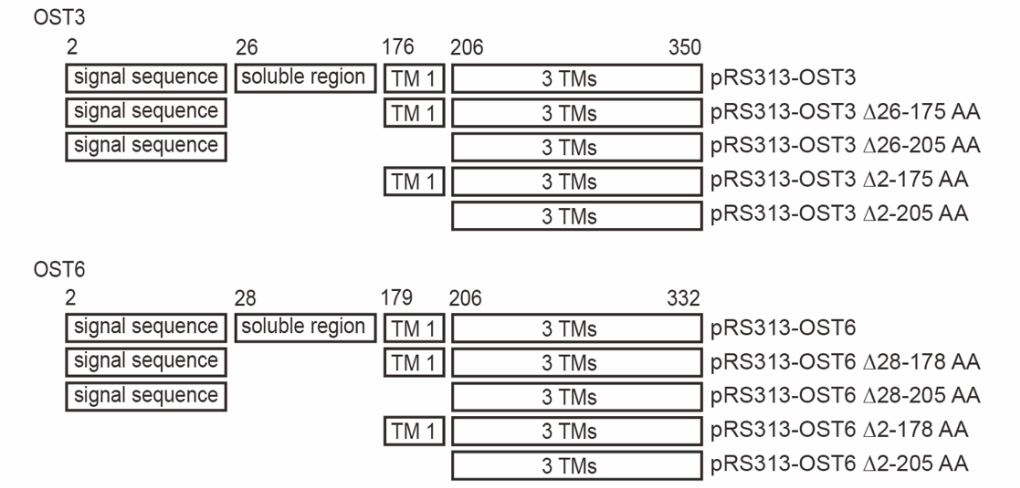

Figure 34. Constructs of plasmids.

Schematic diagram of OST3 and OST6 deletion constructs. The full-length construct contains a signal sequence, soluble region, TM 1, and 3 TMs. The numbers indicate the amino acid position of the protein. TM stands for transmembrane.

plasmid* shuffling *and spotting plate assay

*ost3*Δ *ost6*Δ *ost4*PA-pOST3 cells bearing pOST3 encoding the wild-type ost3 were transformed with pRS313-OST3/6 and each mutant. The transformants were grown in SD medium lacking L-histidine until the OD600 reached 1. Collected cells were diluted in a 5-fold series. Aliquots (2 μL) of each dilution were spotted onto SD plates lacking L-histidine and those lacking L-histidine supplemented with 5-FOA, at a final concentration of 1 mg mL-1. After incubation at 30˚C for 3 days, cell growth was assessed.

In this section, I defined the growth phenotypes as follows, lethal means no growth at 30˚C, normal means the same growth as wild-type. Yeast strain did not survive at 30˚C without OST3 and OST6 (Fig. 35). OST3 and human MAGT1 protein are in a homologous relationship, and the characteristic of having a soluble domain and four TMs is also preserved. However, the yeast was able to survive at 30˚C if either OST3 or OST6 C-terminal three TMs were present.

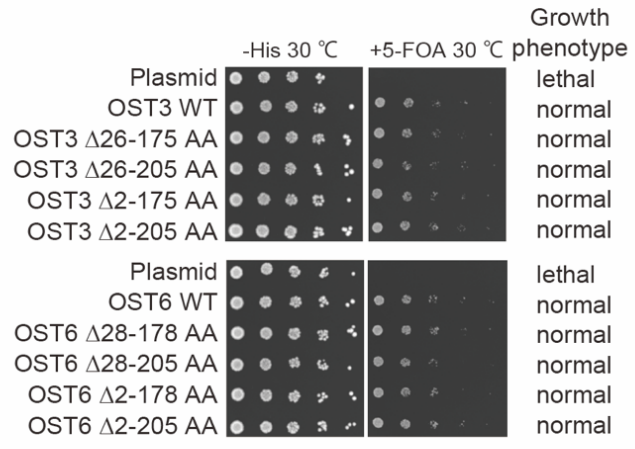

Figure 35. Results of plasmid shuffling.

The yeast strains, *ost3*Δ *ost6*Δ *ost4*PA-pOST3+pRS313-OST3/6 series were spotted on -His + 5-FOA plates. The growths of the colonies were compared after 3 days at 30˚C.

5.3 Comparison of acquired density map vs known structure

PA tag purified OST complex needs to be further purified by gel filtration to obtain good Cryo-EM data. In the case of the OST complex, it was necessary to prepare a high concentration of OST complex solution close to the crystallization [34]. To obtain a new molecular model, I did not set the previously reported OST structures as references.

further purification of OST complex protein

OST[Ost3, OST4-PA] protein was purified the same as described above (chapter 2.4.1). The eluted protein was concentrated using an Amicon Ultra concentrator (Millipore) with a molecular mass cutoff of 100 kDa and further purified by size exclusion chromatography using a Superose-6 (GE Healthcare) column in 20 mM Tris-HCl buffer, pH 7.5, 0.1% digitonin, 150 mM NaCl, 1 mM $MgCl_2$, and 1 mM $MnCl_2$. The fraction was concentrated at 5 mg ml^{-1} using an Amicon Ultra concentrator with a molecular mass cutoff of 100 kDa.

cryo-EM dataset collecting

Collaborated with Dr. Shigematsu and Dr. Mayanagi for grid preparation and dataset collection.

Aliquots of 3 μ l of purified OST at a concentration of 5 mg ml^{-1} were placed on glow-discharged holey carbon grids (Quantifoil Au R1.2/1.3, 200 mesh) and flash-frozen in liquid ethane using an FEI Vitrobot. Electron microscopic image datasets were collected.

cryo-EM image processing

Movie frames were aligned to correct the dose-induced and dose-weighted motions of the specimens using MotionCor2 [71]. The contrast transfer function was determined for each image using the CTFFIND4 program [72]. Particle images were picked automatically, using crYOLO [73]. The output coordinates of the picked particles were used for the particle extraction program of Relion [74].

A total of 348,937 particles were extracted from the OST complex images, and after the 2D classification procedure, particles classified as "bad" were removed from the data set. In total, 138,000 particles were subjected to the 3D classification procedure in Relion (Class3D), assuming eight classes. Particles classified as the best (class 1 73,166 particles) 3D classes were further used for refining (Refine3D in RELION).

The obtained 3D density map had a resolution of 5.0 A (Fig. 36A). Because this resolution does not allow for the construction of a de novo molecular model. I decided to compare it with a known structure [35]. I superimposed the obtained 3D density maps on the known structures and found that they matched well entirely (Fig. 36B). As reported, there was no evidence of an excess density map corresponding to OST3. By increasing the volume of the obtained density map, I could confirm a density map that seems to be a soluble domain of OST3 that was not visible before. The soluble domain of OST3 was located far from the active center of STT3.

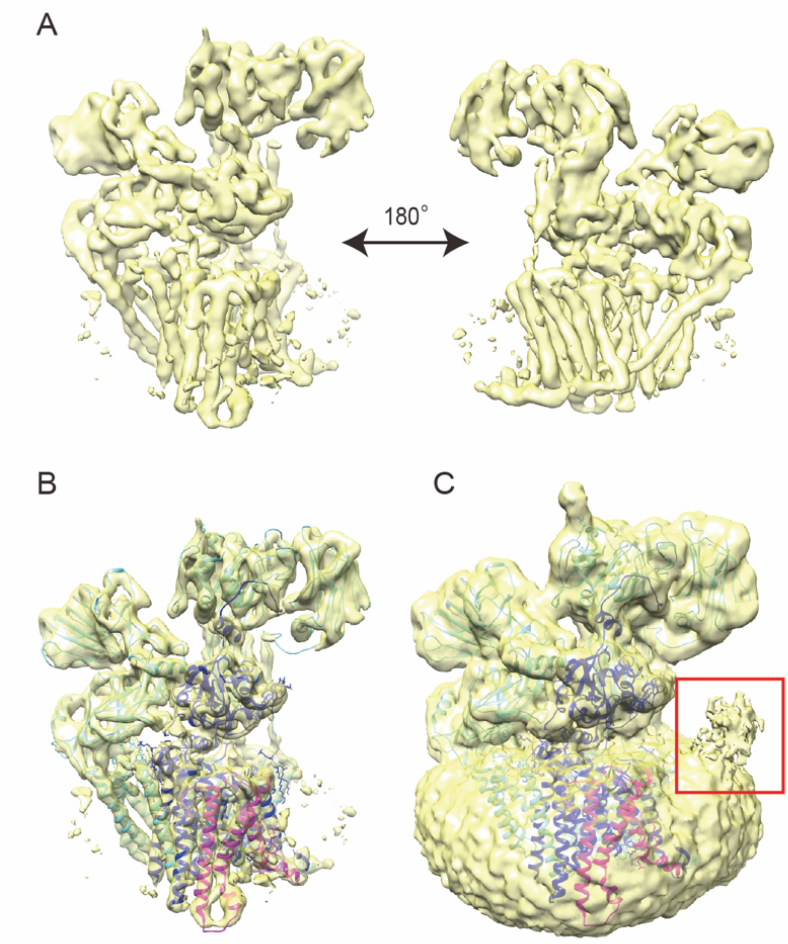

Figure 36. Comparison of structures.

A. The refined 3D density map was shown yellow. *B*. The cartoon model was shown cyan color adopted from yeast OST complex (PDB entry 6C26). The blue color indicated the STT3 subunit. The magenta color indicated the OST3 subunit. Two structures were opened in the UCSF Chimera program and superimposed. *C*. The volume of the refined 3D density map was increased on UCSF Chimera program [75]. The presumed soluble domain of the OST3 density map was surrounded by the red color square.

5.4 Discussion

The structure of the C-terminal three TMs of OST3 resembled the DC2 protein structure of the human STT3A complex [35,59]. Figure 35 showed that the yeast was able to grow at 30˚C with C-terminal three TMs of either OST3 or OST6. These results indicated that the structures of C-terminal three TMs of OST3 and OST6 are preserved as core structures for OST complex function. The reported electron microscopic

structures of yeast OST lack information on the soluble domain and 1st transmembrane of OST3/6 so far [34,35]. Also, information on the soluble domain and 1st transmembrane were missing for MAGT1 contained in the human STT3B complex [76]. OST3 and MAGT1 are homologous proteins, suggesting that they move and function flexibly in both yeast and humans in the same way. Because not only the number of glycoproteins but also the number of cysteines near the sequon has increased significantly during evolution, OST3 / MAGT1 with the thioredoxin domain is presumed to play an important role [70,77]. The core structure of OST obtained in this study is almost the same as that reported, which indicated that the flexibility of the core structure was low in the apo state. The density map observed at increased volume is likely to be the soluble domain of OST3 based on the placement of transmembranes in the OST complex. There was little high-resolution structural information in the OST3 region than in other regions, which may be an overlap of many OST3 structures. I expected that OST3 would be located closer to the active center for its function, but it is difficult to clarify in the apo state. Also, it is said that the human STT3B complex has a structure close to the substrate-bound state as a result of structural analysis in which dolichol phosphate and peptide were fortunately left during preparation [76]. Nevertheless, the soluble domain and 1st transmembrane of MAGT1 were not visible. More aggressive preparation of the OST complex in the substrate-bound state is needed in future studies. Indeed, archaeal OST, which does not have a high affinity for peptides, had succeeded in determining the peptide complex structure by introducing cysteine into each the OST and peptides to induce disulfide bond formation [60]. In yeast, some glycoproteins with a strong dependence on OST3 or OST6, respectively, for the addition of glycans have been reported [36]. Also, the glycosylation status of Sil1 protein changed to reflect the reduction state of the cell [78]. Based on these findings, I will create the peptides of some proteins that are strongly dependent on OST3/OST6 for glycosylation and determine the peptide bound structure of OST by tethering the peptide to OST3 / 6 with a disulfide bond.

Chapter 6. Conclusion

I started this study to resolve the following questions.

1. Is OST-catalyzed FNG generation activity just a side reaction that correlates with oligosaccharyl transfer activity?

If FNG generation activity is a side reaction of glycosyltransferase activity for OST, it is expected that the changes in the oligosaccharyl transfer activity correlate with the changes in the FNG generation activity because they use the same enzymatic mechanism. If the relationship between the oligosaccharyl transfer activity and the FNG generation activity is a simple trade-off mechanism, then introducing mutations in the peptide-binding motif would enhance the FNG generation activity. In this study, I measured separately the oligosaccharyl transfer activity and the hydrolytic activity of LLO in vitro using the purified OST complexes. I found that point mutations and the composition of subunits induced the decoupling of the two activities. The mutations in the first DXD motif increased the FNG generation activity relative to the oligosaccharyl transfer activity, both in vitro and in vivo, while mutations in the DKM motif had the opposite effect. Also, the OST3-containing OST complex had higher oligosaccharyl transfer activity than the Ost6-containing OST complex, whereas the two OST complexes had similar FNG generation activities. Furthermore, only OST3-containing OST complex showed enhancing the FNG generation activity by reducing the environment. These results indicated that OST-catalyzed FNG generation activity is not just a side reaction that correlates with glycosylation activity. I hypothesized that OST has two distinct enzymatic activities, are similar but different mechanisms. The decoupling of the two activities may facilitate future deconvolutions of the reaction mechanism.

2. What effect does the generation and accumulation of FNG in the ER by OST have on the survival of organisms?

I did not find a clear answer to this question. The correlations with the growth phenotype suggested that FNG in the ER was dispensable for the growth of yeast cells under laboratory conditions. However, there is no enzyme other than OST that can

hydrolyze mature LLO consisting of 14 monosaccharides, the FNG generation activity of OST is evolutionarily conserved even though that it can be significantly reduced by the amino acid mutation, and that OST-derived FNGs rapidly increase or decrease in response to the cellular environment. Therefore, I believe that FNGs may play an important function under special conditions or in other species.

In this study, I developed the OST purification method, found the mutation and stress-induced changes in the activity and amount of FNG in the cells, improved the substrate peptides, and showed the findings from electron microscopy analysis. I believe that these will contribute as a toolbox for future OST and FNG research.

Statistical analysis

Statistical analyses were performed with Excel (Microsoft) and EZR statistical software [79], an open-source statistical software program that is based on R and R commander [80,81]. Data were analyzed by Welch's t-test for single comparisons and by one-way analysis of variance (ANOVA) with Dunnett post hoc test for multiple comparisons.

Reference

1. Mann M, Jensen ON. Proteomic analysis of post-translational modifications. *Nat Biotechnol*. 2003;21(3):255-261. doi:10.1038/nbt0303-255
2. Larsen MR, Trelle MB, Thingholm TE, Jensen ON. Analysis of posttranslational modifications of proteins by tandem mass spectrometry. *Biotechniques*. 2006;40(6):790-798. doi:10.2144/000112201
3. Cohen P. The regulation of protein function by multisite phosphorylation - A 25 year update. *Trends Biochem Sci*. 2000;25(12):596-601. doi:10.1016/S0968-0004(00)01712-6
4. Wu D, Jin J, Qiu Z, Liu D, Luo H. Functional Analysis of O-GlcNAcylation in Cancer Metastasis. *Front Oncol*. 2020;10(October):1-11. doi:10.3389/fonc.2020.585288
5. Ohtsubo K, Marth JD. Glycosylation in Cellular Mechanisms of Health and Disease. *Cell*. 2006;126(5):855-867. doi:10.1016/j.cell.2006.08.019
6. Cherepanova N, Shrimal S, Gilmore R. N-linked glycosylation and homeostasis of the endoplasmic reticulum. *Curr Opin Cell Biol*. 2016;41:57-65. doi:10.1016/j.ceb.2016.03.021
7. Aebi M. N-linked protein glycosylation in the ER. *Biochim Biophys Acta - Mol Cell Res*. 2013;1833(11):2430-2437. doi:10.1016/j.bbamcr.2013.04.001
8. Breitling J, Aebi M. N-linked protein glycosylation in the endoplasmic reticulum. *Cold Spring Harb Perspect Biol*. 2013;5(8):a013359. doi:10.1101/cshperspect.a013359
9. Hartley MD, Imperiali B. At the membrane frontier: A prospectus on the remarkable evolutionary conservation of polyprenols and polyprenyl-phosphates. *Arch Biochem Biophys*. 2012;517(2):83-97. doi:10.1016/j.abb.2011.10.018
10. Kohda D. Structural basis of protein asn-glycosylation by oligosaccharyltransferases. *Adv Exp Med Biol*. 2018;1104:171-199. doi:10.1007/978-981-13-2158-0_9
11. Harada Y, Buser R, Ngwa EM, Hirayama H, Aebi M, Suzuki T. Eukaryotic oligosaccharyltransferase generates free oligosaccharides during N-glycosylation. *J Biol Chem*. 2013;288(45):32673-32684. doi:10.1074/jbc.M113.486985
12. Harada Y, Masahara-Negishi Y, Suzuki T. Cytosolic-free oligosaccharides are predominantly generated by the degradation of dolichol-linked oligosaccharides in mammalian cells. *Glycobiology*. 2015;25(11):1196-1205. doi:10.1093/glycob/cwv055

13. Rolf Apweiler HH, Nathan Sharon. On the frequency of protein glycosylation, as deduced from analysis of the SWISS-PROT database. *Biochim Biophys Acta*. 1999;1(2):4-8. doi:10.1097/00013611-198607000-00004
14. Frappaolo A, Karimpour-Ghahnavieh A, Sechi S, Giansanti MG. The Close Relationship between the Golgi Trafficking Machinery and Protein Glycosylation. *Cells*. 2020;9(12):2652. doi:10.3390/cells9122652
15. Ondruskova N, Cechova A, Hansikova H, Honzik T, Jaeken J. Congenital disorders of glycosylation: Still "hot" in 2020. *Biochim Biophys Acta - Gen Subj*. 2021;1865(1). doi:10.1016/j.bbagen.2020.129751
16. Chantret I, Moore SEH. Free oligosaccharide regulation during mammalian protein N-glycosylation. *Glycobiology*. 2008;18(3):210-224. doi:10.1093/glycob/cwn003
17. Chantret I, Kodali VP, Lahmouich C, Harvey DJ, Moore SEH. Endoplasmic reticulum-associated degradation (ERAD) and free oligosaccharide generation in Saccharomyces cerevisiae. *J Biol Chem*. 2011;286(48):41786-41800. doi:10.1074/jbc.M111.251371
18. Hirayama H, Seino J, Kitajima T, Jigami Y, Suzuki T. Free oligosaccharides to monitor glycoprotein endoplasmic reticulum-associated degradation in Saccharomyces cerevisiae. *J Biol Chem*. 2010;285(16):12390-12404. doi:10.1074/jbc.M109.082081
19. Fermaintt CS, Sano K, Liu Z, et al. A bioactive mammalian disaccharide associated with autoimmunity activates STING-TBK1-dependent immune response. *Nat Commun*. 2019;10(1):2377. doi:10.1038/s41467-019-10319-5
20. Lu H, Fermaintt CS, Cherepanova NA, Gilmore R, Yan N, Lehrman MA. Mammalian STT3A/B oligosaccharyltransferases segregate N-glycosylation at the translocon from lipid-linked oligosaccharide hydrolysis. *Proc Natl Acad Sci U S A*. 2018;115(38):9557-9562. doi:10.1073/pnas.1806034115
21. Katsube M, Ebara N, Maeda M, Kimura Y. Cytosolic Free N-Glycans Are Retro-Transported Into the Endoplasmic Reticulum in Plant Cells. *Front Plant Sci*. 2021;11(January). doi:10.3389/fpls.2020.610124
22. Wang Y, Hirata T, Maeda Y, Murakami Y, Fujita M, Kinoshita T. Free, unlinked glycosylphosphatidylinositols on mammalian cell surfaces revisited. *J Biol Chem*. 2019;294(13):5038-5049. doi:10.1074/jbc.RA119.007472
23. Hirayama H, Matsuda T, Tsuchiya Y, et al. Free glycans derived from O-mannosylated glycoproteins suggest the presence of an O-glycoprotein

degradation pathway in yeast. *J Biol Chem*. 2019;294(44):15900-15911. doi:10.1074/jbc.RA119.009491

24. Kimura N, Uchida M, Nishimura S, Yamaguchi H. Promotion of polypeptide folding by interactions with Asn-glycans. *J Biochem*. 1998;124(4):857-862. doi:10.1093/oxfordjournals.jbchem.a022190
25. Jitsuhara Y, Toyoda T, Itai T, Yamaguchi H. Chaperone-like functions of high-mannose type and complex-type N-glycans and their molecular basis. *J Biochem*. 2002;132(5):803-811. doi:10.1093/oxfordjournals.jbchem.a003290
26. Kelleher DJ, Karaoglu D, Mandon EC, Gilmore R. Oligosaccharyltransferase isoforms that contain different catalytic STT3 subunits have distinct enzymatic properties. *Mol Cell*. 2003;12(1):101-111. doi:10.1016/S1097-2765(03)00243-0
27. Niu G, Shao Z, Liu C, Chen T, Jiao Q, Hong Z. Comparative and evolutionary analyses of the divergence of plant oligosaccharyltransferase STT3 isoforms. *FEBS Open Bio*. 2020;10(3):468-483. doi:10.1002/2211-5463.12804
28. Nasab FP, Schulz BL, Gamarro F, Parodi AJ, Aebi M. All in one: Leishmania major STT3 proteins substitute for the whole oligosaccharyltransferase complex in Saccharomyces cerevisiae. *Mol Biol Cell*. 2008;19(9):3758-3768. doi:10.1091/mbc.e08-05-0467
29. Kelleher DJ, Gilmore R. An evolving view of the eukaryotic oligosaccharyltransferase. *Glycobiology*. 2006;16(4):47-62. doi:10.1093/glycob/cwj066
30. Schwarz M, Knauer R, Lehle L. Yeast oligosaccharyltransferase consists of two functionally distinct sub-complexes, specified by either the Ost3p or Ost6p subunit. *FEBS Lett*. 2005;579(29):6564-6568. doi:10.1016/j.febslet.2005.10.063
31. Knauer R, Lehle L. The oligosaccharyltransferase complex from Saccharomyces cerevisiae. Isolation of the OST6 gene, its synthetic interaction with OST3, and analysis of the native complex. *J Biol Chem*. 1999;274(24):17249-17256. doi:10.1074/jbc.274.24.17249
32. Nothaft H, Liu X, McNally DJ, Li J, Szymanski CM. Study of free oligosaccharides derived from the bacterial N-glycosylation pathway. *Proc Natl Acad Sci U S A*. 2009;106(35):15019-15024. doi:10.1073/pnas.0903078106
33. Chung CY, Majewska NI, Wang Q, Paul JT, Betenbaugh MJ. SnapShot: N-Glycosylation Processing Pathways across Kingdoms. *Cell*. 2017;171(1):258-258.e1. doi:10.1016/j.cell.2017.09.014

34. Bai L, Wang T, Zhao G, Kovach A, Li H. The atomic structure of a eukaryotic oligosaccharyltransferase complex. *Nature*. 2018;555(7696):328-333. doi:10.1038/nature25755
35. Wild R, Kowal J, Eyring J, Ngwa EM, Aebi M, Locher KP. Structure of the yeast oligosaccharyltransferase complex gives insight into eukaryotic N-glycosylation. *Science (80-)*. 2018;359(6375):545-550. doi:10.1126/science.aar5140
36. Poljak K, Selevsek N, Ngwa E, Grossmann J, Losfeld ME, Aebi M. Quantitative profiling of N-linked glycosylation machinery in yeast Saccharomyces cerevisiae. *Mol Cell Proteomics*. 2018;17(1):18-30. doi:10.1074/mcp.RA117.000096
37. Kung LA, Tao SC, Qian J, Smith MG, Snyder M, Zhu H. Global analysis of the glycoproteome in Saccharomyces cerevisiae reveals new roles for protein glycosylation in eukaryotes. *Mol Syst Biol*. 2009;5(308):1-11. doi:10.1038/msb.2009.64
38. Hossain TJ, Harada Y, Hirayama H, Tomotake H, Seko A, Suzuki T. Structural analysis of free N-glycans in α-glucosidase mutants of Saccharomyces cerevisiae: Lack of the evidence for the occurrence of catabolic α-glucosidase acting on the N-glycans. *PLoS One*. 2016;11(3). doi:10.1371/journal.pone.0151891
39. Igura M, Maita N, Kamishikiryo J, et al. Structure-guided identification of a new catalytic motif of oligosaccharyltransferase. *EMBO J*. 2008;27(1):234-243. doi:10.1038/sj.emboj.7601940
40. Li G, Yan Q, Nita-Lazar A, Haltiwanger RS, Lennarz WJ. Studies on the N-glycosylation of the subunits of oligosaccharyl transferase in Saccharomyces cerevisiae. *J Biol Chem*. 2005;280(3):1864-1871. doi:10.1074/jbc.M410969200
41. Hese K, Otto C, Routier FH, Lehle L. The yeast oligosaccharyltransferase complex can be replaced by STT3 from Leishmania major. *Glycobiology*. 2009;19(2):160-171. doi:10.1093/glycob/cwn118
42. Sikorski RS, Boeke JD. [20] In vitro mutagenesis and plasmid shuffling: From cloned gene to mutant yeast. In: *Methods in Enzymology*. Vol 194. ; 1991:302-318. doi:10.1016/0076-6879(91)94023-6
43. Karaoglu D, Kelleher DJ, Gilmore R. The highly conserved Stt3 protein is a subunit of the yeast oligosaccharyltransferase and forms a subcomplex with Ost3p and Ost4p. *J Biol Chem*. 1997;272(51):32513-32520. doi:10.1074/jbc.272.51.32513

44. Spirig U, Glavas M, Bodmer D, et al. The STT3 protein is a component of the yeast oligosaccharyltransferase complex. *Mol Gen Genet*. 1997;256(6):628-637. doi:10.1007/s004380050611
45. Chavan M, Chen Z, Li G, Schindelin H, Lennarz WJ, Li H. Dimeric organization of the yeast oligosaccharyl transferase complex. *Proc Natl Acad Sci U S A*. 2006;103(24):8947-8952. doi:10.1073/pnas.0603262103
46. Chavan M, Rekowicz M, Lennarz W. Insight into functional aspects of Stt3p, a subunit of the oligosaccharyl transferase: Evidence for interaction of the N-terminal domain of Stt3p with the protein kinase C cascade. *J Biol Chem*. 2003;278(51):51441-51447. doi:10.1074/jbc.M310456200
47. Spirig U, Bodmer D, Wacker M, Burda P, Aebi M. The 3.4-kDa Ost4 protein is required for the assembly of two distinct oligosaccharyltransferase complexes in yeast. *Glycobiology*. 2005;15(12):1396-1406. doi:10.1093/glycob/cwj025
48. Funakoshi M, Hochstrasser M. Small epitope-linker modules for PCR-based C-terminal tagging in Saccharomyces cerevisiae. *Yeast*. 2009;26(3):185-192. doi:10.1002/yea.1658
49. Matsumoto S, Shimada A, Nyirenda J, Igura M, Kawano Y, Kohda D. Crystal structures of an archaeal oligosaccharyltransferase provide insights into the catalytic cycle of N-linked protein glycosylation. *Proc Natl Acad Sci U S A*. 2013;110(44):17868-17873. doi:10.1073/pnas.1309777110
50. Harada Y, Ohkawa Y, Kizuka Y, Taniguchi N. Oligosaccharyltransferase: A gatekeeper of health and tumor progression. *Int J Mol Sci*. 2019;20(23). doi:10.3390/ijms20236074
51. Igura M, Kohda D. Quantitative assessment of the preferences for the amino acid residues flanking archaeal N-linked glycosylation sites. *Glycobiology*. 2011;21(5):575-583. doi:10.1093/glycob/cwq196
52. Yamasaki T, Kohda D. A Radioisotope-free Oligosaccharyltransferase Assay Method. *BIO-PROTOCOL*. 2019;9(5). doi:10.21769/BioProtoc.3186
53. Studier FW. Protein production by auto-induction in high density shaking cultures. *Protein Expr Purif*. 2005;41(1):207-234. doi:10.1016/j.pep.2005.01.016
54. Widlund PO, Davis TN. A high-efficiency method to replace essential genes with mutant alleles in yeast. *Yeast*. 2005;22(10):769-774. doi:10.1002/yea.1244
55. Gadaleta MC, Iwasaki O, Noguchi C, Noma KI, Noguchi E. New vectors for epitope tagging and gene disruption in Schizosaccharomyces pombe. *Biotechniques*. 2013;55(5):257-263. doi:10.2144/000114100

56. Fujii Y, Kaneko M, Neyazaki M, Nogi T, Kato Y, Takagi J. PA tag: A versatile protein tagging system using a super high affinity antibody against a dodecapeptide derived from human podoplanin. *Protein Expr Purif*. 2014;95:240-247. doi:10.1016/j.pep.2014.01.009
57. Einhauer A, Jungbauer A. Affinity of the monoclonal antibody M1 directed against the FLAG peptide. *J Chromatogr A*. 2001;921(1):25-30. doi:10.1016/S0021-9673(01)00831-7
58. Locatelli-Hoops SC, Gorshkova I, Gawrisch K, Yeliseev AA. Expression, surface immobilization, and characterization of functional recombinant cannabinoid receptor CB2. *Biochim Biophys Acta*. 2013;1834(10):2045-2056. doi:10.1016/j.bbapap.2013.06.003
59. Shrimal S, Gilmore R. Oligosaccharyltransferase structures provide novel insight into the mechanism of asparagine-linked glycosylation in prokaryotic and eukaryotic cells. *Glycobiology*. 2019;29(4):288-297. doi:10.1093/glycob/cwy093
60. Matsumoto S, Taguchi Y, Shimada A, Igura M, Kohda D. Tethering an N-glycosylation sequon-containing peptide creates a catalytically competent oligosaccharyltransferase complex. *Biochemistry*. 2017;56(4):602-611. doi:10.1021/acs.biochem.6b01089
61. Kushnirov V V. Rapid and reliable protein extraction from yeast. *Yeast*. 2000;16(9):857-860. doi:10.1002/1097-0061(20000630)16:9<857::AID-YEA561>3.0.CO;2-B
62. Zielinska DF, Gnad F, Schropp K, Wiśniewski JR, Mann M. Mapping N-Glycosylation Sites across Seven Evolutionarily Distant Species Reveals a Divergent Substrate Proteome Despite a Common Core Machinery. *Mol Cell*. 2012;46(4):542-548. doi:10.1016/j.molcel.2012.04.031
63. Dwivedi R, Nothaft H, Reiz B, Whittal RM, Szymanski CM. Generation of free oligosaccharides from bacterial protein N-linked glycosylation systems. *Biopolymers*. 2013;99(10):772-783. doi:10.1002/bip.22296
64. Hou J, Tang H, Liu Z, Österlund T, Nielsen J, Petranovic D. Management of the endoplasmic reticulum stress by activation of the heat shock response in yeast. *FEMS Yeast Res*. 2014;14(3):481-494. doi:10.1111/1567-1364.12125
65. Guerra-Moreno A, Ang J, Welsch H, Jochem M, Hanna J. Regulation of the unfolded protein response in yeast by oxidative stress. *FEBS Lett*. 2019:1873-3468.13389. doi:10.1002/1873-3468.13389

66. Cui HJ, Cui XG, Jing X, et al. GAS1 deficient enhances UPR activity in saccharomyces cerevisiae. *Biomed Res Int*. 2019;2019. doi:10.1155/2019/1238581
67. Nakamura T, Ando A, Takagi H, Shima J. EOS1, whose deletion confers sensitivity to oxidative stress, is involved in N-glycosylation in Saccharomyces cerevisiae. *Biochem Biophys Res Commun*. 2007;353(2):293-298. doi:10.1016/j.bbrc.2006.12.012
68. Schulz BL, Stirnimann CU, Grimshaw JPA, et al. Oxidoreductase activity of oligosaccharyltransferase subunits Ost3p and Ost6p defines site-specific glycosylation efficiency. *Proc Natl Acad Sci U S A*. 2009;106(27):11061-11066. doi:10.1073/pnas.0812515106
69. Ron D, Walter P. Signal integration in the endoplasmic reticulum unfolded protein response. *Nat Rev Mol Cell Biol*. 2007;8(7):519-529. doi:10.1038/nrm2199
70. Shrimal S, Cherepanova NA, Mandon EC, Venev S V., Gilmore R. Asparagine-linked glycosylation is not directly coupled to protein translocation across the endoplasmic reticulum in Saccharomyces cerevisiae. *Mol Biol Cell*. 2019;30(21):2626-2638. doi:10.1091/mbc.E19-06-0330
71. Zheng SQ, Palovcak E, Armache JP, Verba KA, Cheng Y, Agard DA. MotionCor2: Anisotropic correction of beam-induced motion for improved cryo-electron microscopy. *Nat Methods*. 2017;14(4):331-332. doi:10.1038/nmeth.4193
72. Rohou A, Grigorieff N. CTFFIND4: Fast and accurate defocus estimation from electron micrographs. *J Struct Biol*. 2015;192(2):216-221. doi:10.1016/j.jsb.2015.08.008
73. Wagner T, Merino F, Stabrin M, et al. SPHIRE-crYOLO is a fast and accurate fully automated particle picker for cryo-EM. *Commun Biol*. 2019;2(1):1-13. doi:10.1038/s42003-019-0437-z
74. Scheres SHW. A bayesian view on cryo-EM structure determination. *J Mol Biol*. 2012;415(2):406-418. doi:10.1016/j.jmb.2011.11.010
75. Pettersen EF, Goddard TD, Huang CC, et al. UCSF Chimera - A visualization system for exploratory research and analysis. *J Comput Chem*. 2004;25(13):1605-1612. doi:10.1002/jcc.20084
76. Ramírez AS, Kowal J, Locher KP. Cryo–electron microscopy structures of human oligosaccharyltransferase complexes OST-A and OST-B. *Science (80-)*. 2019;366(6471):1372-1375. doi:10.1126/SCIENCE.AAZ3505

77. Cherepanova NA, Shrimal S, Gilmore R. Oxidoreductase activity is necessary for N-glycosylation of cysteine-proximal acceptor sites in glycoproteins. *J Cell Biol*. 2014;206(4):525-539. doi:10.1083/jcb.201404083
78. Stevens KLP, Black AL, Wells KM, et al. Diminished Ost3-dependent N-glycosylation of the BiP nucleotide exchange factor Sil1 is an adaptive response to reductive ER stress. *Proc Natl Acad Sci*. 2017;114(47):12489-12494. doi:10.1073/pnas.1705641114
79. Kanda Y. Investigation of the freely available easy-to-use software "EZR" for medical statistics. *Bone Marrow Transplant*. 2013;48(3):452-458. doi:10.1038/bmt.2012.244
80. R Core Team. R: A language and environment for statistical computing. 2020. https://www.r-project.org/.
81. Fox J. The R Commander: A Basic-Statistics Graphical User Interface to R. *J Stat Softw*. 2005;14(9):1902. doi:10.18637/jss.v014.i09